MECHANICAL CHARACTERIZATION OF BONE FROM THE TISSUE DOWN TO THE LAMELLAR LEVEL BY MEANS OF NANOINDENTATION

THÈSE N^{O} 2538 (2002)

PRÉSENTÉE À LA FACULTÉ STI SECTION DE GÉNIE MÉCANIQUE

ÉCOLE POLYTECHNIQUE FÉDÉRALE DE LAUSANNE

POUR L'OBTENTION DU GRADE DE DOCTEUR ÈS SCIENCES

PAR

Stefan HENGSBERGER

Diplom-Physiker, Universität des Saarlandes, Saarbrücken, Allemagne
et de nationalité allemande

acceptée sur proposition du jury:

Prof. Ph. Zysset, directeur de thèse
Prof. J. Currey, rapporteur
Dr A. Kulik, rapporteur
Prof. J.-J. Meister, rapporteur
Prof. R. Rizzoli, rapporteur

Lausanne, EPFL
2002

diese Doktorarbeit ist meinem Vater Uwe Hengsberger
und
- in Gedenken -
meiner Mutter Renate Hengsberger gewidmet

Abstract

Osteoporosis has become an important health and economic problem of our aging western society. This metabolic illness leads to a net bone loss and to a deterioration of trabecular architecture. Motivated by the fact that osteoporosis may also result in a degradation of intrinsic tissue quality this thesis focuses on the micro- and nanomechanical properties of human, bovine and rat bone.

For the first time, to the best of our knowledge, mechanical properties of single bone lamellae are tested under dry and physiological conditions. Stable thermal equilibrium conditions can be achieved for the latter that allow for tests at body temperature and under fully wet conditions. This study represents a first step towards extension of knowledge of the structure-function relationships down to the lamellar level. Adjacent thin and thick lamellae of the same bone structural unit (BSU) are significantly different in terms of hardness and indentation modulus. The two types of lamellae show a significantly different increase of mechanical properties when the water content is removed by drying. In this context morphological models are employed to discuss the mechanical properties (bone lamellation theory).

The BSU is found to be the basic bone component with individual morphological and also mechanical properties. Significant differences are seen between BSU of osteonal, trabecular and interstitial microstructures dissected from the human femoral neck. Human interstitial and bovine plexiform bone do not show a significantly different indentation modulus. Depth-dependent indentation measurements, which are done for this purpose, further extend our current knowledge of the technique.

Structure-function relationships are investigated on the BSU-level by applying two morphological and two mechanical techniques on identical BSUs of two donors. The dependence of the mechanical properties on the mineral content (as measured by microradiography) and the orientation of the collagen fibers (as measured by polarized light microscopy) are investigated.

The reported correlations between macroscopic mechanical properties and these morphological parameters are not generally confirmed on the BSU-level by the nanoindentation data of this two-case study.

The indentation modulus is validated by a comparison with a traction experiment of a bovine bone microspecimen. This experiment raises confidence in the absolute value of this elastic parameter. The influence of the material anisotropy on the measured indentation modulus is determined for bovine cortical bone.

As a first step to apply the nanomechanical tool in the context of preclinical studies, a set of rat vertebrae were tested. Given the small number of specimens, this study does not show a general significance of low protein diet, ovariectomy and essential aminoacids on intrinsic tissue properties.

This thesis proposes further nanoindentation studies on bone tissue for future work. It is expected that relationships between nanomechanical properties and the degree of damage accumulation of aging and/or osteoporotic tissue can be established. This can contribute to development of new strategies aiming at improving tissue quality.

Abriß

Osteoporose wird zunehmend zu einem gewichtigen gesundheitlichen sowie ökonomischen Problem unserer alternden westlichen Gesellschaft. Diese Stoffwechselkrankheit führt zu einem Verlust der Knochenmasse und einer Degradierung der Architektur der Spongiosa. Die Tatsache, daß Osteoporose zusätzlich zu einer Reduktion der Qualität des Knochengewebes führen könnte, motivierte diese Doktorarbeit, welche auf dessen mikro- sowie nanomechanischen Eigenschaften zielt. Hierfür werden menschliches Gewebe sowie Proben der Kuh,- und Rattenkompakta untersucht.

Unseren Kenntnissen nach werden zum ersten mal mechanische Eigenschaften einzelner Knochenlamellen unter trockenen sowie physiologischen Konditionen getestet. Für letztere werden stabile thermische Bedingungen erreicht, die Tests von vollständig in Flüssigkeit eingetauchten Knochenproben bei Körpertemperatur gestatten. Diese Studie soll als erster Schritt zur Erweiterung unserer Kenntnisse, wie die Struktur und die Funktion des Knochengewebes auf lamellarer Ebene zusammenhängen, verstanden werden. Angrenzende dünne und dicke Lamellen innerhalb der selben strukturellen Einheit (BSU) zeigen signifikante Unterschiede bezüglich der Härte und des elastischen Indentationsmodules. Diese zwei Klassen von Knochenlamellen zeigen ebenfalls eine unterschiedliche Änderung der mechanischen Eigenschaften, wenn der Wasseranteil ausgetrocknet wird. Die Nanomechanik der Knochenlamellen werden im Rahmen von bereits bekannten morphologischen Modellen ("Theorie der Knochenlamellation") diskutiert. Die BSU wird als Basiseinheit des Knochens vorgeschlagen, da neben individuellen morphologischen auch individuelle mechanische Eigenschaften festgestellt werden.

Signifikante Unterschiede werden zwischen BSUs der osteonalen, trabekularen und interstitiellen Mikrostruktur des menschlichen Oberschenkelhalses aufgezeigt. Der elastische Indentationsmodul von menschlichem interstitiellen und plexiformen Gewebe einer Kuhkompakta sind hingegen nicht unterschiedlich. Tiefenabhängige Indentationsmessungen, die in diesem Rahmen gemacht werden, tragen zu einem vertieften Vertändnis der Technik bei.

Die Beziehung zwischen der Struktur und der Funktion werden auf dem Niveau der BSU untersucht. Zwei morphologische und zwei mechanische Charakterisierungstechniken werden auf ein identisches Kollektiv von BSUs zweier Spender angewendet. Die mechanischen Eigenschaften werden in Abhängigkeit vom Mineralisierungsgrad (bestimmt mittels Mikroradiographie) sowie der Orientierung der Kollagenketten (ermittelt durch Polarisationsmikroskopie) untersucht. Korrelationen, die zwischen den makroskopischen mechanischen Eigenschaften und diesen morphologischen Größen gefunden wurden, werden im Rahmen dieser Zweifallstudie nicht für den BSU-Level bestätigt. Der Indentationsmodul wird mittels eines Vergleiches mit einem Traktionstest einer Mikroprobe eines Kuhknochens validiert. Diese Studie weckt Vertrauen in den absoluten Wert dieses elastischen Parameters. In diesem

Zusammenhang wird auch der Einfluß der Anisotropie der Kuhkompakta auf den gemessenen Indentationsmodul ermittelt.
In einem ersten Schritt, diese nanomechanische Charakterisierungsmethode im Rahmen einer präklinischen Studie anzuwenden, wird ein Kollektiv von Rattenwirbelkörpern gemessen.
Diese Studie, die sich auf eine eventuell zu niedrige Zahl an Tieren stützt, zeigt keinen generellen Einfluß der zugrundeliegenden Behandlung. Weder eine operative Entnahme der Gebährmutter in Verbindung mit einer geringen Aufnahme an Eiweissen noch eine Behandlung mit essentiellen Aminosäuren zeigen eine globale Beeinflussung der intrinsischen Gewebeeigenschaften.
Diese Doktorarbeit motiviert, die bisherigen Kenntnisse bezüglich der intrinsischen Eigenschaften des Knochengewebes durch weitere Nanoindentationsstudien zu erweitern. Es wird erwartet, daß Zusammenhänge zwischen den nanomechanischen Parametern und dem Beschädigungsgrad von alterndem und/oder osteoporotischem Gewebe gefunden wird. Dies kann einen wesentlichen Beitrag zur Entwicklung neuer Strategien, um die Qualität des Knochengewebes zu verbessern, leisten.

Table of Contents

Introduction

Osteoporosis has become an important health and economic problem in our aging society. In the United States, this metabolic illness causes annual health care costs of 13.8 billion US$ (Packard & Heaney, 1997). Osteoporosis is manifested in a loss of trabecular and cortical bone mass and in a deterioration of trabecular architecture. The associated increased risk of fracture primarily effects anatomical sites like the femoral neck, the vertebral bodies and the wrist. These sites consist of a thin shell of cortical bone with trabecular bone as an important internal support (see Figure 1).

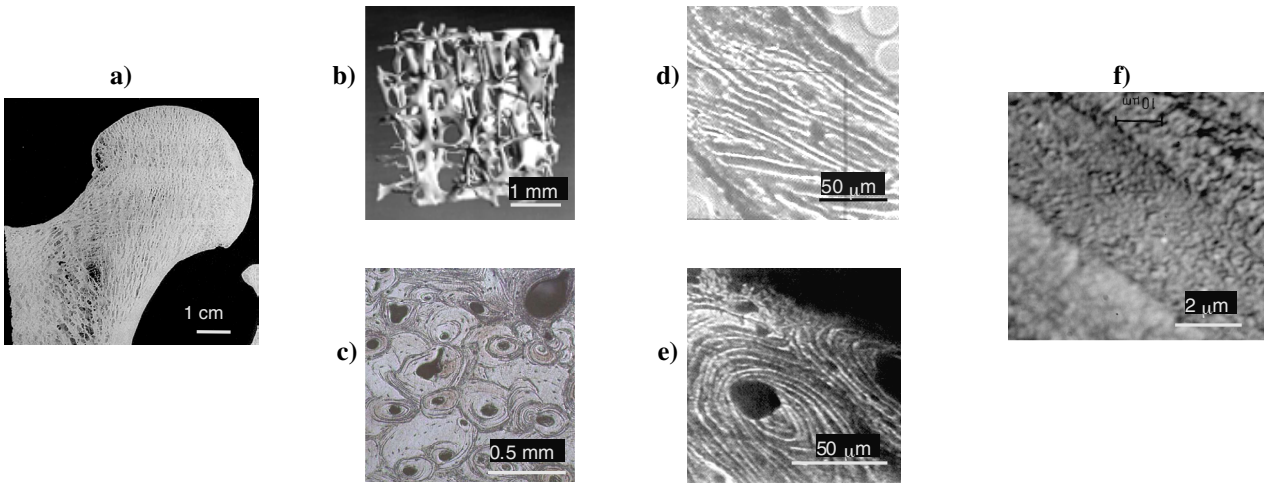

Figure 1: Hierarchy of the human femoral neck
Figure **a** shows a cut through a frontal plane of the femoral neck. The outer shell is constituted of compact bone while the inside is constituted of the spongious trabecular bone. Figure **b** shows the trabecular structure and Figure **c** a transverse cut of the compact shell that shows vascular canals. Figure **d** shows packets of lamellae within trabeculae and Figure **e** an osteon, a vascular canal surrounded by concentric lamellae. On Figure **f**, a single lamella is seen that is mainly constituted of collagen fibers and hydroxyapatite crystals.

Clinical diagnosis of osteoporosis relies on bone mineral density (BMD) measured at sites like the femoral neck. This parameter, that is determined from DEXA (dual energy X-ray absorption), integrates the total quantity of mineral and combines indistinguishably cortical and trabecular bone volume fraction and the degree of mineralisation. The fact, that the mechanical properties depend apart of geometry also with different power laws on volume fraction (Carter & Hayes, 1977; Schaffler & Burr, 1988) and mineralisation (Currey, 1988), causes their moderate correlation with BMD.

Osteoporotic loss of bone mass results from unbalanced bone remodeling, a metabolic process, that might be recalled at this point. Bone completes ossification at the age of 16, reaches full maturity at 30 and the mechanical properties start to deteriorate after this age (Mc Calden et al.,

1993; Zioupos, 2001). During the whole life, ongoing cellular activity remodels the bone tissue. This continuous turnover process is based on two cell types: the multinuclear osteoclasts, that are responsible for the resorption of the bone material, and the mononuclear osteoblasts that ensure the bone formation. The latter provide the organic collagen fibers of the extracellular matrix by synthesizing osteoid on the remodeling site. The osteoblasts are trapped in the lacunae of the matrix and become osteocytes that remain interconnected by canaliculae. A mineralisation process whereby calcium and phosphate diffuse into the matrix and precipitate into hydroxyapatite follows. The end result of this remodeling cycle represents a bone structural unit (BSU). For compact bone a BSU is constituted of a Haversian canal (vascular canal) that is surrounded by concentric bone lamellae, called Haversian system or osteon. For trabecular bone, a packet of several bone lamellae constitutes a BSU (Eriksen et al, 1994). In this context we also consider the fibrolamellar structure of bovine bone as BSUs. The reported ultrastructural properties of bone lamellae (1-4 μm thickness) are controversial and suggest alternating collagen fiber orientation and/or variation in density and/or cholesteric fiber arrangement (Gebhardt, 1906; Ascenzi, 1988; Marotti, 1993; Giraud-Guille, 1998).

In healthy bone, the resorption and formation processes are balanced, while for osteoporosis this equilibrium is lost and a net loss of bone results. Clinical studies have discovered some potential factors that lead to this bone loss. Among those risk factors are a postmenopausal lack of estrogen for female patients or a lack of Vitamin D and reduced physical activity that concern female as well as male patients. For elderly people, the associated high fracture risk is additionally increased due to a reduced muscular capacity to compensate loss of balance and impacts. The aforementioned factors differently influence the balance of the bone turnover process. Estrogen serves as an inhibitor of the resorption processes while Vitamin D is involved in the absorption of calcium in the intestine. Increased physical activity stimulates bone formation while rest promotes bone resorption. It is widely accepted that the decrease of bone mass and the deteriorated architecture are the main factors for the reduced mechanical competence of osteoporotic bone. Current treatments employ estrogen, biphosphonate, SERM or calcitonin that result in an increase of BMD by mainly inhibiting bone resorptive processes. However, the effects of these agents on the bone metabolism are still not fully understood. In the last years, it has become evident that aging may also reduce the mechanical properties of bone tissue instead of just affecting the balance of the remodeling activity (Mc Calden et al, 1993; Zioupos, 2001).

At this point, it is appropriate to define the hierarchical organization levels of bone that are relevant for this thesis. The tissue level includes several BSUs and the mechanical tests therefore include vascular, lacunar and canalicular porosities. Tests of the tissue properties are performed with single trabeculae or with microspecimens of compact bone. On the BSU level, an average of the lamellae within a single BSU is done where canalicular porosity has an influence. The lamellar level considers tests on single bone lamellae and represents an average response of the

extracellular matrix (ECM). The ECM is the composition of collagen fibers and hydroxyapatite platelets.

The need for assessment of intrinsic properties of the bone tissue was recognised in the 1950s by Amprino (Amprino, 1958). He performed Vickers microhardness tests that characterize the resistance of the material against the penetration of a diamond indenter. He applied indentations of 15 and 50 gram loads that resulted in hardness imprints of approximately 20 and 36 micrometers respectively. The microhardness results of avian and calf cortical bone ranged from 0.2 to 0.8 GPa and varied significantly with anatomical site, mineralisation and collagen fiber orientation (using polarized light microscopy).

Eight years later, Weaver focussed on microhardness of human cortical and trabecular bone (Weaver, 1966). He reported differences between cortical and trabecular bone, the latter being on average softer. He studied the effect of storage, drying, embedding, mineralisation and collagen fiber orientation. He confirmed trends with mineralisation but did not detect any dependence on collagen fiber orientation. Microhardness showed a continuous increase until the age of 30 while low variations were detected among older donors. Surprisingly, bone tissue of osteoporotic donors did not have reduced microhardness values. However, this result is moderated by the fact that it is based on only four osteoporotic patients. A weakness of hardness is that it combines indistinguishable elastic and postyield deformation that makes an interpretation of its physiological relevance difficult. The Young's modulus on the other hand characterizes the deformation in the elastic regime and therefore represents a measure of the strain due to physiological loading conditions.

In the following years, many efforts were done to measure the Young's modulus of trabecular and cortical bone tissue. For this purpose numerical studies and mechanical tests of microspecimens down to single trabeculae and beams of cortical bone were performed (Towsend & Rose, 1975; Mente & Lewis, 1989; Choi et al, 1990; Rho & Ashman, 1993; Ryan & Williams, 1989). A comprehensive literature review reported a range of 0.76 to 20 GPa for trabecular and 2.5-20.7 GPa for cortical bone tissue (Guo & Goldstein, 1997). The values vary strongly with specimen size and the applied experimental technique. The size effect has to be attributed to the influence of geometrical artefacts like lacunae, resorption cavities, Haversian canals and cement lines (thin layer between osteonal and interstitial bone). This wide spread of experimental results raises the need for mechanical testing methods on the bone lamellar level where the aforementioned artefacts have no influence.

Approximately twenty years after Weavers study, the further development of Vicker´s microhardness device reached the submicron level. Improved sensitivity of the sensor components allows continuous load and displacement acquisition during the indentation. Theoretical approaches developed a method to derive - apart of the (nano)hardness – also an elastic indentation modulus from this test (Sneddon, 1965; Doerner & Nix, 1986; Oliver & Pharr,

1992). In recent years, several nanoindentation studies focussing on human and bovine bone tissue were performed (Rho et al, 1999b; Zysset et al, 1999; Hoffler et al, 2000a; Hoffler et al, 2000b; Turner et al, 1999). Young's modulus was found to vary with preparation and testing protocol, anatomical site and tissue type, while no significance of age was reported. Typical values for the elastic modulus were 22.4 ±1.2 GPa for osteonal, 25.7 ±1 GPa for interstitial (remnants of partially resorbed osteons) and 19.4 ±2.3 GPa for trabecular tissue of dried tibial bone (Rho et al, 1999b). Under moist conditions, Zysset et al. measured an elastic modulus of 15.8 ±5.3 GPa for osteonal, 17.5 ±5.3 GPa for interstitial and 11.4 ±5.6 GPa for trabecular bone from the femoral diaphysis. These results show that the elastic modulus of trabecular and cortical bone lamellae are close and coincide with (or exceed) the higher boundary of the aforementioned literature range.

The development of this nanomechanical device has opened a new spectrum of possibilities in the field of biomechanics of bone tissue.

The **general goal of this thesis** was to extend the knowledge of the structure-function relationships (Guo & Goldstein, 1997) from the tissue down to the lamellar level. For this purpose, mechanical tests were performed on human, bovine and rat bone. All studies include nanoindentation to characterize trabecular and/or compact bone on the lamellar level (see Chapter 2), the BSU level (Chapter 1,3,4) or on the tissue level (see Chapter 5 & 6). The order of the Chapters reflects the chronological order of data acquisition. Each study contains an individual literature review and discussion of the results.

The reader should note that two different nanoindentation devices were employed. The first is a combined nanoindenter with AFM that allows both topography scan and indentation tests using the same tip (Figure 2 left, Hysitron). This results in highly precise indenter positioning (<100nm). On the other hand, this device is limited to indents with 6mN maximum force within a

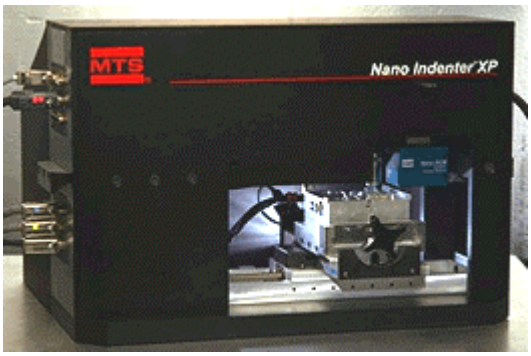

Figure 2 left: Photo of the combined AFM and nanoindenter (Hysitron Inc., Minneapolis, MN). This combination allows for topography scans and indentation tests using the same tip. This device provides a high precision to position the indenter tip, but the tests are confined to a small window of 100µm x 100µm
right: Photo of the nanoindenter combined with optical microscope (MTS, Systems Corporation Minneapolis). This device allows for testing within a window of several cm^2 but is less accurate in terms of positioning the indenter.

window of 100μm x 100μm (smaller than a single BSU). The second device is a combination of optical microscope and nanoindenter (Figure 2 right, MTS). This instrument allows for higher loads up to 600mN (indentation depths) and a characterization of greater areas since the structures of interest are chosen with the optical microscope. On the other hand, the precision to position the indenter is less accurate (>1μm).
The theoretical basis of the nanoindentation test is addressed in the first two chapters. The derivation of the elastic parameter "indentation modulus", that combines local Young's modulus and Poisson ratio, will be explained. The major prospects of the following chapters will now be shortly addressed and explained with respect to available data from the literature.

Work with combination of nanoindenter with AFM (Hysitron): Chapter 1-2
To our current knowledge, we were the first team to apply the combination of nanoindentation with AFM to bone tissue. **Chapter 1** represents a description of this recently developed device and a first application to a few human osteonal and trabecular BSUs. Chapter 1 was already published in Cells & Materials **1**:2001, p.12-16.
Most of the published nanoindentation data derive from indents to 500–1000 nm depth. These results represent the composite modulus of multiple lamellae. Reported values of wet tissue were further obtained keeping the tissue moist by contact with a thin layer of water (<100μm) on the surface or by contact with water below the surface (Rho & Pharr, 1999a; Zysset et al, 1999; Hoffler et al, 2000a). This may not simulate true physiological conditions.
The combination of nanoindenter with AFM allows proper positioning and low indentation depths of 100nm on individual lamellae. **Chapter 2** addresses the mechanical properties of single bone lamellae under dry and wet conditions (Section 2.1) and their relative change as a result of drying (Section 2.2). In this context, bone lamellation theories will be recalled. For the tests under physiological conditions, the bone sample were installed in a plexiglas cup and fully immersed into a liquid. A shortened version of Section 2.1 – containing less figures and tables and without the appendix - is published in Bone **30/1**:2002. Chapter 2 is introduced with a preliminary study to quantify time-dependent deterioration of the mechanical properties when the tissue is exposed to a physiologic solution.

Work with combination of nanoindenter with optical microscope (MTS): Chapter 3-6
Chapter 2 demonstrates depth dependent variations of bone lamellar properties for depths ranging from 100 up to 500nm. **Chapter 3** quantifies depth dependent effects of the mechanical parameters in a range of 100nm to 2300nm. This study was performed to determine an ideal indentation depth for a characterization of single BSUs. This article also demonstrates a comparison of three microstructures of human femoral bone and bovine plexiform tissue.

Mineral content and collagen fiber orientation are recognised factors for the macroscopic elastic and postyield properties respectively (Currey, 1988; Martin & Ishida, 1989). The following **Chapter 4** aimed at quantifying the influence of these factors on the mechanical properties on the BSU level. For this purpose, four different techniques were applied to a collective of BSUs dissected from a 30-year old male and from an 86-year old female donor. Two methods addressed morphological properties: microradiography and polarised light microscopy (PLM) while two further methods characterize mechanical properties: nanoindentation and scanning acoustic microscopy (SAM). The variations of the mechanical properties are discussed in the light of the morphological parameters.

Chapter 5 represents a validation study of the indentation modulus for bovine bone. The literature provide studies where a correlation between the intrinsic tissue properties and the macroscopic bending modulus was demonstrated (Rho et al, 2001). The goal of this project was to convert the local indentation modulus into an absolute Young's modulus of a microspecimen containing several BSUs. For this purpose the elastic response of a bovine microspecimen loaded in traction was related to its porosity (obtained by 3D-tomography) and its intrinsic tissue properties (obtained by nanoindentation).

The potential of nanoindentation motivates the investigation of the effect of medical agents on the intrinsic mechanical properties of the tissue. However, few studies were done to apply this nanomechanical method in the context of preclinical research. **Chapter 6** demonstrates a contribution of nanoindentation to a preclinical study on rat bone. The effects of ovariectomy, low protein intake and treatment with essential aminoacids on the intrinsic tissue properties of rat vertebral bodies were investigated.

References

- Ascenzi A (1988) The micromechanics versus the macromechanics of cortical bone - a comprehensive presentation. J Biomech Eng **110**:357-363
- Amprino R (1958) Investigations on some physical properties of bone tissue. Acta Anatom **34**:161-168
- Carter DR, Hayes WC (1977) The compressive behavior of bone as a two-phase porous material. J Bone Jt Surg **59A**:954-962
- Choi K Kuhn JL, Ciarelli MJ, Goldstein SA (1990) Elastic moduli of human subchondral trabecular and cortical bone tissue and the size-dependency of cortical bone modulus. J Biomech **23/11**:1103-1113
- Currey JD (1988) The effect of porosity and mineral content on the Young's modulus of elasticity of compact bone. J Biomech **21/2**:131-139
- Doerner MF, Nix WD (1986) A method for interpreting the data from depth-sensing indentation instruments. J Mater Res **1/4**: 601-609
- Eriksen EF, Axelrod DW, Melsen FM (1994) Bone Histomorphometry. 1ed. Raven Press Ltd, New York
- Gebhardt, 1906 über funktionell wichtige Anordnungsweisen der feineren und gröberen Bauelemente des Wirbeltierknochens. II. Spezieller Teil.: der Bau der Haversschen

Lamellensysteme und seine funktionelle Bedeutung. Arch Entw Mech Org **20**:187-322
- Giraud-Guille MM (1998) Plywood structures in nature. Curr Op Solid State & Mat Sc **3**:221-227
- Guo XE, Goldstein SA (1997) Is trabecular bone tissue different from cortical bone tissue? FORMA **12**:185-196
- Hoffler CE, Moore KE, Kozloff K, Zysset PK, Brown MB, Goldstein SA (2000a) Heterogneity of bone lamellar-level elastic moduli. Bone **26/6**:603-609
- Hoffler CE, Moore KE, Kozloff K, Zysset PK, Goldstein SA (2000b) Age, gender, and bone lamellae elastic moduli. J Orth Res: Official Publication of the Orthopaedic Research Society, **18/3**:432-437
- Marotti G (1993) A new theory of bone lamellation. Calcif Tissue Int **53**(Suppl I):47-56;
- Martin RB, Ishida J (1989) The relative effects of collagen fiber orientation, porosity, density and mineralization on bone strength. J Biomech **22/5**: 419-426
- Mc Calden RW, Mc Geough JA, Barker MB, Court-Brown CM (1993) Age-related changes in the tensile properties of cortical bone. J Bone Jt Surg **75A/8**: 1193-1205
- Mente PL, Lewis JL (1989) Experimental method for the measurement of the elastic modulus of trabecular bone tissue. J Orthopaed Res **7**:456-461
- Oliver WC, Pharr GM (1992) An improved technique for determining hardness and elastic modulus using load and displacement sensing indentation experiments. Mat Res Soc **7/6**:1564-1583
- Packard PT, Heaney RP (1997) Medical nutrition therapy for patients with osteoporosis. J Amer Diet Ass **97/4**:414-417
- Rho JY, Ashman RB (1993) Young's modulus of trabecular and cortical bone material: ultrasonic and microtensile measurements. J Biomech **26**:111-119
- Rho JY, Pharr GM (1999a) Effects of drying on the mechanical properties of bovine femur measured by nanoindentation. J Mat Sc: Mat Med **10**:485-488
- Rho JY, Roy ME, Tsui TY, Pharr GM (1999b) Elastic properties of microstructural components of human bone tissue as measured by nanoindentation. J Biomed Mat Res **45**:48-54
- Rho JY, Zioupos P, Currey JD, Pharr GM (2001) Microstructural elasticity and regional heterogeneity in human femoral bone of various ages examined by nanoindentation. J Biomech: in press
- Ryan SD, Williams JL (1989) Tensile testing of rodlike trabeculae excised from bovine femoral bone. J Biomech **26**:77-83
- Schaffler MB, Burr DB (1988) Stiffness of compact bone: effects of porosity and density. J Biomech **21/1**:13-16
- Sneddon IN (1965) The relation between load and penetration in the axisymmetric Boussinesq problem for a punch of arbitrary profile. Int J Eng Sc **3**:47-57
- Townsend PR, Rose RM (1975) Buckling study of single human trabeculae. J Biomech **8**:199-201
- Turner CH, Rho JY, Takano Y, Tsui TY, Pharr GM (1999) The elastic properties of trabecular and cortical bone tissues are similar: results from two microscopic measurement techniques J Biomech **32**:437-441
- Weaver JK (1966) The microscopic hardness of bone. J Bone Joint Surg **A48**:273-288
- Zioupos P (2001) Ageing human bone: factors affecting its biomechanical properties and the role of collagen. J Biomat App **15**:187-229

- Zysset PK, Guo XE, Hoffler CE, Moore KE, Goldstein SA (1999) Elastic modulus and hardness of cortical and trabecular bone lamellae measured by nanoindentation in the human femur. J Biomech **32**:1005-1012

Chapter 1

A combined atomic force microscopy and nanoindentation technique to investigate the elastic properties of bone structural units*

*This article was published (under the above-mentioned title) by Cells and Materials **1**:2001 p. 12-16.* *Authors: S. Hengsberger, A. Kulik* & Ph. Zysset. Laboratory of Applied Mechanics and Reliability Analysis, Department of Physics*, Swiss Federal Institute of Technology, Lausanne; Switzerland*

Introduction

Osteoporosis leads to excessive bone fragility and impairs increasingly the quality of life of the elderly. The deteriorating influences of this metabolic disease on the mechanics of human bone are increasingly well understood in terms of bone density and architecture. Recent studies aimed at quantifying damage accumulation in bone tissue down to the extracellular matrix (ECM) level. It becomes also accepted that the ECM plays the role of a local mechanical sensor providing the cells with the strain or stress information to control the remodeling process and maintain bone tissue. Material characterization of the ECM contributes to the understanding of the biomechanical implications of the normal remodeling process and its perturbation by osteoporosis.

The spectrum of applied experimental techniques to quantify mechanical properties at the bone tissue level range from buckling (Townsend et al., 1975), bending (Mente et al., 1989), 3-point-bending (Choi et al., 1990), microtensile and ultrasonic tests (Rho et al., 1993, Ryan et al., 1989) to ultrasonic microscopy (Katz et al., 1993). The reported Young's moduli range from 0.76 GPa to 20 GPa for trabecular bone and from 5 GPa to 27 GPa for cortical bone. These values were found to vary strongly with the experimental technique mostly due to distinct strain rates, representative volume element sizes and the associated influence of structural artifacts like lacunae, cement lines and vascular channels. For ultrasonic microscopy, the measured impedance change between the sample and a coupling liquid depends on both Young's modulus and the local material density that cannot easily be distinguished.

More recently, a nanoindentation technique was developed that allows measurement of some mechanical properties within a bone structural unit (BSU[1]). Previous nanoindentation studies (Rho et al., 1997, Zysset et al., 1999, Rho et al., 1999c) characterized the dependence of the elastic modulus of cortical and trabecular bone with age, anatomical site, microstructural orientation and tissue preparation. However, the influence of surface roughness of the tested

[1] *The bone structural unit (BSU) represents the end result of a remodeling cycle; in cortical bone, it constitutes a haversian system (or cortical osteon), and in cancellous bone, it is a wall or "packet" of bone (or trabecular osteon) (Eriksen94)*

specimens was not reported. The results by Zysset et al. (1999) for the femoral neck demonstrated standard deviations exceeding 20% of the mean value, which may be attributed to the inclusion of several bone structural units with quite different properties. The present study focussed on the application of a combined atomic force microscopy and nanoindentation technique to measure elastic modulus and hardness of human bone tissue.

The first aim was to check if the preliminary characterization of the surface with the available AFM-mode improves the reliability of the measurements. As a second aim, we investigated if the separate evaluation of single BSUs would give significantly lower standard deviations than 20% of the mean value.

Materials and methods

A: Technique

The combination of an AFM and a nanoindenter (Hysitron, Incorporated 2010 East Hennepin Avenue Minneapolis, MN 55413) is a further development of the traditional Vickers microhardness testing device. This instrument allows for two measurement modes. It provides a surface topography of constant contact force in AFM mode (see Figure 1) and a force displacement curve in nanoindentation (see Figure 2) mode using the same tip. This feature provides a high spatial resolution to position the tip on the microstructure of interest. The sample

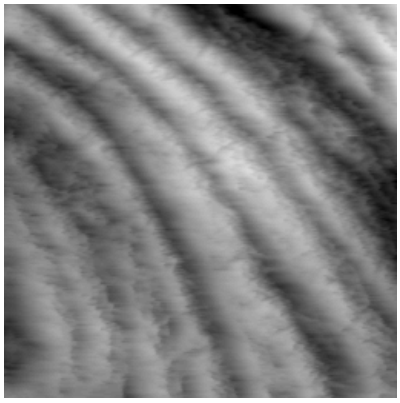

Figure 1 topography of compact bone in AFM-mode (scan size 50μm times 50μm)

is mounted on a scanner that allows for a movement in the plane normal to the axial motion of the tip. The transducer consists of a three-plate capacitor on whose central plate a tetrahedral diamond Berkovich-tip is mounted. A nanoindentation curve (see Figure 2) consists of a loading phase where the tip is pressed into the material up to a maximal force, a holding period where the tip creeps into the material and an unloading phase where the force on the material is released. The loading and holding phases result in both plastic and elastic deformation that cannot be distinguished. The unloading phase shows the elastic recovery of the material while the load is released. For isotropic elastic materials, the following relationship based on the analytical solution by Sneddon (1965) holds for indenters of revolution:

$$S(h_{max}) = \frac{dP}{dh}(h_{max}) = \frac{2}{\sqrt{\pi}} E_r \sqrt{A_c(h_{max})} \qquad \text{(eq.1)}$$

where $S(h_{max})$ describes the derivative of the unloading part at the point of initial unloading and $A_c(h_{max})$ the contact area, over which the material and the indenter are in contact at that position and time. The unloading stiffness $S(h_{max})$ is determined by fitting the unloading curve between 40% and 95% of maximum force. The contact area $A_c(h_{max})$ is determined by a procedure derived by Oliver et al. (1992). The calibration of the instrument is commonly performed by

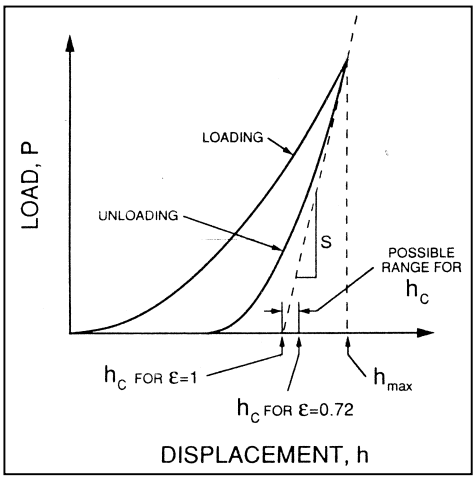

Figure 2 typical nanoindentation curve. The unloading part allows to determine elastic modulus and hardness

doing indents of increasing depth in fused silica with a known reduced modulus of 69.9 GPa. The reduced modulus E_r depends on the deformation of the material and the deformation of the diamond tip:

$$\frac{1}{E_r} = \frac{1-\nu_{specimen}^2}{E_{specimen}} + \frac{1-\nu_{tip}^2}{E_{tip}} \qquad \text{(eq.2)}$$

The material properties of the diamond tip are $\nu_{tip} = 0.07$ and $E_{tip} = 1140\ GPa$. The indentation modulus is defined by

$$E_{ind} = \frac{E_{specimen}}{1-\nu_{specimen}^2} \qquad \text{(eq.3)}$$

This variable contains Young's modulus and Poisson's ratio. Often, Poisson's ratio is assumed to be $\nu = 0.3$ for bone tissue, but we prefer to report indentation moduli to avoid this assumption. For the purpose of comparison, Young's modulus calculated for $\nu = 0.3$ is approximately 90% of the indentation modulus.

A second mechanical property can be calculated from the nanoindentation curve: hardness. This variable describes the mean pressure the material can resist and is defined by the ratio of maximum load P_{max} over the contact area:

$$H = \frac{P_{max}}{A_c(h_{max})} \qquad \text{(eq.4)}$$

The stress field imposed by the indentation process is heterogeneous and leads to plastic deformation around the tip. To achieve reproducible measurements, the average roughness of the sample in the contact area should be well below the applied indentation depth. The minimal distance between neighbor indents was set to approximately 3 times the contact diameter (i.e. $\approx 18\, h_{max}$ for a Berkovich tip geometry).

B: Specimen preparation and measurements:

The femoral head of an 86 year old female was cut in 3mm slices perpendicular to the axis of the neck. For this purpose, a diamond band saw with continuous water irrigation was employed. The marrow was dissolved applying about 3 alternated treatments with 0.5 % bleach and ordinary soap solution in an ultrasonic cleaner for 5 minutes (Zysset et al. 1994). The specimen was then embedded in PMMA without fixation to prevent possible deterioration of the mechanical properties (McElhaney et al. 1964, Sedlin et al. 1966). The sample was then polished, first with successive grades of silicon carbide paper, followed by a treatment with diamond slurry and finishing with a 0.05μm alumina solution. The water content of bone promotes the enzymatic degradation of collagen and reduction in mechanical properties within several hours at ambient temperature. Since characterization of each BSU took at least one entire day, it was necessary to stabilize the mechanical properties for several days with an additional drying procedure for 24 hours at 50 degrees. After drying the sample was first scanned in AFM-mode with a typical size of 60 μm times 60 μm, a frequency of 0.3 Hz and a contact force of 5 μN. The topography measurement helped to characterize the polishing quality and to choose precisely the region of interest. The piezoelectric scanner of the AFM allows for a higher positioning accuracy than the x-y translation table that equips nanoindentation devices relying on optical microscopy. First, we tested if the high contact force of the tip damaged the specimen surface. For this purpose several successive scans with the same center and increasing scan size were performed. Then, 3 indents of 2.5 mN maximum force on the same osteon were done each day during a period of one week. The purpose was to check if the mechanical properties remained constant over time. After these preliminary tests, two BSU in cortical and two BSU in trabecular bone were tested. The tests included 24 indents in each BSU with a maximum force of 5 mN. The load-controlled indentations reached depths of about 550 nm that varied in correlation to the stiffness of the tested region. All tests included a preliminary thermal drift correction limited to a maximum drift

of $0.05\frac{nm}{s}$. The indentations contained a linear loading part of 15s, a 10s holding period at maximum force and a linear unloading part of 15s. These parameters correspond to an average strain rate of

$$\frac{1}{h}\frac{dh}{dt} \approx 0.067\frac{1}{s} \qquad \text{(eq.5)}$$

According to the orientation of the femur section and for best identification of the BSU, the indents were applied parallel to the osteon axes in compact bone. On cancellous bone the indents were applied perpendicular to the long axes of transversely orientated trabeculae.

Results

AFM

The successive topography measurements with increasing scan size showed that the selected contact force of 5 μN did not affect the surface appearance and topography. After polishing, bone lamellae showed an excellent contrast in the AFM-scan. Those lamellae that appeared bright under AFM (peaks) corresponded to the optically bright lamellae and similarly, the dark lamellae (valleys) corresponded to the optically dark lamellae. Neighboring lamellae showed typical height differences on the order of 60 nm but could range from 20 to 140 nm. The average roughness, calculated for the entire scan area, was typically between 30 nm and 100 nm.

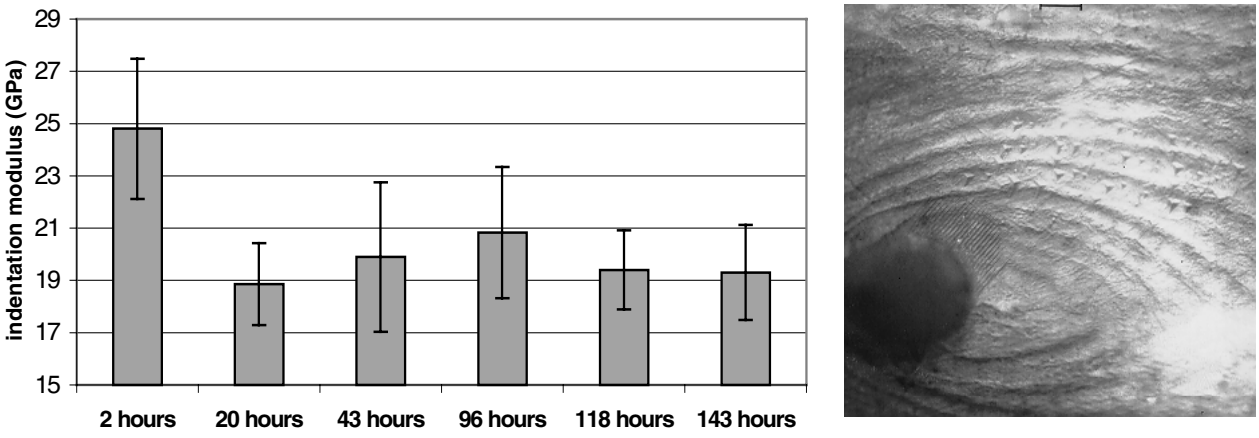

Figure 3 left: Time dependence of indentation modulus of compact bone after drying. After one day, the indentation modulus reached a stabilized level and did not change in a significant way any more.
right: Optical image of an osteon after data acquisition. The triangular marks are the remaining imprints of the indents.

Effect of drying

The indentation modulus was highest immediately after drying and was decreased by about 20% within the next 24 hours. The following days, the modulus (see Figure 3) did not change in a significant way ($p>0.05$). The standard deviations of the elastic moduli (error bars) within single BSU were approximately 10%. A similar evolution of the mechanical properties after drying could be reproduced for trabecular bone. The hardness followed the same trend and changed from 1.2±0.15 GPa to 0.9±0.2 GPa within the first 24 hours and became stable. The right picture in Figure 3 shows an osteon after data acquisition. The location of the indentations can be recognized as triangular imprints. The effect of decreasing indentation modulus after the first day may be attributed to rehydration of the bone tissue under the normal humidity conditions of the laboratory.

Test of four BSUs

The graphic in Figure 4 represents the mean indentation moduli of 550 nm (5 mN) indents for the 4 BSUs. The error bars indicate standard deviations. The indentation modulus ranged from 18±1.7 GPa in compact bone to 22.5±3.1 GPa in trabecular bone. According to our ANOVA analysis, the mean indentation modulus of the 4 BSU was significantly different ($p<0.0001$). The two BSU of compact bone showed also significantly different indentation moduli ($p<0.01$). The latter effect is most probably due to differences in mineralization (Currey, 1969). The nanoindentation parameters of the 5 mN indents correspond to those applied by Zysset *et al.* (1999) who investigated eight human femoral heads under moist conditions. According to this study the indentation moduli were 12.5±6.15 GPa for trabecular bone and 17.4±5.8 GPa for

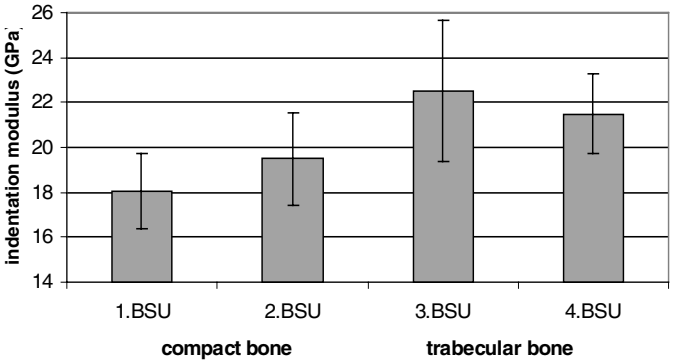

Figure 4 Average indentation modulus of 5mN indents for the 4 tested BSU. The variations are most probably due to differences in mineral content.

compact bone. Surprisingly, the elastic properties of trabecular bone were found to be higher than those of compact bone in the present study. Due to the very limited statistics, we attribute this finding to the random selection of the four BSU. The standard deviations of the indentation

moduli are within 10% of the mean value and therefore substantially lower than previous studies including several BSUs for each donor (Zysset et al., 1999).

The hardness values for the four tested BSUs showed similar trends as the indentation moduli (see Figure 5). This observation compares favorably with the microindentation study by Evans et al. (1990) and the nanoindentations performed by Rho et al. (1999a), where a relatively high correlation between elasticity and hardness was found (r^2 =0.96 given by Evans). The hardness

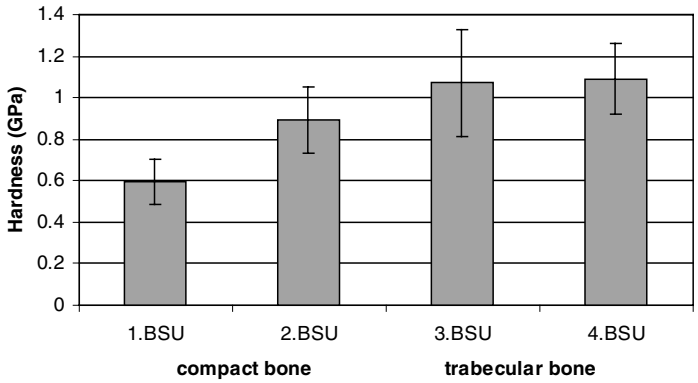

Figure 5 Hardness values of 5mN indents for the 4 BSU. You see variations with comparable trends like the indentation modulus.

ranged from 0.6±0.11 GPa for compact bone to 1.1±0.17 GPa for trabecular bone. For moist conditions, Zysset et al. (1999) found averages between 0.234 GPa for trabecular bone and 0.76 GPa for compact bone.

Discussion

The combination of AFM and nanoindentation has proven to be a powerful tool to provide reliable micromechanical properties of bone tissue. The strong advantage of the available AFM-mode over the conventional nanoindentation technique lies in the possibility to select the location of the indentations within a few tenths nanometers and to quantify the sample's surface topography, hence the quality of the sample preparation.

Drying the bone specimens for 24 hours at 50°C increased but conserved the mechanical properties for several days. BSUs from the same anatomical site of the same donor and undergoing the same preparation process showed significant variations in mean mechanical properties that may be attributed to differences in mineral content. The higher standard deviations found in previous nanoindentation studies were probably associated with averaging over multiple BSU and/or donors. The influence of nanoindentation parameters on bone results should therefore be determined within the same BSU. The here-reported standard deviation of approximately 10% of mean value are mainly due from biological variation of the bone ECM and the canalicular porosities.

This study allowed comparing several BSU from the femoral neck of a single donor. The results indicated that, in first approximation, bone might be seen as an assembly of structural units with

distinct mechanical properties between them but rather homogeneous properties within the same BSU. This finding has potentially important implications in the process of fracture propagation that is clearly related to tissue heterogeneity.

The major limitation of the nanoindentation data analysis remains the hypothesis of isotropy of the tested material. In fact, the indentation curve depends to a widely unknown extent on all anisotropic elastic constants of the tested material. Since bone tissue and most probably also the bone ECM (Rho et al., 1999b) is elastically anisotropic, the reported results are some weighted average of the elastic moduli along the various material orientations.

References

- Ascenzi A (1988) The micromechanics versus the macromechanics of cortical bone - a comprehensive presentation. J Biomech Eng **110**:357-363
- Choi K Kuhn JL, Ciarelli MJ, Goldstein SA (1990) Elastic moduli of human subchondral trabecular and cortical bone tissue and the size-dependency of cortical bone modulus. J Biomech **23/11**:1103-1113
- Currey JD(1969) The mechanical consequences of variation in the mineral content of bone. J Biomech **2**:1-11
- Eriksen EF, Axelrod DW, Melsen FM (1994) Bone Histomorphometry. 1ed. Raven Press Ltd, New York
- Evans GP, Behiri JC, Currey JD, Bonfield W (1990) Microhardness and Young's modulus in cortical bone exhibiting a wide range of mineral volume fractions, and in a bone analogue. J Mat Sc: Mat Med **1**:38-43
- Katz JL, Meunier A (1993) Scanning acoustic microscope studies of the elastic properties of osteons. J Biomech Eng **115**:543-548
- McElhaney J, Fogle J, Byars E Weaver G (1964) Effect of embalming on the mechanical properties of beef bone. J Appl Physiol **19**:1234-1236
- Mente PL, Lewis JL (1989) Experimental method for the measurement of the elastic modulus of trabecular bone tissue. J Orthopaed Res **7**:456-461
- Oliver WC, Pharr GM (1992) An improved technique for determining hardness and elastic modulus using load and displacement sensing indentation experiments. Mat Res Soc **7/6**:1564-1583
- Rho JY, Ashman RB (1993) Young's modulus of trabecular and cortical bone material: ultrasonic and microtensile measurements. J Biomech **26**:111-119
- Rho JY, Tsui YT, Pharr GM (1997) Elastic properties of human cortical and trabecular lamellar bone measured by nanoindentation. Biomat **18/20**:1325-1330
- Rho JY, Pharr GM (1999a) Effects of drying on the mechanical properties of bovine femur measured by nanoindentation. J Mat Sc: Mat Med **10**:485-488
- Rho JY, Roy ME, Tsui TY, Pharr GM (1999b) Elastic properties of microstructural components of human bone tissue as measured by nanoindentation. J Biomed Mat Res **45**:48-54
- Rho JY, Roy ME, Tsui TY, Evans, ND, Pharr GM (1999c) Mechanical and morphological variation of the human lumbar vertebral cortical and trabecular bone. J Biomed Mat Res

44:191-199
- Ryan SD, Williams JL (1989) Tensile testing of rodlike trabeculae excised from bovine femoral bone. J Biomech **26**:77-83
- Sedlin ED, Hirsch C (1966) Faktors affecting determination of the physical properties of femoral cortical bone. Acta Orthop Scand **37**:29-48
- Sneddon IN (1965) The relation between load and penetration in the axisymmetric Boussinesq problem for a punch of arbitrary profile. Int J Eng Sc **3**:47-57
- Townsend PR, Rose RM (1975) Buckling study of single human trabeculae. J Biomech **8**:199-201
- Weaver JK (1966) The microscopic hardness of bone. J Bone Joint Surg **A48**:273-288
- Ziv V, Wagner HD, Weiner S (1996) Microstructure-Microhardness relations in parallel-fibered and lamellar bone. Bone **18/5**:417-428
- Zysset P, Sonny M, Hayes WC (1994) Morphology-mechanical property relations in trabecular bone of the osteoarthritic proximal tibia. J Arthroplasty **9**:203-216
- Zysset PK, Guo XE, Hoffler CE, Moore KE, Goldstein SA (1999) Elastic modulus and hardness of cortical and trabecular bone lamellae measured by nanoindentation in the human femur. J Biomech **32**:1005-1012

Discussion with reviewers

S. Weiner: Did the authors find any systematic trend with increasing distance from the lamellar boundary plane?

Authors: We did not examine the dependence of indentation modulus with increasing distance to the lamellar boundary because single lamellae are not sufficiently large to position several neighboring indents. We did observe a dependence of the indentation modulus with depth that is described in a paper that is currently submitted elsewhere.

S. Weiner: Error obtained for repeated measurements should decrease with increasing indent size.

Authors: Surprisingly, our standard deviations were not influenced by indentation depth, which we attribute to the high force and displacement sensitivity of our instrument and the minimal roughness of the tested surface selected on the AFM scan.

S. Weiner: Anisotropy is not a probable property of lamellar bone but a certainty.

J. Currey: There is no doubt that bone is anisotropic, many, many studies have shown this.

Authors: We agree. From a mechanical standpoint, we distinguish the anisotropy of the ECM from the anisotropy of bone at the macroscopic level (mm) that includes oriented vascular channels and lacunae. However, the studies by Ziv et al. (1996) and Rho *et al.* (1999c) provide experimental evidence for mechanical anisotropy also at the ECM level.

J. Currey: Indents parallel to the osteon axes will be parallel to the grain of the bone. On the other hand indents perpendicular to the transversely orientated trabeculae will be normal to the grain of the bone. Why have authors chosen a different orientation for the two tissue types?
JY Rho: Indentations were made in only one plane in the cortical and the trabecular bone surfaces. What was the rationale behind choosing those planes over the other planes? Given the anisotropic nature of bone, would data in planes transverse to those tested be worth obtaining. Finally, it is clear which plane the cortical bone specimen was indented, relative to the long axis. Please be more explicit with regard to which plane was indented in the trabecular bone, relative to the long axis.
Authors: The grain of a trabecular BSU can be defined by the normal of the lamellae and the axis of the trabeculae, but to our knowledge there is no evidence that the ECM ultrastructure of the trabecular BSU will be identical to that of a compact BSU in their respective grain coordinate system. In fact, the ECM ultrastructure seems even to vary within compact bone and motivate a classification of osteons as longitudinal, alternate and transverse.
In practice, the directions defining trabecular grain are difficult to determine. The identification of the contours of a single BSU in the transverse section of a trabecula is also difficult. Since the goal of this study was not to compare compact and trabecular bone tissue, we tested the BSU along the most accessible direction that belonged to the plane of the lamellae for both tissues.

J.Y. Rho: A bleach solution will affect the collagen in bone. In general, these solutions have been used for decollagenization. Will this cause a serious deterioration of the mechanical properties of bone?
Authors: The bleach concentration of 0.5% used in our study is extremely low and this protocol was not found to degrade the physical properties of human cancellous bone in Zysset *et al.* (1994). Since the sensitivity of mechanical data to biochemical treatments is probably increased when testing a superficial layer of tissue, we selected the indentation locations at least 30 μm away from the bone edge.

JY Rho: "…rather homogenous properties within the same BSU": This suggestion is not supported from the results of the present study, because as the authors mentioned the elastic properties are significantly different between a BSU of compact bone (18.1±1.7 GPa) and a BSU of trabecular bone (22.5±3.1 GPa).
Authors: BSU was a significant global factor for all tested units, but indeed the two trabecular bone units were not significantly different according to the pairwise comparison of means. The other 5 pairs were significantly different, which supports our statement.

Chapter 2
Preliminary study: Does hardness and indentation modulus of bone tissue change with time under physiological conditions?

Introduction

The combination of nanoindenter with AFM allows for proper positioning of the indenter on the structure of interest that motivates to test single bone lamellae. Chapter 2.1 & 2.2 focus on the properties of single bone lamellae tested under dry and physiological (i.e. fresh, fully wet tissue tested at 37° Celsius) conditions.

Chapter 1 has shown that after drying and an adaptation period to the laboratory conditions the mechanical properties of the dry bone tissue remained constant over days.

Wet conditions on the other hand promote the enzymatic degradation of the collagen molecules that leads to a time-dependent degradation of the mechanical properties (Weaver, 1966). Additionally, diffusion may occur in the liquid environment that results in dissolution of the mineral phase. The latter effect could strongly affect the surface sensitive nanoindentation measurements. Increasing the measurement temperature from 20° to 37° Celsius also results in an acceleration of chemical reactions. These effects lead to additional experimental constraints for tests of fresh tissue under physiological conditions.

The prospect of this preliminary study was to find an appropriate liquid that allows the conservation of the nanomechanical properties of fresh bone tissue for at least 8 hours. For this purpose, a human bone sample was immersed in a Calcium-buffered Ringer's solution containing sodium azide and tested by nanoindentation. This solution has shown to conserve the bending properties of macroscopic bone specimens (7.5mm x 7.5mm x 3mm in size) for several days (Gustafson et al, 1996).

As a reference we also present a preceding test of a bovine bone sample that was tested in pure water.

Materials and Methods

From the femoral diaphysis of a cow, a sample containing plexiform bone was removed. Another cortical bone specimen was dissected from the posterior part of the femoral neck of an 86 year old female. Both specimens were polished with successive grades of silicon carbide paper and finished with a 0.05μm alumina solution. The specimens were then glued to the bottom of a specimen holder that contains a Plexiglas cup. The Plexiglas cup was designed to allow for measurements while the sample is fully immersed in a liquid. The nanoindentation device was installed in a thermal chamber and heated up to 37° Celsius (see Chapter 2.1 for a detailed description).

Test A: The bovine bone sample was immersed in pure water. 8 indents to 400 μN maximum load were done within a 40μm x 40μm area of the plexiform structure, after 0, 8 and 14 hours (with respect to the moment when thermal equilibrium was achieved).

Test B: For the test of the human bone sample, a Calcium-buffered Ringer's solution containing sodium azide was prepared with 2.5 10^{-4} mol/l $CaCl_2$, 0.9g/l salt and 0.01 % NaN_3 (Gustafson et al, 1996).

After reaching thermal equilibrium, an osteon was scanned and tested by nanoindentation after 0, 3, 6, 12 and 18 hours. The identical pair of thick lamellae was each time tested performing 6 indents to 400 μN maximum load. Statistical analysis was performed with One-Way-ANOVA with "time" as a fixed effect.

Results

***A**: bovine bone sample tested in pure water at 37° Celsius*

After 8 hours in water, the indentation modulus and hardness of the bovine bone sample decreased by 12% and 24% respectively. After 14 hours the decrease was 22% for indentation modulus and 35% for hardness. This continuous decrease was significant for both indentation modulus ($p=0.0034$) and hardness ($p<0.0001$).

***B**: human bone sample tested in Ca-buffered Ringer's solution at 37° Celsius*

The initial test of the human bone sample showed an indentation modulus of 12.2 ±3.5 GPa and a hardness value of 0.37 ±0.16 GPa (see Figure 1). Within the first 12 hours neither indentation modulus ($p=0.68$) nor hardness changed in a significant way ($p=0.5$).

The indentation modulus showed after 18 hours with 8 ±3.5 GPa a significant decrease of 34% with respect to the initial value ($p=0.04$).

After 18 hours, hardness was with 0.25 ±0.17 GPa by 33% lower than the initial value ($p=0.09$).

Figure 1 Variation of hardness (left) and indentation modulus (right) of human osteonal bone under physiological conditions. The specimen was immersed in a Ca-buffered Ringer's solution containing 0.01% NaN_3 and tested at 37° Celsius. Within the first 12 hours, neither variation of hardness ($p=0.5$) nor of indentation modulus ($p=0.68$) were significant.

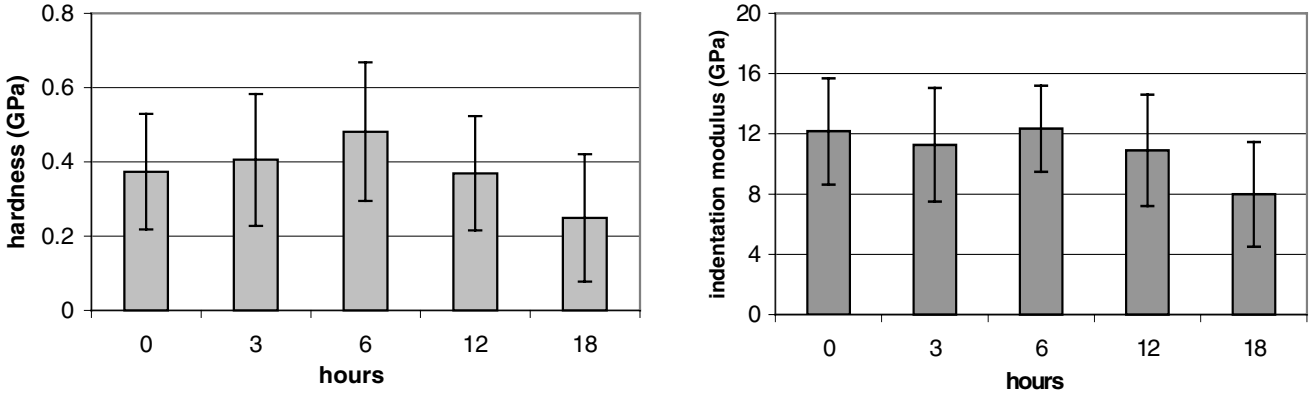

Discussion

This study tested the time dependence of the nanomechanical properties of human compact bone tested in a Calcium-buffered Ringer's solution containing sodium azide. As a reference we presented a recent test of a bovine bone sample that was immersed in pure water. In pure water, the mechanical properties of the bovine bone sample were significantly decreased after 8 hours. In the Calcium-buffered Ringer's solution the variation of the nanomechanical properties of a human bone sample was not significant during the first 12 hours.

The employed solution was proposed by Gustafson (Gustafson et al, 1996). The liquid was buffered in terms of Ca^{2+}-Kations to avoid dissolution of the mineral phase. Sodium azide served as an inhibitor for enzymatic degradation of the collagen. Using this solution, Gustafson studied the variation of the bending properties of equine cortical bone at ambient temperature. According to his data the bending modulus did not change significantly during 10 days.

In our study, a significant decrease of indentation modulus and hardness was already detected after 18 hours.

The large difference between Gustafson's and our results suggest additional constraints involved in nanomechanical tests. It is probable that effects play a role which have a greater influence on the nanomechanical parameters than on macroscopic properties. The ratio between the surface that is in contact with the liquid and the deformed volume can be estimated for these indentation experiments with $149mm^{-1}$ (taking into account a half-ellipsoidal volume, see Appendix of the following study for a dimensional discussion). The corresponding surface to volume ratio for Gustafsons four point bending test was $0.92mm^{-1}$. This demonstrates the surface sensitivity of nanoindentation in comparison to other mechanical tests. It is therefore probable that the change of indentation modulus is due to an effect on the surface. It is possible that the here-applied concentration of $CaCl_2$ (that is based on tests at ambient temperature) does not represent the saturation level at 37° Celsius. For most of the inorganic salts in a watery environment the concentration of the dissolved phase increases with temperature. The saturation level at 37° Celsius may therefore be underestimated with tests at ambient temperature. A partially buffered solution could have lead to a slow dissolution of the bone mineral phase and may have decreased the indentation modulus.

A deposition of mineral crystals on the surface might be excluded since this effect should be detected by the topography scans that were done in combination with the indentation tests.

The temperature employed for this nanoindentation study was approximately 17° Celsius higher than for Gustafson's bending experiments. The associated acceleration of chemical processes may also play a role for the faster degradation of the nanomechanical properties.

The maximum measurement time for subsequent nanoindentation tests of bone tissue under physiological conditions was therefore set to 12 hours (period to reach thermal equilibrium + measurement time).

References

- Gustafson MB, Martin RB, Gibson V, Storms DH, Stover SM, Gibeling J, Griffin L (1996) Calcium buffering is required to maintain bone stiffness in saline solution. J Biomech **29/9**:1191-1194
- Weaver JK (1966) The microscopic hardness of bone. J Bone Joint Surg **A48**:273-288

2.1

Nanoindentation discriminates the elastic properties of individual human bone lamellae under dry and physiological conditions[1]

Introduction

Besides reduction in bone mineral density, there is growing evidence that bone fragility might be linked to the degradation of the intrinsic mechanical properties of the bone extracellular matrix (ECM) that is associated with alteration of the bone remodeling process and fatigue damage accumulation (Meunier & Boivin, 1997; Burr et al, 1998). It has also become widely accepted that the bone ECM determines the mechanical environment of the osteocytes and bone lining cells, and may therefore play an important role in mechanotransduction. These issues call for a better understanding of the intrinsic mechanical properties of the human bone ECM and their evolution with age and disease.

The literature provides a wide spectrum of studies that focused on the characterization of intrinsic properties of bone tissue. Ascenzi and coworkers performed tension, compression, torsion and bending tests of single osteons dissected from human bone and reported a strong dependence of Young's modulus on average collagen fiber orientation and mineral content (Ascenzi, 1988). Other investigators carried out microhardness tests (Amprino, 1958; Weaver, 1966) with imprint sizes of approximately 50μm. Their results indicated a high correlation between microhardness and mineralization, anatomical site, Young's modulus, yield strength and tissue preparation. Surprisingly, Weaver did not observe a dependence of bone microhardness on donor, age and osteoporosis. Based on microhardness tests, Hodgskinson et al. (1989) hypothesized that Young's modulus for trabecular bone tissue and compact bone were comparable. Evans et al. (1990) reported a dependence of microhardness on the links between the mineral phase and the organic matrix. Ziv et al. (1996) found a strong dependence of microhardness on collagen fiber orientation (determined by SEM). Unfortunately, hardness is a complex mechanical property that involves both elastic and postyield properties and cannot be easily converted to continuum level properties such as Young's modulus or shear strength. In addition, hardness can show a certain depth-dependence even for homogeneous materials (Oliver & Pharr, 1992)

Another attractive technique to investigate mechanical properties of individual bone BSU is ultrasound microscopy. The bone structural unit (BSU) represents the end result of a remodeling cycle; in cortical bone, it constitutes a Haversian system (or cortical osteon), and in cancellous bone, it is a wall or "packet" of bone (trabecular osteon) (Eriksen et al, 1994). The reported

---

[1] *a shortened version of this article is (with the above-mentioned title) accepted for publication in Bone 2002. Authors: S. Hengsberger, A. Kulik* & Ph. Zysset. Laboratory of Applied Mechanics and Reliability Analysis, Department of Physics*, Swiss Federal Institute of Technology, Lausanne; Switzerland*

experiments showed a relatively uniform acoustic reflectivity within each BSU, but significant differences between BSUs (Katz & Meunier, 1993). However, acoustic reflectivity depends on both elastic properties and local material density, which makes the quantitative determination of Young's modulus difficult.

Nanoindentation, which evolved from traditional Vickers microhardness testing, allows measuring mechanical properties at the nanometer scale. As a substantial improvement with respect to the above-mentioned techniques, the measured force displacement curves provides a local indentation modulus, a purely elastic property. The first nanoindentation studies applied on bone (Rho et al, 1997 & 1999a; Zysset et al, 1999) examined the influence of microstructure, drying, anatomical location, and age and compared the mechanical properties of compact versus trabecular bone. It was reported that drying increases Young's modulus of compact bone by approximately 9-16%, but does not change the relative stiffness of the bone constituents. For identical anatomical sites, interstitial bone showed highest Young's modulus, followed by osteonal bone and then by trabecular bone.

Further studies (Rho et al, 1999b & 1999c; Roy et al, 1999) investigated factors such as the anatomical orientation of the plane of indentation for vertebral and tibial bone and the site of indentation within secondary osteons. They measured significantly higher indentation moduli and hardness for compact and trabecular bone tissue tested in load-bearing directions with respect to transverse directions. Within single osteons, they observed a decrease of Young's modulus with increasing distance to the Haversian channel. Most of these studies reported indentations of 500-1000nm depth that result in imprint sizes of 3 μm to 6 μm and therefore exceeded the typical dimensions of single lamellae (typically between 1 μm to 3 μm for thin lamellae and 2 μm to 4 μm for thick lamellae). In a recent study, thick lamellae were tested with a depth of 200nm (Rho et al, 1999c), but due to the difficulty in positioning the indenter tip in the submicron regime, no comparison between thick and thin lamellae was possible.

In an effort to extend our current knowledge of the mechanical properties of single bone lamellae, our objective was to quantify indentation modulus and hardness of both thin and thick lamellae selected from human trabecular and compact bone structural units (BSU). The influence of lamella type (thick or thin) and indentation depth were examined under both dry and physiological conditions. For this purpose, we applied a combination of atomic force microscopy (AFM) and nanoindentation that provided the required accuracy (better than 0.1μm) to position the indenter tip in the center of a single lamella and perform reliable indentations with depths as low as 100 nm.

Materials and methods

Technique

The combination of an AFM and a nanoindenter (Hysitron Inc. Minneapolis, MN) is sketched in Figure 1. A Berkovich (three-sided pyramid) diamond tip is mounted on a transducer that allows for displacements in the z-direction in nanoindentation mode. The sample is mounted on a scanner that allows for motion in the x,y-plane that is perpendicular to the tip axis. This

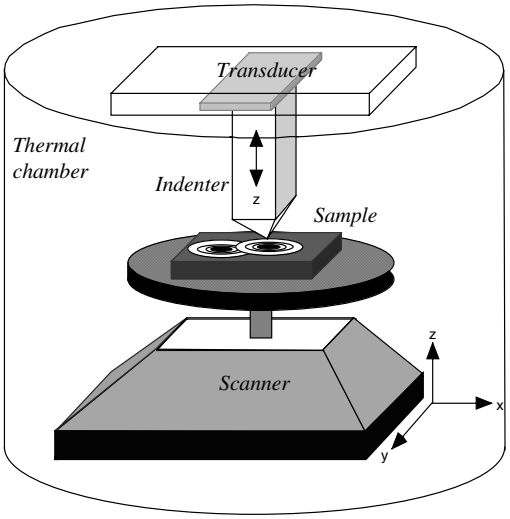

Figure 1. Combined AFM and nanoindentation instrument (Hysitron Inc.):
The sample is mounted on a scanner that allows movement in x,y and z-direction in AFM-mode. The diamond indenter is mounted on a transducer that allows for force-displacement curves in z-direction in nanoindentation-mode.
For the liquid cell tests the sample was placed in a plexiglass cup for the addition of liquids and the device was installed in a thermal chamber.

combination allows for measuring both topography of the sample surface with a constant contact force criterion in the AFM scanning mode and force displacement curves in nanoindentation mode using the same tip. Based on the AFM image, the tip can be positioned on the indentation area with a high spatial resolution (<0.1μm). Figure 2 shows a typical force displacement curve in nanoindentation mode. First, the tip is loaded into the material, resulting in indistinguishable elastic and plastic deformation. The tip is then held at maximum force, resulting in creep of the material under the tip. Finally, unloading allows elastic recovery of the material. The experiment lasts 15 to 180 seconds per indent, representing a compromise between a desired quasistatic strain rate and the thermal drift of the instrument. The available device works in a load-controlled mode and linearly increasing and decreasing loading protocols were applied. This corresponds to a loading rate of

$$\frac{dP}{dt} = \frac{P_{max}}{T_{loading}} \tag{1}$$

where P_{max} is the maximum load and $T_{loading}$ the loading time. Based on the analytical work by Sneddon (1965), Oliver and Pharr (1992) derived the following relationship for force-displacement curves obtained with an indenter of revolution pressed into an isotropic elastic material:

$$S(h_{max}) = \frac{dP}{dh}(h_{max}) = \frac{2}{\sqrt{\pi}} E_r \sqrt{A_c(h_{max})} \tag{2}$$

This relationship has been shown to be a good approximation for a Berkovich indenter tip (Pharr et al, 1992). Here *P* represents the applied load. $S(h_{max})$ is the derivative of the unloading curve at the point of initial unloading h_{max}, that is determined by fitting 40 % to 95 % of the unloading curve.

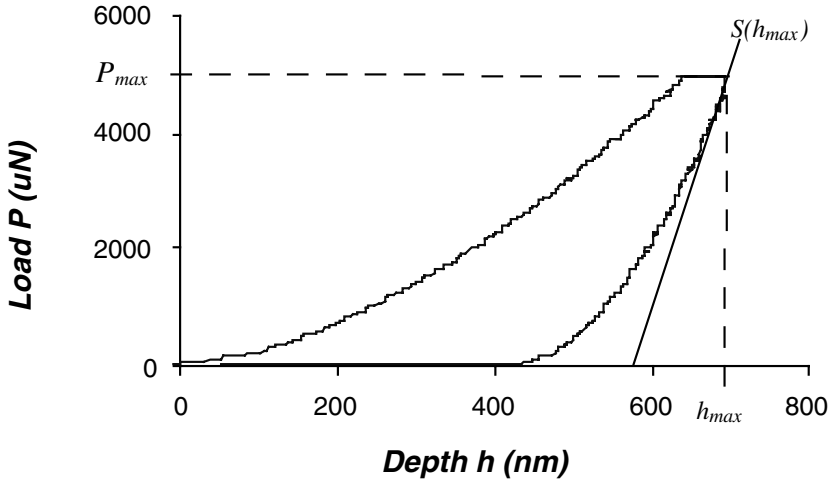

Figure 2. Nanoindentation curve: Force-displacement curve of a typical nanoindentation experiment. The test consists of three parts, the loading part where the tip is pressed into the material, a holding period where the tip creeps into the material and an unloading part where the load is released. $S(h_{max})$ is the slope of the unloading part at the point of initial unloading. and allows the determination of the local indentation modulus of the material.

$A_c(h)$ is the contact area over which the material and the indenter are in instantaneous contact. The latter function is determined by a calibration procedure described by Oliver & Pharr (1992). The reduced modulus E_r depends on the deformation of the material and the diamond tip as well. According to Hertz it consists of the sum of two contributions (Johnson, 1985):

$$\frac{1}{E_r} = \frac{1-\nu_{specimen}^2}{E_{specimen}} + \frac{1-\nu_{tip}^2}{E_{tip}} \tag{3}$$

The indentation modulus

$$E_{ind} = \left(\frac{1}{E_r} - \frac{1-\nu_{tip}^2}{E_{tip}} \right)^{-1} \tag{4}$$

can be calculated with the reduced modulus and the elastic properties of the diamond indenter tip $\nu_{tip} = 0.07$ and $E_{tip} = 1140\ GPa$. This variable represents with

$$E_{ind} = \frac{E_{specimen}}{1-\nu_{specimen}^2} \tag{5}$$

a combination of the local Young's modulus $E_{specimen}$ and the local Poisson ratio $\nu_{specimen}$ whereby the material is assumed to be isotropic.

The calibration of the device was performed applying fused silica with $E_{ind} = 74.4 \pm 2.2$ GPa and the determined area function was validated with a polycarbonate sample with $E_{ind} = 3.4 \pm 0.26$ GPa. The nanoindenter was therefore calibrated with two materials that frame the properties of bone in terms of elastic modulus, viscoelasticity and time-dependent plasticity. For this study, which includes 550 indents, the tip calibration procedure was performed four times.

The classical hardness property represents the mean pressure under the tip at maximum load $P(h_{max})$:

$$H = \frac{P(h_{max})}{A_c(h_{max})} \tag{6}$$

Specimen preparation

The femoral neck of an 86 year old female that was free of evident bone disease was cut perpendicular to its long axis applying a diamond band saw under continuous water irrigation. Several bone specimens from a central region of the neck that included both compact bone and trabeculae were dissected from 3 mm thick slices. The interstitial marrow was removed employing 3 alternate treatments with the very low concentration of 0.5% bleach and ordinary soap solution in an ultrasonic cleaner for 5 minutes. This concentration was shown to have a minor effect on the mechanical properties of bone tissue (Zysset et al, 1994). The specimens were then embedded in PMMA without alcoholic fixation to avoid a possible deterioration of the collagen. After polymerization, the surface lying in the plane perpendicular to the long axis of the femoral neck was polished. Increasing grades of silicon carbide paper, 1 μm and 0.25 μm diamond slurry were employed finishing with a 0.05μm alumina solution.

further preparation and measurement protocol for dry specimen

After polishing the specimen were dried for 24 hours at 50 degrees to remove the water content that supports the enzymatic degradation of collagen (Weaver, 1966). In a preliminary experiment, the indentation modulus of several lamellae of compact and of trabecular bone were measured each day during one week. The process of drying increased but maintained the bone indentation modulus for several days ($p>0.5$) in both compact and trabecular bone and therefore allowed for extended measurement time (Hengsberger et al, 2001).

The experiments included 4 BSU: 2 osteons and 2 trabecular packets. Within each BSU six neighboring lamellae (3 thick and 3 thin and for each type separately numbered with lamella number 1 to 3) were each tested with 16 indents, 4 at each of the following maximum loads: 0.4mN (~120nm), 1mN (~250nm), 2mN (~360nm) and 5mN (~530nm). The corresponding indentation depths are indicated in brackets. Each BSU was first scanned in AFM-mode with a typical window size of 50μm x 50μm with about 5μN contact force and 0.3Hz scan rate. We

checked that this relatively high contact force did not deteriorate the surface by scanning successively windows with the same center but increasing scan size. The lamellae could be distinguished in the AFM image due to topographical differences. This allowed us to position each indent individually on thin and thick lamellae. Each indent included a preliminary thermal drift rate correction limited to a maximum of $0.05\frac{nm}{s}$. The indentations contained a linear loading part of 15s, a holding period at maximum force of 10s and a linear unloading part within 15s. This corresponds to a loading rate of $\frac{dP}{dt} = \frac{P_{max}}{15s}$ (for example $\frac{dP}{dt} = 0.33\frac{mN}{s}$ for the indents to 5mN maximum load). To avoid proximity effects, neighboring indents were applied keeping a minimum distance of 3 times the diameter of the remaining imprints. The experiments on the dried specimen included 4x 100 indentations for the four chosen BSU of one single donor and one anatomical site.

further preparation and measurement protocol for the liquid cell

After polishing, four additional specimens were chosen for the liquid cell experiments. The samples were glued to the bottom of plexiglas cups and kept frozen until testing. The AFM and nanoindentation instrument was installed in a thermal chamber with a controlled temperature ranging between 37°C and 39°C. To prevent enzymatic degradation of the collagen and partial dissolution of the mineral during testing, a Ringer's solution containing 0.01% NaN_3 and saturated with $2.5 \cdot 10^{-4}\frac{mol}{l} CaCl_2$ was prepared (Gustafson et al, 1996). The specimens were completely immersed in the solution, the surface being at least 2mm under the liquid level. By intermittent topography scans during the indentation tests it was verified that this solution did not cause any deposition of minerals on the surface.

The preliminary experiment demonstrated that bone immersed in this solution did not change the indentation modulus in a significant way for the first 12 hours after installation ($p>0.5$). The maximum time for thermal stabilization and testing was therefore limited to 12 hours. For these tests, a liquid cell tip, i.e. a Berkovich tip that is mounted on a 10mm long holder, was used. The experiments included 4 BSU, 2 osteons and 2 trabecular packets. Due to the additional constraint to reach thermal stability and to carry out the experiments within a few hours, the number of observations had to be reduced. The number of lamellae was confined to two neighboring lamellae (1 thick and 1 thin). Each was tested with the following maximum loads adapted to match the identical indentation depths employed for the dry specimens: 0.2mN (~100nm), 0.4mN (~180nm), 1mN (~320nm), 2mN (~440nm) for trabecular bone and 0.2mN, 0.5mN 1.1mN, 2.5mN for compact bone. Each lamella was tested with 6, 7 or 8 indents at the lowest depth and 4 indents at the other depths. The thermal equilibrium conditions produced a drift rate of less than $0.1\frac{nm}{s}$. The periods of the loading and unloading segments were reduced to 10s to reduce the

influence of the time-dependent drift on the detected indentation depth. This study on fresh specimens tested in the liquid cell includes 150 indentations for one anatomical site and donor.
For statistical analysis of the data set, mean values and standard deviations were calculated. Multiple-Way-Analysis of Variance (ANOVA) were run based on a mixed model with BSU as a random effect and lamella number, depth and type as fixed effects.

Results

Dry conditions

The comparisons of the AFM-scans and the optical microscope images showed that the thick lamellae corresponded to the peaks in the topography and the thin lamellae to the valleys.

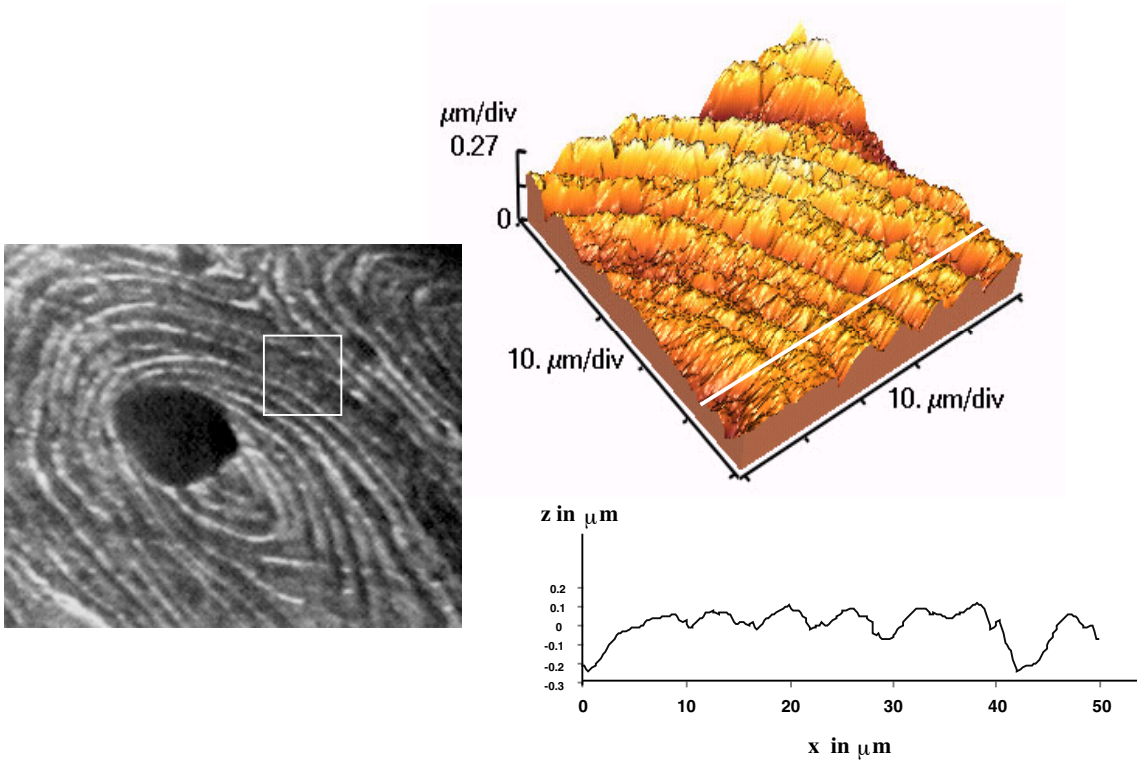

Figure 3. Correlation of lamellar structure with topography:
Optical image of an osteon (left), the corresponding AFM topography of the area within the white square (right) and a two-dimensional slice along the white line. Please note that magnification in the z-direction is more than 20 times greater than magnification in the x,y,-directions.

Typically, the topographical differences between thin and thick lamellae ranged between 50nm to 130nm (Fig. 3). Thin lamellae showed a thickness between less than 1 µm and 3 µm while the thickness of thick lamellae ranged between 2 µm and 4 µm. Figure 4 shows an AFM image after nanoindentation. The triangular marks are the remaining imprints of the indents. Young's moduli based on an assumed Poisson ratio[2] of $\nu_{specimen} = 0.3$ ranged from 11.06 GPa to 31.6 GPa. Figure

[2] *A recent report showed that the resulting error caused by a variation of the actual Poisson ratio between* $\nu_{specimen} = 0.2$ *and 0.4 remains within 10% (Zysset, 1999).*

5 summarizes the indentation modulus data of the four dried BSU separately for the two lamella types and the different indentation loads. The data of the three lamellae of the same type could be pooled, since in each BSU the three thick and the three thin lamellae showed indistinguishable results ($p=0.27$). A 3-way-ANOVA demonstrated that lamella type ($p=0.029$) and load ($p=0.0002$) were globally significant. In all four BSU, the thick lamellae showed higher indentation modulus than the thin lamellae for the 0.4mN indents and the lamella type was found to be of high significance for the low load indents ($p<0.0001$).

Surprisingly, the load and the load*type interaction were both of high global significance ($p<0.0001$). In fact, the thick lamellae showed a decreasing modulus with increasing load, while

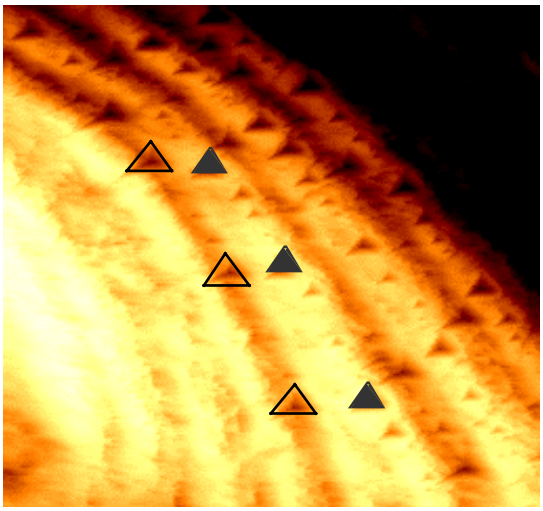

Figure 4. Topography scan after indentation tests: AFM scan of a BSU after nanoindentation (50µm x 50µm) that shows the remaining imprints of the indentations. Open and closed triangles indicate the position of some 500nm indents in thin and thick lamellae respectively.

no significant dependence with load was observed for the thin lamellae. A two-way ANOVA showed that load was a significant factor ($p<0.0001$) for thick lamellae but not for thin lamellae ($p=0.15$). All 4 BSU's showed the same trend and it is remarkable, that the higher modulus of the thick lamellae for 0.4mN indents was inverted into a lower modulus for the 5mN indents.

The results for hardness ranged between 0.48±0.1 GPa and 1.25±0.26 GPa and showed the same trends as indentation modulus (see Figure 5), but with different statistical results. The lamella type was highly significant ($p<0.0001$), while load did not reach significance ($p=0.092$). See Table 1 for the ANOVA-results in tabulated form.

Physiological conditions

Despite the presence of the liquid phase the AFM scan provided sufficient contrast to distinguish thin and thick lamellae. The thermal stability in the heating chamber allowed reducing the drift of the nanoindenter to less than 0.1nm/s. The experiments on dry bone were done first and showed that the lamella number was an insignificant factor ($p=0.27$). For the experiments under physiolo-

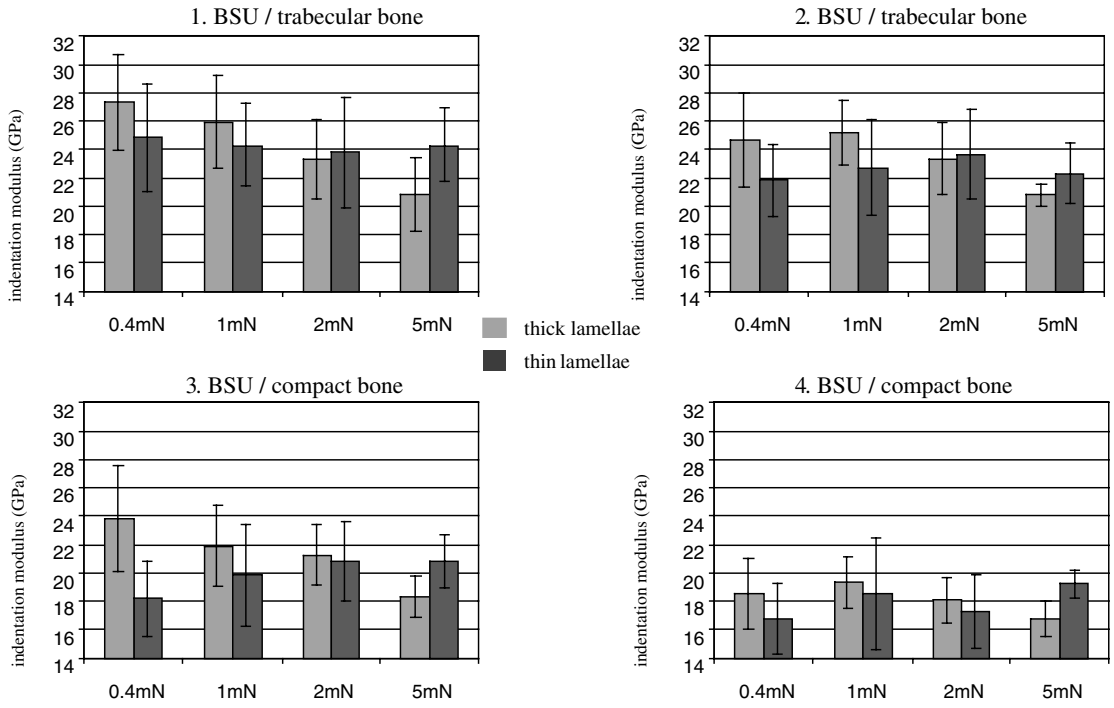

Figure 5. Indentation moduli (top) and hardness (bottom) of 4 BSU of trabecular and compact bone tested under dry conditions. The bars show thin and thick lamellae separately, and also show the different loads. Each cell contains 12 indents. The error bars indicate standard deviations.

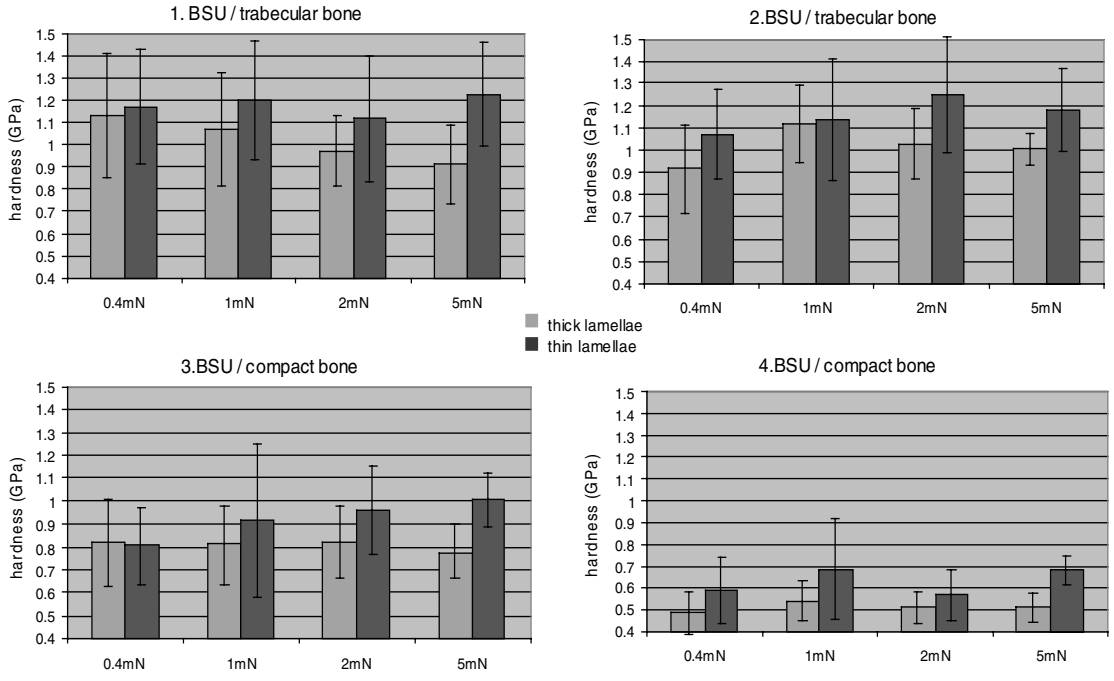

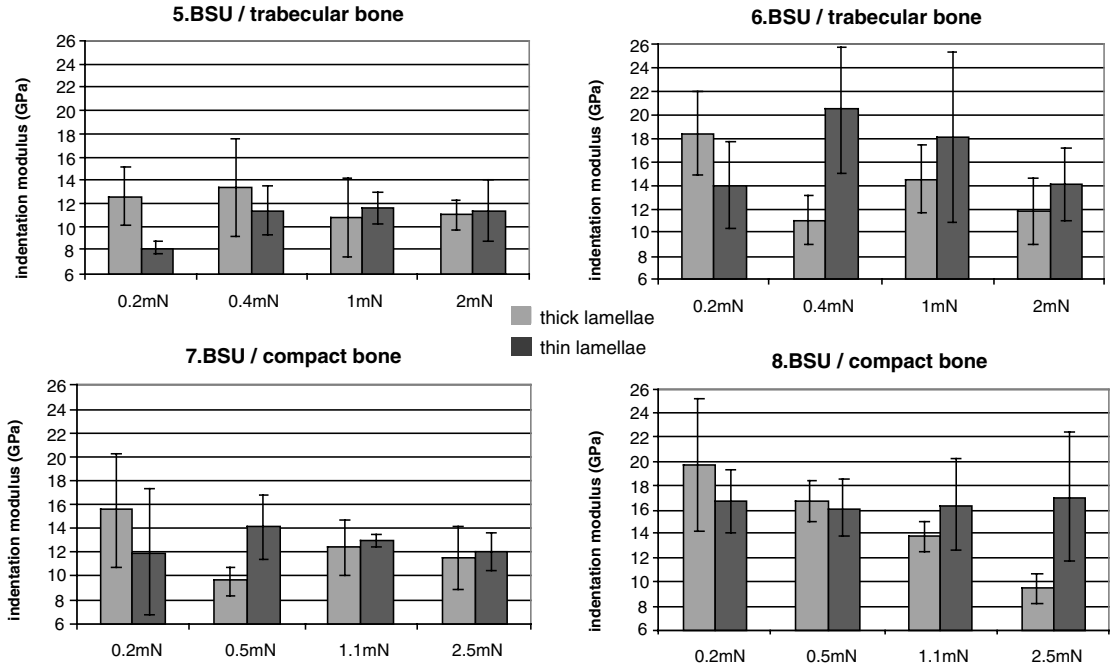

Figure 6. Indentation moduli (top) and hardness (bottom) of 4 BSU of trabecular and compact bone tested under physiological conditions (fully wet, body temperature). Each cell contains 4 indents.

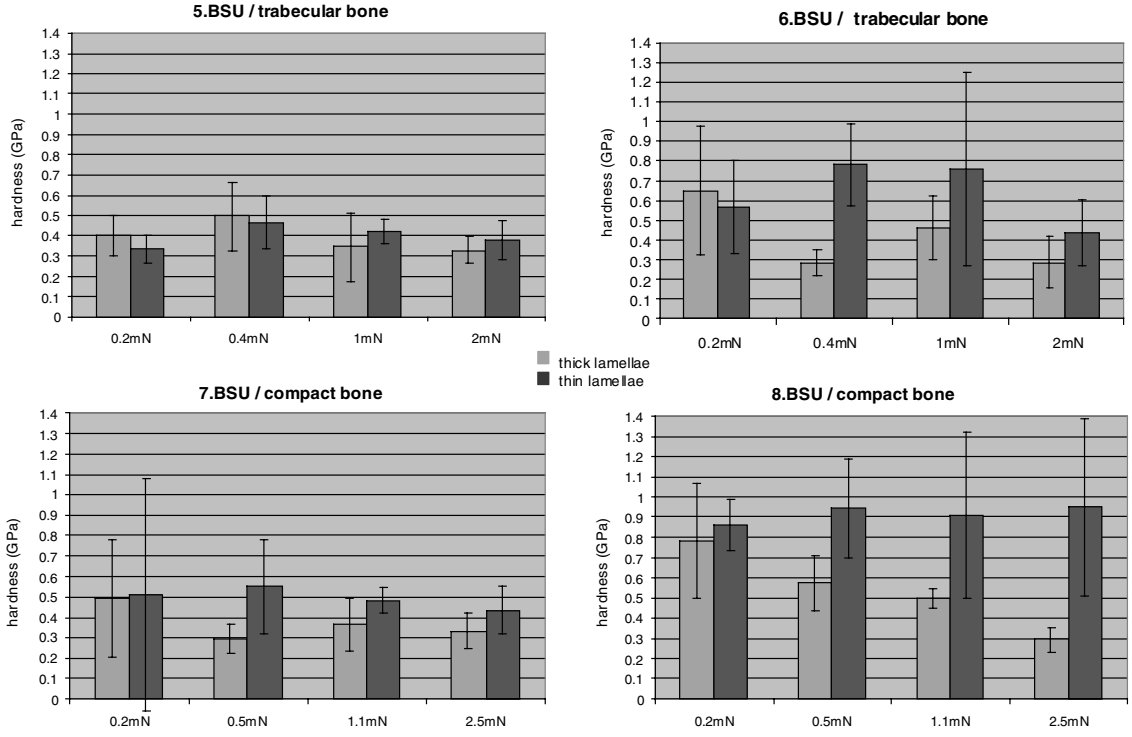

gical conditions, the protocol was reduced to one lamella of each type in order to respect the maximum experimentation time of 12 hours. The measured elastic moduli based on an assumed Poisson ratio of $\nu_{specimen} = 0.3$ ranged from 7.4±0.45GPa to 18.5±4.9GPa and were in average lower than the range for the dry specimens.

Figure 6 shows the indentation moduli data for four BSU tested under physiological conditions. A 3-way-ANOVA showed again that indentation load was a significant factor (p=0.021). In contrast to the results under dry conditions, lamella type was not found to be significant (p=0.68) but interacted strongly with the load factor (load*type p<0.0001). Using one-way ANOVA, thick lamellae showed significantly higher indentation moduli than thin lamellae for the low depth indents (p=0.0003). In general, the indentation moduli of thick lamellae decreased significantly with load (p<0.0001), while for thin lamellae this factor was much less significant (p=0.037).

Hardness values ranged from 0.29±0.13 GPa to 0.95±0.44 GPa and also demonstrated comparable trends as indentation modulus (see Figure 6). Both the lamella type (p=0.0001) and the applied indentation load (p=0.015) were significant. See Table 1 for the ANOVA-results in tabulated form.

factors for indentation modulus	***p-value (dry)***	***p-value (wet)***
lamella number	*p=0.27*	*- - -*
lamella type (globally)	*p=0.029*	*p=0.68*
load (globally)	*p=0.0002*	*p=0.021*
*load*type*	*p<0.0001*	*p<0.0001*
load (for thick lamellae)	*p<0.0001*	*p<0.0001*
load (for thin lamellae)	*p=0.15*	*p=0.037*
lamella type (for 0.4mN indents)	*p<0.0001*	*p=0.0003*
factors for hardness		
lamella type (globally)	*p<0.0001*	*p=0.0001*
load (globally)	*p=0.092*	*p=0.015*

Table 1 Significance level of the investigated factors for the results under dry and under wet conditions.

Discussion

The goal of this study was to investigate the influence of lamella type (thick and thin) and indentation depth on the indentation modulus of human bone ECM under dry and physiological conditions. According to our measurements on dry specimens, the lamellar number in each BSU was not significant. Rho et al. (1999c) found a weak but significant decrease of indentation modulus of thick lamellae with increasing distance from the Haversian channel and therefore

reported a dependence on the lamellar number. Since the lamellae tested in the present study were close neighbors, this variation had a negligible influence.

The influence of lamella type and indentation depth was determined for both thin and thick lamellae between 100nm and 500nm. Thick lamellae showed a higher indentation modulus than thin lamellae for the low depth indents. Further more, thick lamellae showed a significant decrease of indentation modulus with increasing depth while for thin lamellae depth was not a significant factor.

A first interpretation may presume that surface roughness plays a major role for these variations. But since surface roughness changes its relative influence with increasing depth the standard deviations of the results should also show a depth-dependence.

The intrinsic variability of the calibration material could also have an influence. The standard variation of the calibration material PC was on the order of 8% and for fused silica below 3%. Since the here discussed decrease of indentation modulus of thick lamellae are on the order of 25% (see BSU 1 & 3) or even up to 50% (see BSU 8) a pure calibration artifact can be excluded.

To get a better understanding of the results, it becomes necessary to estimate the tested volume as a function of the indentation depth. An estimation based on Hertz's theory (Johnson, 1985) is derived in the appendix. The mechanical properties measured by nanoindentation correspond to a semi-ellipsoidal volume extending to about 9 times the indentation depth in the vertical direction (z) and about 7 times this same depth in the radial direction (r). In this perspective, the low load indents are probably the most appropriate to compare the intrinsic properties of thick and thin lamellae, since they include with indentation depths around 100nm a confined volume of 700nm (7x100nm) in lateral and 900nm (9x100nm) in vertical direction. The results of the 100nm indents showed consistently higher indentation moduli for thick lamellae under both dry and physiological conditions.

Unfortunately, this estimation of the deformed volume using an elastic analysis does not explain the detected decrease of indentation modulus for thick lamellae when the load is increased. It is evident that the 500nm indents (the tested volume corresponds to 3.5μm in lateral direction) will measure a composite modulus that is also influenced by neighbored lamellae. This may explain the detected depth dependence of the thick lamellae but leaves the question open why for thin lamellae this does not lead to the inverse trend. It is more likely that the here-discussed trends represent mainly intrinsic properties of the individual lamellae.

In order to gain further insight in this issue, the postyield behaviour of bone ECM needs to be discussed. At the macroscopic level, human bone exhibits a simultaneous accumulation of plastic deformation and degradation of elastic moduli, which means that the damaged bone volume does not recover with an intact elastic modulus like a metal during unloading. If the same behaviour is assumed at the ECM level and the volume of damaged bone ECM is of importance when compared to the elastically deformed volume, then the elastic properties measured by nanoindentation may be to some extent lower than those of the intact tissue. According to this hypothesis, the measured mechanical properties may depend on indentation depth and collagen

architecture because they affect the mode and extent of the damage process at the ultrastructural level. This point of view is supported by the fact that SEM images of the dried BSU showed many transverse cracks in the thick lamellae, but no cracks in the thin lamellae. This suggests that damage accumulation may be more prone to occur in a longitudinal plane in thick than in thin lamellae. It is important to note that the discussed trends with increasing loads were also observed under physiological conditions and therefore do not represent artifacts of the drying cracks. It is more likely that the here-discussed damage accumulation occurs during the loading cycle when the indenter is pressed into the bone matrix. In this perspective thin and thick lamellae showed different properties with respect to this loading process.

The key to this difference must be due to compositional and/or architectural effects and should be discussed in the frame of published bone lamellation theories. See Table 2 to have an overview of the structural and compositional characterization of thick and thin lamellae for compact bone.

Based on observations with polarized light microscopy, Gebhardt (1906) distinguished transverse and longitudinal lamellae consisting of collagen fibers lying perpendicular (transverse) or parallel (longitudinal) to the long axes of the secondary osteon respectively. Gebhardt demonstrated various types of osteons with mainly transverse, longitudinal or alternate collagen fiber orientations. Gebhardt's model is still the most accepted and has found support in more recent studies (Ascenzi, 1988). Weiner & Traub (1992) proposed the rotated plywood model based on the interpretation of SEM and TEM images of rat bone and mineralized turkey tendon. They explained the lamellar appearance of the BSU after polishing by changes in the orientation of both the collagen fibers and the hydroxyapatite (HAP) platelets. One year later, Marotti (1993) reported new findings obtained with SEM and TEM. He claimed that the lamellar appearance of bone was due to density changes of the collagen fiber network and the associated HAP crystals. The thick lamellae were less dense in terms of the collagen network but more dense in HAP.
In our study thick lamellae demonstrated a higher indentation modulus for low depth indents and a decrease of the indentation modulus with increasing depth. In addition the topography scans showed that thick lamellae were more resistant to the mechanical stresses imposed by polishing, which confirms observations reported by Reid (1986). Weiner proposed for thick lamellae an orientation of the fibres that is longitudinal and therefore parallel to the direction of load application of the nanoindents. According to Marotti the relative density of the HAP-crystals is higher for thick lamellae (Marotti, 1993). This higher resistance to polishing and the higher indentation modulus for thick lamellae for the low load indents could be a result of both the collagen fibre orientation and the higher relative HAP-crystal density. The decrease of the indentation modulus with increasing load for this type may correlate to the orientation of the collagen fibres. It is conceivable that this orientation is more prone to effects like buckling and/or the above discussed damage accumulation in comparison to transverse lying fibres when the load is increased. A more detailed interpretation of these mechanical data requires a better understanding of the intrinsic mechanical properties of the bone matrix constituents and

especially the strength of the bonds between the organic and mineral component. Moreover, the application of the above mentioned bone lamellation theories (that consider osteonal lamellae) to trabecular bone has to be validated. Tests of the mechanical anisotropy of individual bone lamellae could become a first step in this clarification.

author(s)	thin lamellae	thick lamellae	characterization
Marotti (1993)	• dense in collagen • less dense in HAP	• loose in collagen • dense in HAP	SEM & TEM
Gebhardt (1906) and Ascenzi (1993)	• transverse orientation of collagen fibers • bright (birifringent)	• longitudinal orientation of collagen fibers • extinguished	PLM (transmission)
Gebhardt (1906)	• anisotropic	• isotropic	PLM (transmission)
Weidenreich (1923)	• striped	• stippled or dotted	Ordinary light (reflection)
Weiner & Traub(1992)	• transverse orientation of collagen fibers with vertically orientated HAP	• longitudinal orientation of collagen fibers with obliquely orientated HAP	SEM & TEM
this study	• lower levels in topography • more compliant for low depths indents • little variation with increasing indentation depth	• higher levels in topography from polishing • stiffer for low depths indents • decreasing stiffness with increasing indentation depth.	AFM & Nanoindenter

Table 2. Overview of reported bone lamellation theories: Reported characterization of thick and thin bone lamellae for compact bone. Transverse and longitudinal orientation is given with respect to the long axes of the Haversian channel. The most recent studies proposed that the lamellar appearance of bone was due to variations in collagen fiber and HAP-crystal orientation (Weiner & Traub, 1992) or in successive density changes of the organic and inorganic components (Marotti, 1993).

To conclude, the combined AFM and nanoindenter has proven to be a powerful tool to characterise single bone lamellae under dry and physiological conditions. Thick and thin lamellae of this 86 year old bone showed significant differences, which is attributed to distinct compositional and/or morphological features leading to distinct damage behavior. Drying influenced the level of indentation modulus and hardness of human bone tissue but did not affect the comparative trends of indentation depth and lamella type. Since the four BSUs tested under dry conditions were distinct from the four BSUs tested in the liquid cell, no precise determination of the influence of water content on the examined mechanical properties could be done. On the one hand, the physiological conditions provide a better estimate of the mechanical properties of bone ECM in vivo, but involve strong additional experimental constraints in terms of thermal drift and measurement time. On the other hand, the dry conditions may be affected by air moisture content that may change over longer periods of time or between laboratories. However, the dry conditions may be well suited for comparative studies performed under similar air moisture conditions.

References

- Ascenzi A (1988) The micromechanics versus the macromechanics of cortical bone - a comprehensive presentation. J Biomech Eng **110**:357-363
- Amprino R (1958) Investigations on some physical properties of bone tissue. Acta Anatom **34**:161-168
- Burr DB, Turner CH, Naick P, Forwood MR, Ambrosius W, Hasan MS, Pidaparti R (1998) Does microdamage accumulation affect the mechanical properties of bone? J Biomech **31**:337-345
- Choi K, Kuhn JL, Ciarelli MJ, Goldstein SA (1990) Elastic moduli of human subchondral trab. and cort. bone tissue and the size-dependency of cortical bone modulus. J Biomech **23/11**:1103-1113
- Eriksen EF, Axelrod DW, Melsen FM (1994) Bone Histomorphometry 1st ed. Raven Press Ltd, New York
- Evans GP, Behiri JC, Currey JD, Bonfield W (1990) Microhardness and Young's modulus i cortical bone exhibiting a wide range of mineral volume fractions, and in a bone analogue. Mat Sc: Mat Med **1**:38-43
- Gebhardt W (1906) Ueber funktionell wichtige Anordnungsweisen der feineren und gröberen Bauelemente des Wirbeltierknochens. II. Spezieller Teil.: der Bau der Haversschen Lamellensysteme und seine funktionelle Bedeutung. Arch Entw Mech Org **20**:187-322
- Gustafson MB, Martin RB, Gibson V, Storms DH, Stover SM, Gibeling J, Griffin L (1996) Calcium buffering is required to maintain bone stiffness in saline solution. J Biomech **29/9**:1191-1194
- Hengsberger S, Kulik A, Zysset P (2001) A combined atomic force microscopy and nanoindentation technique to investigate the elastic properties of bone structural units. Europ Cells Mat **1**:12-16
- Hodgskinson R, Currey JD, Evans GP (1989) Hardness, an indicator of the mechanical competence of cancellous bone. J Orthop Res **7**: 754-758
- Johnson KL (1985) Contact Mechanics 1st ed, Cambridge University Press:84-106
- Katz JL, Meunier A (1993) Scanning acoustic microscope studies of the elastic properties of osteons. J Biomech Eng **115**:543-548
- Marotti G (1993) A new theory of bone lamellation. Calcif Tissue Int **53**(Suppl I):47-56
- Mente PL, Lewis JL (1989) Experimental method for the measurement of the elastic modulus of trabecular bone tissue. J Orthopaed Res **7**:456-461
- Meunier PJ, Boivin G (1997) Bone mineral density reflects bone mass but also the degree of mineralization of bone: therapeutic implications. Bone **21/5**:373-377
- Oliver WC, Pharr GM (1992) An improved technique for determining hardness and elastic modulus using load and displacement sensing indentation experiments. Mat Res Soc **7/6**:1564-1583
- Pharr GM, Oliver WC, Brotzen FR (1992) On the generality of the relationship among contact stiffness, contact area, and elastic modulus during indentation. J Mater Res **7/3**:613-617
- Reid SA (1986) A study of lamellar organization in juvenile and adult human bone. Anat Embryol **174**:329-338
- Rho JY, Tsui YT, Pharr GM (1997) Elastic properties of human cortical and trabecular lamellar bone measured by nanoindentation. Biomat **18/20**:1325-1330
- Rho JY, Ashman RB, Turner CH (1993) Young's modulus of trabecular and cortical bone material: ultrasonic and microtensile measurements. J Biomech **26**:111-119
- Rho JY, Pharr GM (1999a) Effects of drying on the mechanical properties of bovine femur

measured by nanoindentation. J Mat Sc: Mat Med **10**:485-488

- Rho JY, Roy ME, Tsui TY, Pharr GM (1999b) Elastic properties of microstructural components of human bone tissue as measured by nanoindentation. J Biomed Mat Res **45**:48-54
- Rho JY, Zioupos P, Currey JD, Pharr GM (1999c) Variations in the individual thick lamellar properties within osteons by nanoindentation. Bone **25/3**:295-300
- Roy ME, Rho JY, Tsui TY, Evans NS, Pharr GM (1999) Mechanical and morphological variation of the human lumbar vertebral cortical and trabecular bone. J Biomed Mat Res **44**:191-199
- Ryan SD, Williams JL (1989) Tensile testing of rodlike trabeculae excised from bovine femoral bone. J Biomech **26**:77-83
- Sneddon IN (1965) The relation between load and penetration in the axisymmetric Boussinesq problem for a punch of arbitrary profile. Int J Eng Sc **3**:47-57
- Townsend PR, Rose RM (1975) Buckling study of single human trabeculae. J Biomech **8**:199-201
- Weaver JK (1966) The microscopic hardness of bone. J Bone Joint Surg **A48**:273-288; 1966
- Weidenreich F (1923) Knochenstudien über Aufbau und Entwicklung des Knochens und den Charakter des Knochengewebes. Z Anat Entw Gesch **69**:382-466
- Weiner S, Traub W (1992) Bone structure:from angstroms to microns. FASEB J **6**:879-885
- Ziv V, Wagner HD, Weiner S (1996) Microstructure-Microhardness relations in parallel-fibered and lamellar bone. Bone **18/5**:417-428
- Zysset P, Guo XE, Hoffler CE, Moore KE, Goldstein SA (1999) Elastic modulus and hardness of cortical and trabecular bone lamellae measured by nanoindentation in the human femur. J Biomech **32**:1005-1012
- Zysset P, Sonny M, Hayes WC (1994) Morphology-mechanical property relations in trabecular bone of the osteoarthritic proximal tibia. J Arthroplasty **9**:203-216

Appendix

The stress field generated by the indentation process is heterogeneous and leads to plastic deformation and damage in the vicinity of the tip. Using Hertz's theory (Johnson, 1985), the spatial dependence of the stress components during indentation can be estimated by considering the elastic contact of a spherical indenter with a semi-infinite half space. In the direction of loading (z-axis), the stress component below the indenter decreases according to

$$\frac{\sigma_{zz}}{p_0} = -\left(1+\frac{z^2}{a^2}\right)^{-1} \tag{A.1}$$

where p_0 indicates the maximum pressure below the indenter and a the contact radius.

In a horizontal plane (z=0) the radial and circumferential components of the stress field next to the contact area obey

$$\frac{\sigma_{rr}}{p_0} = -\frac{\sigma_{\theta\theta}}{p_0} = \frac{(1-2\nu)a^2}{3r^2} \tag{A.2}$$

where θ and r are the cylindrical coordinates of the periphery of the indenter and ν is the Poisson ratio. For $\nu=0.3$ the stress field components reach their 10%-boundary defined by $\sigma_{zz} = -0.1p_0$ and $\sigma_{rr} = -\sigma_{\theta\theta} = 0.1p_0$ at a depth of $z \cong 3a$ or in lateral direction at $r \cong \frac{2}{\sqrt{3}}a$. For the Berkovich tip used in our study, the ratio between maximum indentation depth and contact radius is about $a \cong 3h_{\max}$. The mechanical properties measured by nanoindentation correspond to a semi-ellipsoidal volume extending to about 9 times the indentation depth ($z \cong 3a \cong 9h_{max}$) in the vertical direction (z) and about 7 times this same depth ($2r \cong \frac{4}{\sqrt{3}}a \cong 7h_{max}$) in the radial direction (r).

2.2
The effect of drying and re-wetting on the stiffness of single bone lamellae

Introduction

Many studies have proven the power of nanoindentation as a tool to discriminate the intrinsic mechanical properties of bone tissue. Due to technical constraints of this sensitive nanomechanical device, the majority of studies present dehydrated or dried tissue properties measured at ambient temperature (Rho et al, 1999b; Hengsberger et al, 2001; Turner et al, 1999; Roy et al, 1999). However, removal of the water content may lead to anisotropic shrinking of the matrix that create microcracks and alter the relative mechanical properties of the bone constituents.

For proper characterization of the mechanical environment of the osteocytes and the bone lining cells, the nanomechanical properties should therefore be measured under physiological conditions. Nanoindentation provides force displacement curves in the submicron regime and requires an accurate detection of the contact force between the indenter and the material. In addition, this mechanical experiment requires excellent thermal equilibrium to avoid drifting of the indenter during data acquisition. The presence of liquid on the surface has important effects on both the detection of contact force and thermal equilibrium and makes the application of nanoindentation under physiological conditions very delicate.

Among recent studies, a few attempts were performed (Zysset et al, 1999; Rho & Pharr, 1999a; Hoffler et al, 2000a) to test the intrinsic mechanical properties of fresh bone tissue. Because of experimental constraints the bone samples were kept moist by a thin layer of liquid (less than a hundred microns) on the surface or by subsurface water irrigation. Local evaporation of the thin liquid layer may have lead to indents on areas that were partially dried out during the test. Testing the bone tissue that is fully immersed in a liquid cell could avoid this problem.

The degradation of the organic component of fresh tissue also results in experimental constraints in terms of the measurement time (Weaver, 1966). Using a Ca-buffered Ringer's solution that contained sodium azide, the mechanical parameters could be conserved for only 12 hours (see preliminary study of Chapter 2). For statistically powerful studies, it seems therefore unavoidable to dry or dehydrate the sample to exclude this time-dependent effect. However the question remains open how the values of the changed tissue can be converted into the properties under physiological conditions.

The preceding chapter presented nanoindentation results on the level of single bone lamellae under dry and fully wet conditions where the samples were fully immersed in a liquid cell. The results showed that both hardness and indentation modulus were increased by drying but that relative trends like the depth dependency of the stiffness were less affected. The high statistical significance of the factor BSU implied, that the effect of drying on the lamellar stiffness cannot be determined based on these data because the four BSUs tested under physiological conditions are not identical with the other four tested under dry conditions.

The objective of this study was to determine the effect of a 24 hour drying protocol on the stiffness of single bone lamellae with respect to their properties under physiological conditions. A further objective was to check if re-wetting of a dried sample revealed the original indentation modulus. This test may give some idea if the absorption of water by the tissue pores and if the linking process to the bone matrix is reversible.
For this purpose, we measured an identical set of lamellae selected from human trabecular and compact BSUs at first under physiological, then under dry, and again under physiological conditions.

Materials and Methods
Two samples containing trabecular and cortical bone were dissected from the medial part of the femoral neck of an 86 year old female. After embedding in PMMA, the samples were polished and finished with 0.05µm alumina solution. Two BSUs, one trabecular packet and one osteon were tested. In each BSU 4 lamellae, 2 thin and 2 thick were identified.
Each BSU was first characterized in terms of hardness and indentation modulus at first under physiological conditions, i.e. being immersed in a Ca-buffered Ringer's solution containing NaN_3 (see preliminary study of Chapter 2) at 37° Celsius.
Then, the specimens were dried for 24 hours at 50° Celsius and indents to an identical depth were carried out under dry conditions.
Afterwards the samples were re-wetted and again tested under physiological conditions.
For each of these conditions 16 indentation tests were done, two indents to 100 nm maximum depth and two to 500 nm maximum depth in each of the four lamellae. To avoid proximity effects of neighbouring indents, an adjacent testing area in the same lamellae was chosen after changing the testing conditions.
This study is based on 96 indents, 48 on each tissue type, and 3*16 indents for the three testing conditions.
For statistical analysis, 4-Way-ANOVA of the absolute values were run with load, environmental conditions, bone type and lamella type as fixed effects. Two-Way-ANOVAs were performed of the ratios (dry/wet) to determine the effect of drying. Here bone type and lamella type were fixed effects.
Additionally, Two-Way-ANOVAs of the absolute values were carried out to compare the mechanical properties under wet and rewet conditions. For this purpose, analysis was done separately for each bone type setting conditions and lamella type to fixed effects.

Results
Indentation modulus:
The characterization of the compact bone sample took 7 hours under wet conditions. After drying and re-wetting the sample was again stored for 8 hours under physiological conditions until the testing protocol could be fulfilled. The trabecular bone sample was tested for 7 hours under fully

wet conditions. After the tests under dry conditions, the trabecular sample was for 3.5 hours again under wet conditions until completion of the testing protocol.

Figure 1 and 2 demonstrate the results of the relative change of indentation modulus for thin and thick lamellae for compact and trabecular bone respectively. The results are normalized with respect to their initial properties under physiological conditions.

The indentation modulus showed for thick lamellae of trabecular bone with +22% (measured at 500nm) lowest and for thin lamellae of osteonal bone with +124% (at 100nm) greatest relative change due to drying.

In both BSU the relative change of indentation modulus after drying was greater for the thin lamellae than for thick lamellae. Pooling the indents at 100nm and 500nm, the relative change of indentation modulus due to drying was +44% (+37%) for thick lamellae and +109% (+78%) for

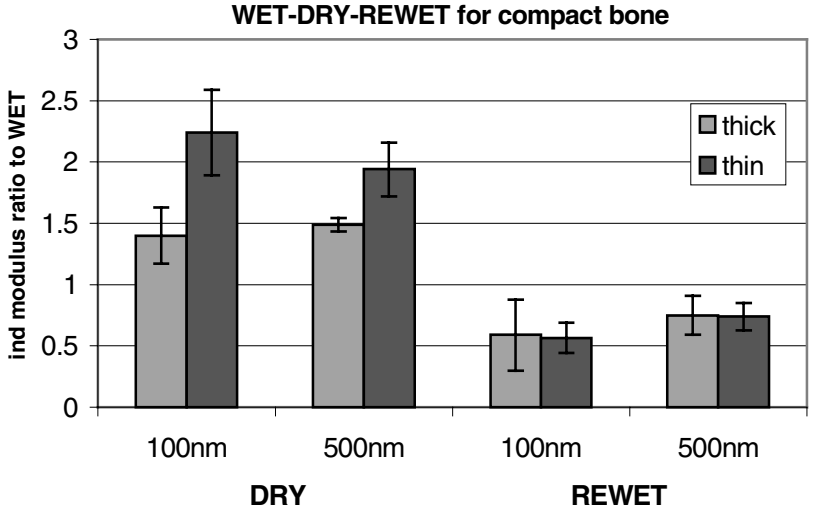

Figure 1: (top) Relative change of lamellar stiffness of osteonal bone after drying (left 4 columns) and re-wetting (right 4 columns). This graphic represents separately the results for the 100nm and 500nm indents and for thin and thick lamellae. Note the greater increase of indentation modulus of thin lamellae as a result of drying.

Figure 2: (bottom) Relative change of the stiffness of trabecular bone lamellae. Note that again the thin lamellae showed greater increase of indentation modulus after drying.

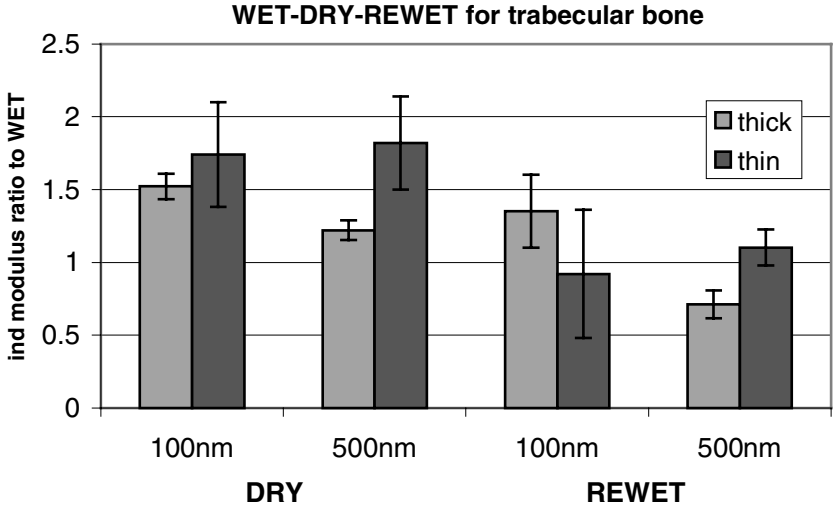

thin lamellae of compact (trabecular) bone.
The effect of re-wetting on the indentation modulus ranged from -43% for thin osteonal lamellae detected at 100nm up to +35% for thick lamellae of trabecular bone as measured at 100nm ("+" means increase and "-" means decrease). Mixing the 100nm and 500nm indents the relative change of indentation modulus due to drying AND re-wetting was -35% (+1%) for thin lamellae and -33% (+3%) for thick lamellae of compact (trabecular) bone.
According to 4-way-ANOVA, the load was not significant (p=0.4), while lamella type (p=0.002), the bone type (p=0.0004) and the testing conditions (p<0.00001) were of high global significance.
A 2-Way-ANOVA for the ratios dry/wet showed a moderate significance of bone type (p=0.03) while the lamella type was highly significant (p<0.00001).
According to 2-Way-ANOVA, rewetting (versus wet) was not significant for trabecular bone (p=0.9) but highly significant for compact bone (p=0.0004).

Hardness:
The results for hardness followed similar trends and are summarized in Table 1.
Pooling the 100nm and 500nm indents the effect of drying was again with +108% (+99%) greater for thin lamellae of compact (trabecular) bone and was weaker with +44% (+56%) for thick lamellae of compact (trabecular) bone. According to 4-Way-ANOVA lamella type (p=0.5), bone type (p=0.2) and load (p=0.33) were not globally significant while conditions (p<0.00001) showed high global significance.
A 2 Way-ANOVA for the ratios dry/wet showed no significance for bone type (p=0.98) while lamella type was significant (p=0.0006) for the effect of drying.
According to 2-Way-ANOVA, the effect of rewetting was weakly significant for trabecular bone (p=0.03) and highly significant for compact bone (p=0.00002).

rel change of hardness	lamella	ind.depth	after drying	after re-wetting
trabecular bone	thin	100nm	+73%	+2%
		500nm	+125%	+47%
	thick	100nm	+58%	+113%
		500nm	+54%	-19%
compact bone	thin	100nm	+107%	-54%
		500nm	+110%	-37%
	thick	100nm	+26%	-53%
		500nm	+62%	-36%

Table 1: relative change of hardness with respect to the initial values under physiological conditions. Note the greater increase of the thin lamellae after drying.

Discussion

The same thin and thick lamellae of 2 BSU's of compact and trabecular bone were successfully tested under physiological, under dried, and ,after re-wetting, under physiological conditions. The testing conditions were highly globally significant for both indentation modulus and hardness. The lamella and bone type reached global significance for indentation modulus.

The effect of drying was highest for thin lamellae of both compact and trabecular bone. It is possible that this observation is due to a different shrinkage behavior of the two lamella types. According to Marotti (Marotti, 1993) the density of collagen is higher in thin lamellae than in thick lamellae. Collagen fibers that are long chains of proteins contain adsorption sites for polar water molecules. It is possible that the higher density of the collagen fibers in the thinner lamellae results in a higher water adsorption capacity.

Rho has postulated that drying leads to a contraction of individual collagen fibrils with a degree of contraction that becomes smaller with increasing mineralization (Rho & Pharr, 1999a). According to Marotti (Marotti, 1993) the thick lamellae are richer in mineral content than thin lamellae and may therefore show a smaller relative contraction after drying.

These observations are also compatible with a study by Ascenzi (Ascenzi, 2000) who dissected single lamellae from osteonal bone. They reported different volume changes of the two lamella types when changing the testing conditions. Thin lamellae showed a lower thickness (3.3±0.88 μm after drying with respect to 3.56±0.93 μm wet) after drying while thick lamellae kept their thickness constant when changing from wet to dry state. They also reported a significant lower height of both lamella types under dry conditions with respect to the wet state. The latter observation corresponds to shrinkage of the matrix in the direction of the indentations.

The different changes of indentation modulus and hardness between the two lamella types seem therefore compatible with the independent findings of Rho, Marotti and Ascenzi.

Rho (Rho & Pharr, 1999a) has reported an increase of indentation modulus by 15.8 % for bovine osteonal bone after drying. This study demonstrates an increase by 76.5% if the results of thin and thick osteonal lamellae are averaged. This high discrepancy may be attributed to distinct preparation and testing protocols. Rho tested the sample at ambient temperature and while kept moist by a thin film (50-100 μm) of deionized water containing thymol while in our study the sample was fully immersed in a Ca-buffered Ringer's solution. Afterwards, Rho dried for 14 days at ambient temperature. The results after this slow drying process may have been influenced by a degradation of the collagen that could have decreased the relative change of indentation modulus. Further, our tests were done at body temperature that probably has increased the detected relative changes with respect to Rho et al. Turner & Burr (1993) reported a 2-4% stiffness decrease when increasing from ambient temperature to 37° Celsius. This confirms again the sensitivity of nanomechanical properties to the preparation and testing protocol.

After rewetting, trabecular bone showed on average the same indentation modulus as under the initial wet conditions ($p=0.9$). However a very high hardness value that corresponds to an 113%

increase with respect to the first wet tests was observed for thick lamellae at 100nm. This may be the reason for the weak significance of rewetting for the hardness values of trabecular bone (p=0.03). Since this value can hardly be explained by the biological variation of the tissue it may represent some artifact of the experiment.

The compact bone sample decreased the mean indentation modulus by 34% and the hardness values decreased by approximately 45% after rewetting. The mechanical properties were therefore lower than under initial physiological conditions. The compact bone sample was for 15 hours in the Ca-buffered solution. According to the degradation study, (see preliminary study in Chapter 2) this exceeded the critical 12 hour period and a partial degradation of the collagen fibers may have influenced the results. It cannot further be excluded that a partial dissolution of the mineral phase is responsible for this decrease after 15 hours. The latter point is supported by the fact that for the 100nm indents, the relative decrease of the mechanical parameters was greater than for the 500nm indents. Clarification of this point is needed before the reversibility of the drying process for the stiffness of single bone lamellae can be proven.

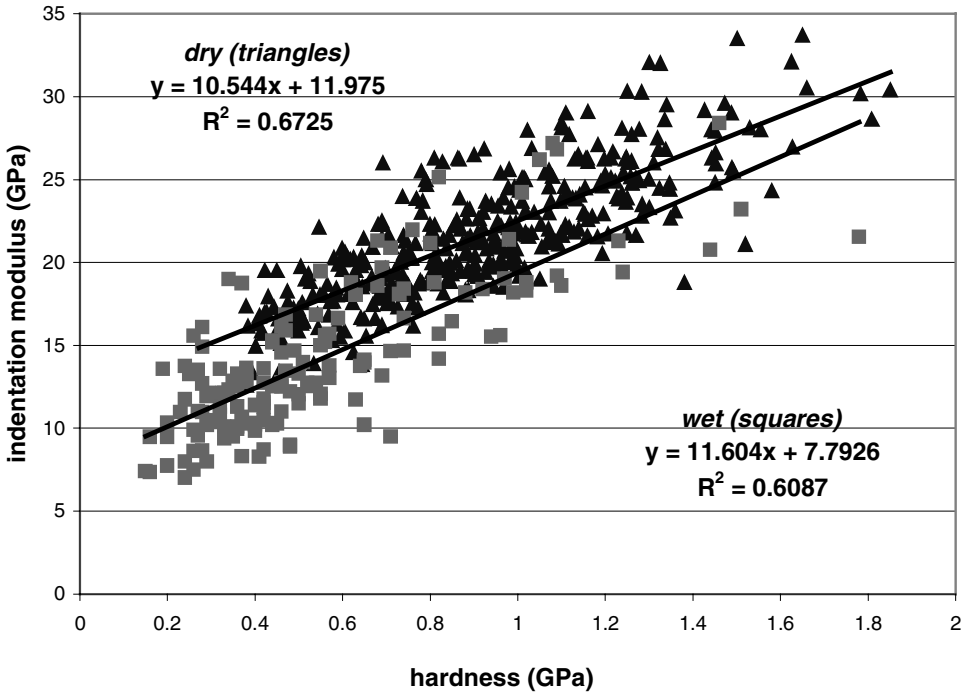

Figure 3: Correlation of indentation modulus with hardness of the data presented in the preceding chapter 2. The 4 BSUs tested under physiological conditions (squares) and the 4 BSUs tested under dry conditions (triangles) show close but significant different regression slopes ($p<0.0001$).

A further point of this discussion pertains to the correlation between indentation modulus and hardness. The empirically proven relationship (Evans et al, 1990) between these two mechanical

parameters may somehow change as a result of drying. For this purpose we checked the data of the 8 BSU presented in the preceding paragraph that are demonstrated in figure 3. The correlation between hardness and indentation modulus is similar under wet (R^2=0.61) and under dry (R^2=0.67) conditions. The slopes of the linear regression show close but significantly different values ($p<0.0001$) for the wet and dry samples. Hardness and indentation modulus therefore show a similar but significantly different relative shift as a result of drying. However, the study in chapter 2.1 demonstrates that relative trends (like the depth-dependence of mechanical properties and differences between lamella types) are not affected by drying.

References

- Ascenzi MG, Benvenuti A, Mango F, Ascenzi A (2000) Structural biomechanical differences in bright and extinct osteonic lamellae. Proceedings ESB 2000
- Evans GP, Behiri JC, Currey JD, Bonfield W (1990) Microhardness and Young's modulus in cortical bone exhibiting a wide range of mineral volume fractions, and in a bone analogue. J Mat Sc: Mat Med **1**:38-43
- Hengsberger S, Kulik A, Zysset P (2001) A combined atomic force microscopy and nanoindentation technique to investigate the elastic properties of bone structural units. Europ Cells Mat **1**:12-16
- Hoffler CE, Moore KE, Kozloff K, Zysset PK, Brown MB, Goldstein SA (2000a) Heterogneity of bone lamellar-level elastic moduli. Bone **26/6**:603-609
- Marotti G (1993) A new theory of bone lamellation. Calcif Tissue Int **53**(Suppl I):47-56;
- Rho JY, Pharr GM (1999a) Effects of drying on the mechanical properties of bovine femur measured by nanoindentation. J Mat Sc: Mat Med **10**:485-488
- Rho JY, Roy ME, Tsui TY, Pharr GM (1999b) Elastic properties of microstructural components of human bone tissue as measured by nanoindentation. J Biomed Mat Res **45**:48-54
- Roy ME, Rho JY, Tsui TY, Evans NS, Pharr GM (1999) Mechanical and morphological variation of the human lumbar vertebral cortical and trabecular bone. J Biomed Mat Res **44**:191-199
- Turner CH, Burr DB (1993) Basic biomechanical measurements of bone: A tutorial. Bone **14**:595-608
- Turner CH, Rho JY, Takano Y, Tsui TY, Pharr GM (1999) The elastic properties of trabecular and cortical bone tissues are similar: results from two microscopic measurement techniques J Biomech **32**:437-441
- Weaver JK (1966) The microscopic hardness of bone. J Bone Joint Surg **A48**:273-288
- Zysset PK, Guo XE, Hoffler CE, Moore KE, Goldstein SA (1999) Elastic modulus and hardness of cortical and trabecular bone lamellae measured by nanoindentation in the human femur. J Biomech **32**:1005-1012

Chapter 3
Depth dependency of indentation modulus and hardness for human and bovine microstructures

Introduction

The following three chapters focus on a higher level in the hierarchy of bone tissue, on the characterization of individual BSU's.

For this task, a nanoindentation device (Nanoindenter XP - MTS Systems Corporation Minneapolis) that is combined with an optical microscope was be used. This combination allows selection of indentation regions on an area of several square centimeters and is therefore appropriate to characterize a large set of BSU's.

The study discussed in chapter 2 presented the intrinsic mechanical properties of individual bone lamellae. Thick lamellae showed a significant depth dependency while for thin lamellae indentation depth was not a significant factor. It is therefore crucial to determine an indentation depth that represents a compromise between the depth dependent effects on the lamellar level and the spatial resolution of the mechanical tests; the latter being directly correlated to the size of the hardness imprint.

The prospect of this study was to test the dependency of the indentation modulus and hardness on the indentation depth for human trabecular, osteonal and interstitial bone and for bovine plexiform bone. For this purpose, indents with multiple unloading between 100nm and 2300nm were run. These tests served to determine an "ideal" indentation depth and to perform a comparison of the selected tissue microstructures.

Materials and Methods

A 3 mm slice containing trabecular and cortical bone was dissected from the lateral part of the femoral neck of an 86 year old female. This slice was cut perpendicular to the long axis of the femoral neck and was embedded in PMMA.

A bovine bone specimen was dissected from the femoral diaphysis and cut perpendicular to the long axis of the bone shaft.

The samples were polished finishing with 0.25 μm diamond paste and then dried for 24 hours at 50° Centigrade. After 24 hours adaptation of the tissue to the laboratory conditions the nanoindentation tests were carried out.

Based on the microscopy image 8 BSU of compact bone, 8 BSU of trabecular bone and 8 regions of interstitial bone. BSUs of trabeculae with axial orientation were selected and the indents were done in the direction of their longitudinal axis. Further more, 29 indents were performed on bovine lamellar and parallel-fibered tissue.

On each type of bone, 29 indents to 2300 nm maximum depth with unloadings at 100nm, 200nm, 350nm, 635nm, 1200nm and 2300 nm were done (see Figure 1). For this purpose, a constant strain rate of $\dot{\varepsilon} = \frac{1}{h}\dot{h} = 0.066\frac{1}{s}$ was applied. Each unloading was preceded by a 5 second holding

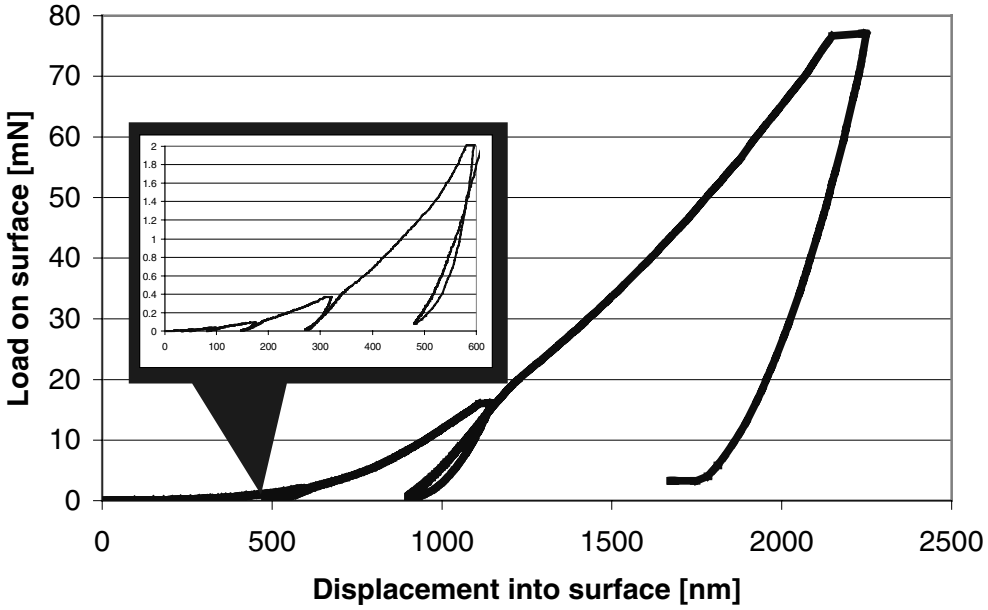

Figure 1: Force displacement curve of an indent to 2300nm maximum depth with multiple unloading. Indents of this displacement history were performed on the three human microstructures and bovine bone to measure the depth dependency of indentation modulus and hardness.

period. At the end of each test a correction for thermal drift was included. The indenter tip calibration was performed with the fused silica standard material. For statistical analysis Multiple Way ANOVA were run based on a mixed model with BSU as a random factor while tissue type and depth were set to fixed effects.

Pairwise comparisons were performed applying 2 Way ANOVAs of the corresponding data subset based on a mixed model with tissue type as a fixed and BSU as a random effect.

Results

Indentation modulus as a function of depth:

The fused silica sample provided an indentation modulus of E_{ind}=70.8±4.6 GPa showing a slight but insignificant increase with increasing depth (p=0.25 for unloadings between 140nm and 2300nm and p=0.06 if unloading at 70nm are also taken into account).

Figure 2 demonstrates the results for the four different bone types as a function of depth. The indentation moduli are normalized with respect to the value at a depth of 2300nm.

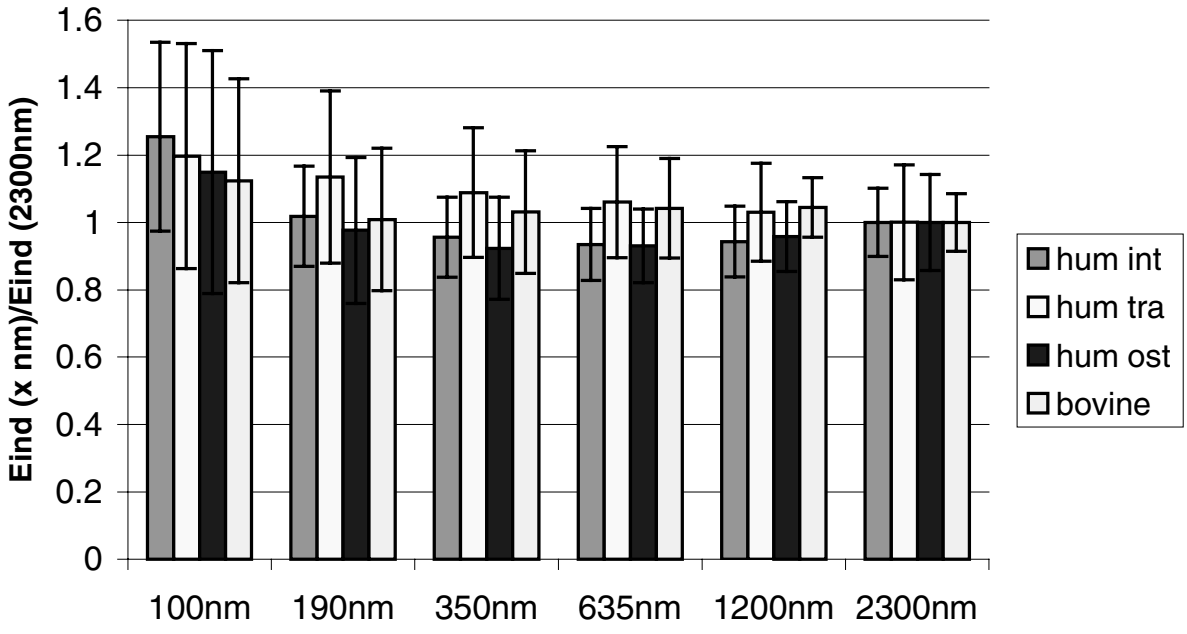

Figure 2: (top) Depth dependency of indentation modulus for human interstitial (int), trabecular (tra), osteonal (ost) and bovine bone. Note that the results are normalized to the value at 2300nm depth representing the relative trends.
Figure 3: (bottom) Absolute values for indentation modulus for the four microstructures at 1200nm depth. Osteonal, interstitial and trabecular bone were pairwise significantly different. Bovine and human intersititial bone were not significant.

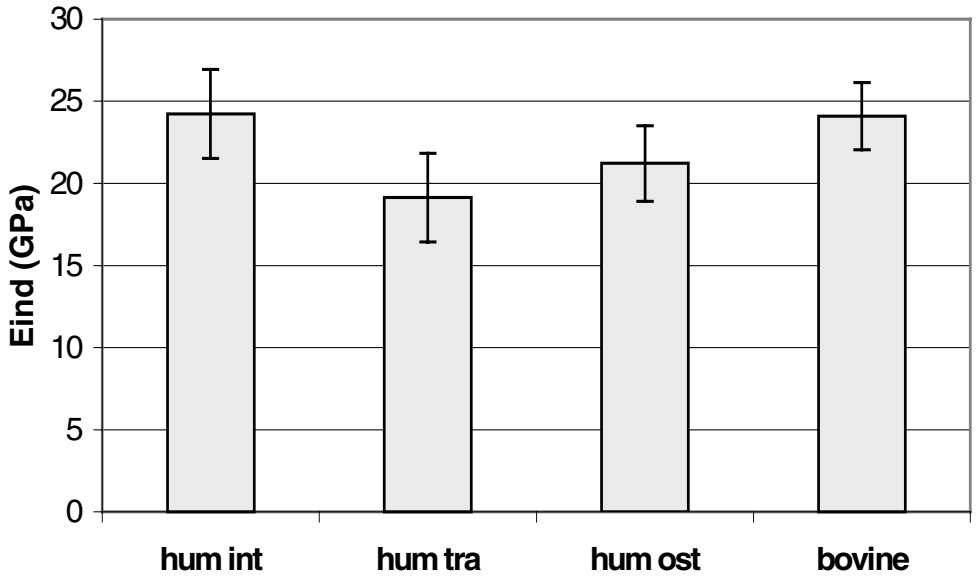

For all bone types indentation modulus was highest at 100nm ranging from 112.4% for bovine bone to 125% for interstitial bone with respect to the value at a depth of 2300nm. For the unloadings at 100nm the standard deviation was highest and exceeded for osteonal bone 30 % of the mean value.

With increasing depth, both the indentation moduli and the standard deviation decreased and reached a constant level at 635nm and higher depths. A 3-Way ANOVA showed that tissue type ($p<0.0001$) and depth ($p<0.0001$) were factors of high global significance. The standard deviations were lowest at 1200nm depth and ranged between 8.5% of the mean value for bovine bone to 14.1% for trabecular bone.

For the indentation modulus of bovine bone, the factor "depth" was not significant ($p=0.22$). For unloading at 190nm and deeper, the variation of indentation modulus was insignificant for osteonal bone ($p=0.3$). This similarly applies to interstitial ($p=0.12$) and trabecular ($p=0.13$) bone for a range of depths between 350nm and 2300nm.

The absolute values of the indentation modulus at a depth of 1200nm are demonstrated for the four microstructures by Figure 3. Table 2 represents the results of the pairwise comparisons of the four tissue types for a depth of 1200nm.While the modulus of human interstitial and bovine bone were not significantly different ($p=0.8$), interstitial bone tissue showed a significantly higher modulus than osteonal ($p=0.0045$) and trabecular bone ($p=0.0003$). A comparison of osteonal bone with trabecular bone indentation modulus reached the significance level ($p=0.03$).

Correlation between Indentation modulus and hardness:

Table 1 shows the correlation coefficients R^2 between indentation modulus and hardness for the different types of bone. These correlations include all depths. The correlation coefficient between these mechanical parameters was lowest for bovine bone, $R^2=0.13$. The three microstructures of human bone showed a similar moderate correlation between $R^2=0.37$ for osteonal and $R^2=0.43$ for interstitial bone.

	R^2 for E_{ind} with hardness
bovine bone	0.13
human trabecular bone	0.4
human osteonal bone	0.37
human interstitial bone	0.43

Table 1: Correlation coefficient between indentation modulus and hardness for the four microstructures for all depths. Note that the correlation is lowest for bovine bone and similar for the three microstructures of human bone.

Hardness as a function of depth:

Figure 4 shows the absolute values of hardness as a function of depth. Hardness showed the reverse trend of indentation modulus. Hardness was lowest for the low depth indents and increased with increasing depth. The standard deviation of the hardness results was also maximum for the low depth indents and became lower with increasing depth. According to the MANOVA results both depth ($p<0.0001$) and tissue types ($p=0.0012$) were factors of high global statistical significance.

The standard deviations for the hardness values of the four microstructures were lowest at 2300nm depth and ranged from 7.6% of the mean value for bovine bone to 14.2% for trabecular bone.

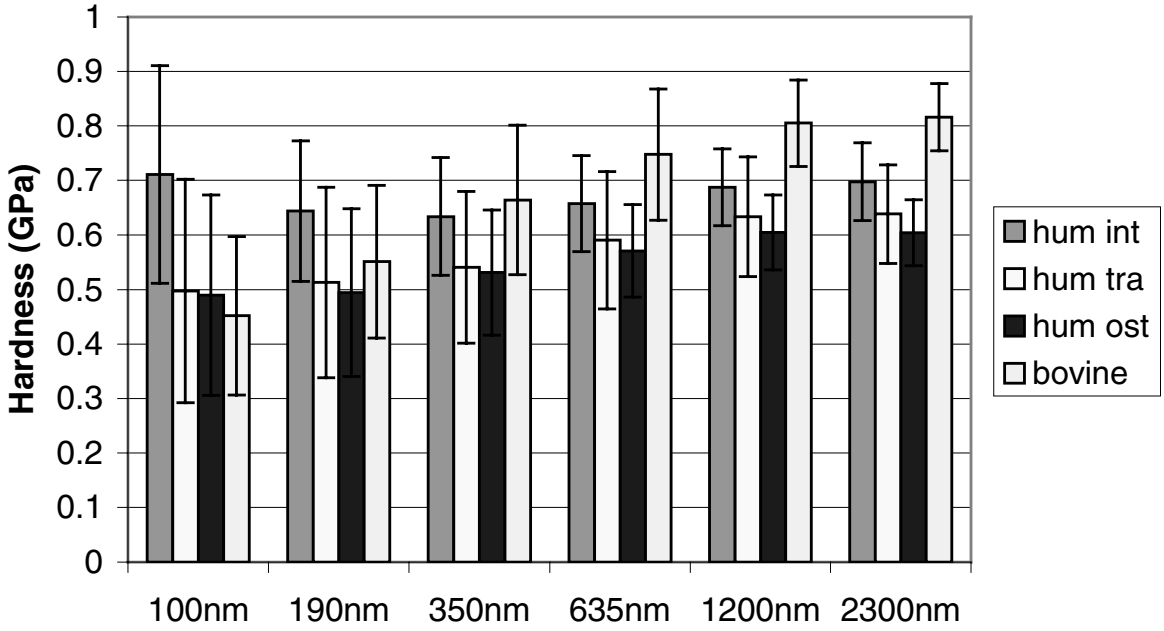

Figure 4: Dependency of the absolute hardness values on the unloading depth. Note that human osteonal and trabecular and bovine bone show an increasing trend with depth. For human interstitial bone the mean hardness remained almost constant with depth.

For the unloading at 635 nm or deeper, the factor "depth" was for human trabecular bone ($p=0.11$), osteonal bone ($p=0.14$) and interstitial bone ($p=0.15$) not significant. For bovine bone this factor was of moderate significance ($p=0.02$) for the same range of depths. For bovine bone the hardness results at 1200nm were not significantly different neither from the results at 635nm ($p=0.053$) nor from the results at 2300nm ($p=0.59$). Table 2 shows the pairwise comparisons of the microstructures at 1200nm for both hardness and indentation modulus. Note, that for hardness, bovine and interstitial bone were significantly different ($p=0.001$), while interstitial and trabecular bone did not show significant differences ($p=0.12$).

p-value	bovine	hum int	hum tb	hum ost
bovine	1			
hum int	0.001 / 0.81	1		
hum tb	0.0002 / <0.0001	0.12 / 0.0003	1	
hum ost	<0.0001 / 0.0002	0.003 / 0.005	0.43 / 0.03	1

Table 2: Pairwise comparison of the hardness / indentation moduli at 1200nm depth of the four microstructures: bovine plexiform bone, human interstitial (int), trabecular (tb) and osteonal (ost) tissue. Two-way-Anovas based on a mixed model were performed of the corresponding data subsets

Discussion

The standard deviations for both indentation modulus and hardness were highest for 100nm depth and decreased with depth. This effect can be due to several factors like the signal to noise ratio of data acquisition, tip irregularity, calibration artifacts and surface roughness. All these three factors decrease their relative influence with increasing depth. The standard deviations for the 100nm unloading were higher than for the low depth indents under dry conditions reported in Chapter 2 (typically 15% of the mean value). This may be attributed to the fact that in this study each cell includes both lamella types and several BSUs while in Chapter 2 single bone lamellae of the same type were averaged. The available AFM scan allowed choice of areas of low local roughness, information that is not accessible for the MTS indenter that is combined with optical microscope. Standard deviation of indentation modulus was lowest for unloading at 1200nm depth. The resulting 7μm imprints correspond to the typical thickness of one pair of thin and thick lamellae and may average the heterogeneity of adjacent lamellae.

Indentation modulus decreases for depths between 100nm and 350nm. Chapter 2 presented results where thick lamellae showed a decrease for depths between 100nm and 500nm while depth was not significant for thin lamellae. The indents of this study represent a composite behavior of both lamella types. Pooling the results of the thin and thick lamellae of the preceding chapter confirms an average decreasing trend of indentation modulus for depths up to 500nm. Although depth was not a significant factor for trabecular bone for unloadings at 635nm and deeper, we note a slightly decreasing trend also for this range of depths. On the spongy bone structure the indents were chosen on axially aligned trabeculae i.e. their long axis being parallel to the direction of load application. The fact that axial trabeculae were measured allows a comparison of the different microstructures all being tested in their physiological main direction. Further, this avoided the fact that this test combines an indentation with bending of the whole structure since interfaces between the tissue and plastic could occur below the trabeculae.

However the results of this study do not exclude that a buckling of the trabecula occurs that leads to the continuously decreasing trend of indentation modulus up to 2300nm depth.
The indentation moduli values were constant for depths above 350nm and the results at 1200nm had lowest standard deviation. A comparison of the absolute values of the four bone types at this depth shows that human interstitial and bovine bone were not significantly different. The fast growing cow bone generates tissue with similar elastic properties like human interstitial tissue that consists of only partially resorbed secondary osteons.
Human interstitial bone showed significantly higher stiffness than Haversian and spongy bone. Osteonal bone had a higher indentation modulus than trabecular bone. Recent studies under moist conditions (Hoffler et al, 2000a; Zysset et al, 1999) support these findings for the human femoral neck. Roy (Roy et al, 1999) has reported an indentation modulus anisotropy for vertebral trabecular bone. Highest values were seen for axially aligned trabeculae being indented in axial direction. If similar property descriptions applied to the femoral neck then the differences would be greater between osteonal bone and transverse trabeculae.

Hardness showed a reverse trend to indentation modulus, that being lowest for the low depth indents and by showing an increase with higher depths. The relative trend was greatest for bovine bone and almost negligible for human interstitial bone. This is also reflected by the correlation coefficients between indentation modulus and hardness that was lowest for bovine with R^2=0.13 and highest for interstitial bone with R^2=0.43. This empirically proven relationship (Evans et al, 1990) between these two mechanical properties could not be confirmed for bovine bone in this study.
The question arises why hardness showed the reverse trend to indentation modulus. Errors of tip calibration for this high range of depths can be excluded. Since indentation modulus and hardness depend both on the inverse of the area function, an erroneous calibration of the indenter should lead to similar depth trends for both parameters. This discrepancy of trends may be attributed to the included holding period that preceded each unloading. During those periods the material creeps under the tip while the load is held constant that results in a continuous change of the apparent hardness value. This creep is due to viscoelastic behavior and to time-dependent plasticity, two effects that may change their relative influence on the detected hardness value with increasing depth. Viscous effects and damage may differently influence the hardness than the indentation modulus results.
Indents of approximately 1μm depth showed lowest standard deviation for indentation modulus and the 2μm indents showed lowest standard deviation for hardness. A few 2μm indents with the resulting 12μm hardness imprints may be sufficient to characterize individual BSU. However according to Hertz (see appendix of chapter 2) indents to this depth average over a

semiellipsoidal volume of 18 μm in vertical direction that could be highly influenced by lacunar porosities.

We concluded for the following three studies in Chapter 4-6 that an indentation depth of approximately 1 μm represents an appropriate compromise between the aforementioned depth-dependent errors, the spatial resolution and the potential influence of lacunar porosities.

References

- Evans GP, Behiri JC, Currey JD, Bonfield W (1990) Microhardness and Young's modulus in cortical bone exhibiting a wide range of mineral volume fractions, and in a bone analogue. J Mat Sc: Mat Med **1**:38-43
- Hoffler CE, Moore KE, Kozloff K, Zysset PK, Brown MB, Goldstein SA (2000a) Heterogneity of bone lamellar-level elastic moduli. Bone **26/6**:603-609
- Roy ME, Rho JY, Tsui TY, Evans NS, Pharr GM (1999) Mechanical and morphological variation of the human lumbar vertebral cortical and trabecular bone. J Biomed Mat Res **44**:191-199
- Zysset PK, Guo XE, Hoffler CE, Moore KE, Goldstein SA (1999) Elastic modulus and hardness of cortical and trabecular bone lamellae measured by nanoindentation in the human femur. J Biomech **32**:1005-1012

Chapter 4
Mineral content, collagen fiber orientation and mechanical properties of human compact BSU: a two-case study

Introduction

There is increasing evidence for the role of the intrinsic bone tissue quality in skeletal fragility and the associated medical treatments. A current method for the assessment of bone quality at the tissue level involves quantification of the mineral content that is recognized as an important predictor of bone stiffness at the macroscopic level (Currey, 1988). The clinically used bone mineral density (BMD) combines volume fraction and the degree of mineralisation and does not allow for a distinct quantification of these parameters. The fact that the mechanical properties depend with different power laws on porosity and mineral content (Carter & Hayes, 1977; Currey, 1988) contributes to their limited predictability by BMD.

It becomes also widely accepted that the morphology of the organic matrix has an important contribution to the mechanical properties of the bone tissue. Based on observations with polarised light microscopy (PLM), Gebhardt (1906) and Ascenzi (1988) distinguished osteons with mainly longitudinal, transverse or alternate orientation of collagen fibers. Weiner & Traub (1992) extended this model by including an analysis of the arrangement of the HAP-crystals that grow within the fibers. Martin & Ishida (1989) showed that the orientation of the collagen fibers significantly influenced the macroscopic postyield properties of bovine bone while the mineral content was less important.

Only a few studies focussed on the influence of the organic and inorganic components on the mechanical properties at the level of bone structural units (BSU: defined in Eriksen et al, 1994). Amprino (1958) reported a correlation of avian bone microhardness with mineralisation and with the orientation of the collagen fibers (determined with PLM). Later, Hodgskinson et al (1989) confirmed the dependence of microhardness on mineralisation for bone of several species. Zioupos (2001) observed a correlation between mineral weight fraction and the indentation modulus (R^2=0.49). A weakness of these studies may be that the data represent average of multiple BSU's. Additionally, the bone volume used for mechanical tests did not always contain the identical BSUs like the volume taken for morphological characterization. The mechanism of the bone remodeling process implies that the individual degree of maturation and the associated morphological properties of each BSU may also result in individual mechanical properties. This suggests that both mechanical and morphological analysis should be done on the identical BSU. In an effort to extend our knowledge of the structure-function relationship down to the level of structural units, we defined a study where morphological and mechanical properties are measured in the same population of BSU.

The object of this study was to evaluate the correlation between mechanical and morphological properties of human osteonal and interstitial bone at the level of BSU. For this purpose, mineralisation and average collagen fiber orientation were compared with the mechanical data obtained by nanoindentation and scanning acoustic microscope (SAM). The hypothesis of this study was that mean collagen fiber orientation measured by PLM and mineralisation measured by microradiography predicted at least 70% of the variation of the mechanical parameters.

Methods

Samples of compact bone were dissected from the posterior part of the proximal femoral diaphysis of an 86-year old female and of a 30-year old male (see Figure 1). Each sample was cut perpendicularly to the Haversian canals generating two adjacent slices of approximately 100 μm and 300 μm thickness. Both faces of the 100-μm slice and the adjacent surface of the 300-μm slice were polished with successive grades of silicon carbide paper and finished with 0.25μm diamond paste.

The material loss between two adjacent slices due to sawing and polishing was approximately 150 μm. Many osteons (single BSU) and regions of interstitial bone could be identified on both slices.

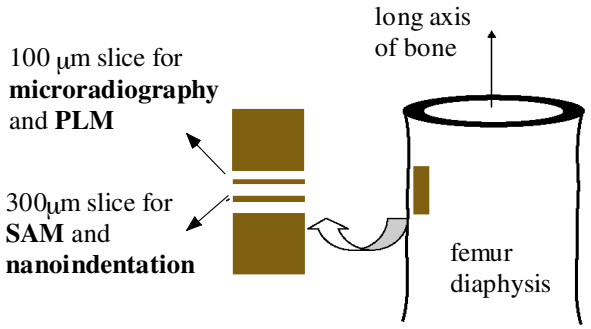

Figure 1: Illustration where the bone samples were dissected and how the slices were oriented. Two adjacent slices were taken for characterization in terms of morphology (microradiography and PLM) and in terms of mechanics (SAM and nanoindentation)

For the female donor, 43 osteons and seven regions of interstitial bone were selected and for the male donor 29 osteons and six regions of interstitial bone were chosen. The 100-μm thin slice was used to characterize these BSUs and regions in terms of morphology by microradiography and polarised light microscopy (PLM). The 300-μm thin slice was used to perform mechanical tests of the same BSUs by nanoindentation and scanning acoustic microscopy (SAM). See Figure 2 for an overview of the four applied measurement techniques.

Mineral content:

Mean degree of mineralisation of bone (MDMB) was determined by quantitative microradiography (Meunier & Boivin, 1997; Boivin, 2000). For this purpose the absorption of transmitted characteristic CuKα X-ray (W=25 keV and λ=1.54 Å) was measured for the 100 μm

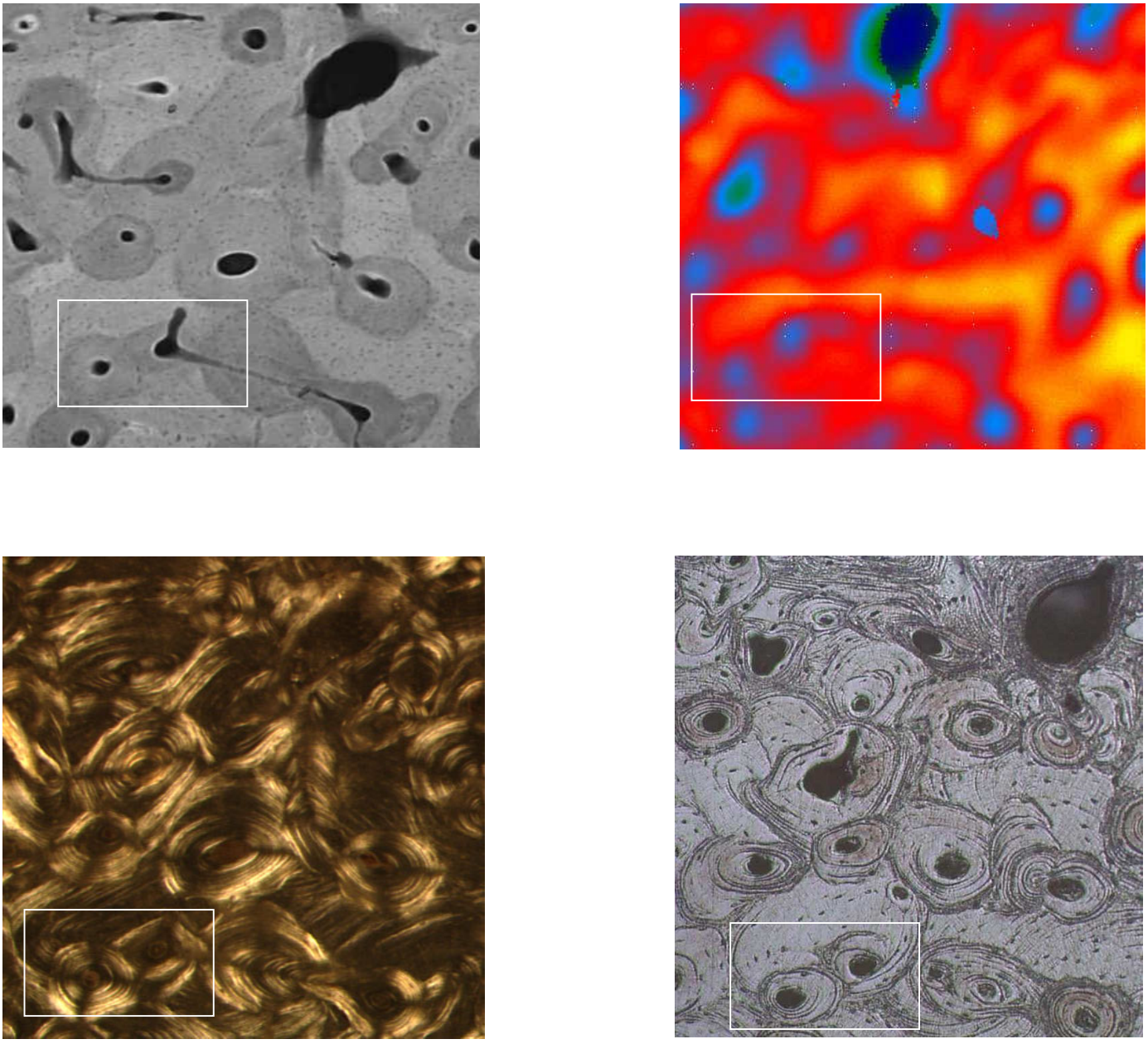

Figure 2: These four figures illustrate the different characterization techniques that were applied. The white rectangle shows the same pair of BSU on each graphic.
On the left: morphological methods: Microradiography (top) and Polarized light microscopy (bottom)
On the right: mechanical tests: Scanning acoustic microscopy (top) and Optical image based on which the nanoindentation tests were located (bottom)

thin slice (see Figure 2 top left). For calibration, 10 aluminum foil slices with known thickness ranging from 10 to 100 micrometers were measured simultaneously with the bone slice. This method accounts for the individual exposure time and allows for a quantification of the local mineralisation. The mean gray level of each BSU and region was evaluated applying image processing software and then compared with the gray level of the aluminum calibration material. Considering the attenuation coefficient of the pure aluminum and of the pure hydroxyapatite at this particular photon energy, the local concentration of the mineral can be determined.

The MDMB was evaluated for each BSU excluding the vascular channels and represents therefore an average value for the matrix including the lacuno-canalicular porosity.

Based on MDMB, the clinically used bone mineral content, BMC can be calculated by correcting for the effect of the vascular pores by

$$BMC = MDMB\left(1 - V_{vasc}\right) \tag{1}$$

Here V_{vasc} represents the volume fraction of the vascular canals, that was estimated to be 0.033.

Based on BMC, the tissue density ρ_{tissue} can be calculated with the relation

$$\rho_{tissue} = \rho_o + \frac{\rho_m - \rho_o}{\rho_m V_{matrix}} BMC \tag{2}$$

Here, a density of pure osteoid of ρ_o=1.46g/cm^3 and a density of the pure mineral phase of ρ_m=2.8g/cm^3 were chosen. The volume fraction of the matrix V_{matrix} (including both vascular and lacunar porosities) was assumed to be 0.95.

Polarised light microscopy:

The 100-μm slice was then analyzed by polarized light microscopy. For this purpose, the method proposed by Martin & Ishida (1989) was employed.

The bone slice was installed on a transmission optical microscope between two linear polarizers. The intensity of transmitted white light was determined for each BSU/region twice, once in bright field with parallel polarizers, and again in dark field with crossed polarizers.

The bright field intensity accounts for the individual absorption of white light of each region due to porosity and mineralisation (see Figure 3 left). The dark field accounts for the birefringence of each structure of interest (see Figure 3 right). According to Ascenzi (1988) and Gebhardt (1906) the relative orientation of the collagen fibers with respect to the propagation direction of the polarized light explain different birefringence phenomena. The collagen fibers do not turn the polarization plane of photons with a Poynting vector parallel to their long axis. Between crossed polarizers, regions with longitudinally oriented collagen fibers appear dark. The polarization of light propagating perpendicularly to the longitudinal axis of collagen fibers is turned. Regions

with transversely oriented collagen fibers are therefore birefringent and appear bright between crossed polarizers. A longitudinal structure index (LSI) was defined by

$$LSI = \frac{Intensity(bright\ field)}{Intensity(dark\ field)} \tag{3}$$

This index is directly proportional to the concentration of longitudinally oriented fibers.

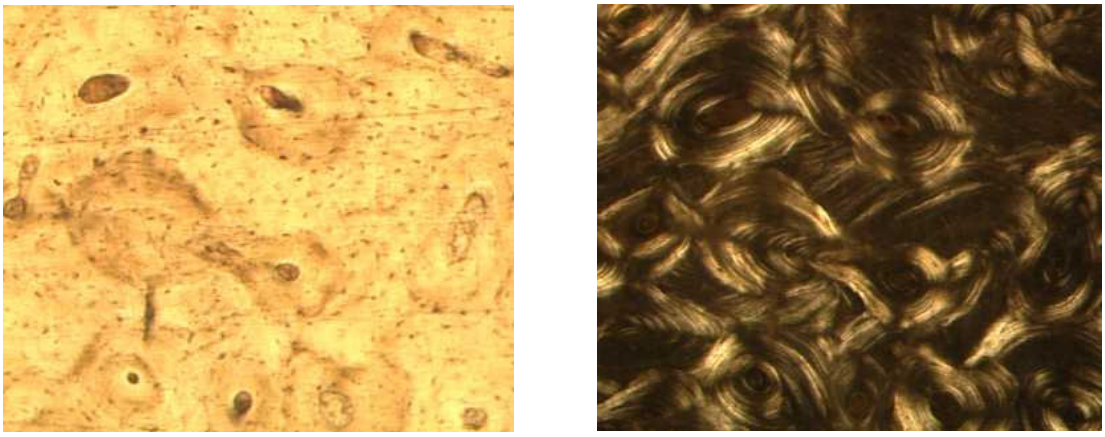

Figure 3 Quantification of the collagen fiber orientation with a longitudinal structure index (LSI). **left:** PLM picture with parallel polarizers (bright field) that accounts for the individual absorption of white light of each region. **right:** PLM picture with crossed polarizers (dark field) showing regions with optical activity.

Nanoindentation:

Indentation modulus and hardness of each BSU/region (after 24 hours drying at 50°C) were measured by nanoindentation using 5 displacement-controlled tests to 0.9 μm depth. For the loading and unloading part an identical strain rate of $\dot{\varepsilon} = 0.066\frac{1}{s}$ was applied. The unloading part allows determinatio of the indentation modulus when the deformation of the diamond tip (with known elastic constants) is subtracted (Oliver & Pharr, 1992),

$$E_{ind} = \frac{E_{Young}}{1 - \nu^2} \tag{4}$$

which combines the Young's modulus E_{Young} and the Poisson ratio ν for an isotropic material. Hardness is defined by

$$H = \frac{P(h_{max})}{A_c(h_{max})} \tag{5}$$

and represents the mean pressure the material can resist. Here $P(h_{max})$ is the applied load and

$A_c(h_{max})$ the actual contact area between the diamond indenter and the material at maximum depth (Oliver & Pharr, 1992).

Scanning acoustic microscopy:

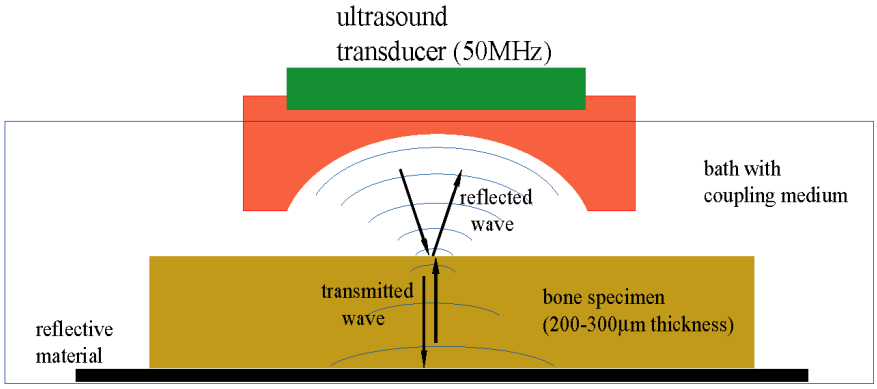

Figure 4: Scanning acoustic microscope. The quantification of local elasticity is achieved by the independent measurement of impedance (reflected wave) and speed of sound in the material (transmitted and back-reflected wave)

The longitudinal wave modulus of the selected regions was characterized by scanning acoustic microscopy (SAM) at 50 MHz under fully wet conditions (see Figure 4). During the scan, the local impedance Z of the material (reflected wave) and the sound velocity v (transmitted and back-reflected wave) within the material were measured independently. This allows for a determination of the local material density (SAM-ρ) by the ratio of these two parameters with

$$\rho = \frac{Z}{\mathrm{v}} \tag{6a}$$

Furthermore, a quantification of the longitudinal wave modulus C (SAM-modulus) is possible with

$$C = Z\ \mathrm{v} \tag{6b}$$

For an isotropic material, the elasticity constant obtained by SAM depends on both Young's modulus and Poisson ratio (Briggs, 1992)

$$C = E_{Young}\left(\frac{1-\nu}{(1-2\nu)(1+\nu)}\right) \tag{7}$$

Equation (7) holds if the sound wavelength is small with respect to the lateral dimensions of the sample. This was the case for a wavelength of approximately 80µm (within the bone material) with respect to 3mm width of the sample.

Results

86-year old female:

Each BSU exhibited an individual degree and a homogenous distribution of MDMB ranging from 1.38 to 1.71 g min/cm^3 with a relatively high mean value (± standard deviation) of 1.55 ±0.085 g min/cm^3. For LSI, a range of 1.35 to 4.98 with an average (± stdev) of 2.88 ±1.07 was obtained.

Mean indentation modulus of the BSU ranged from 9 to 25.7 GPa with an average (± stdev) of 19.3 ±4.4 GPa. Osteonal and interstitial bone were not significantly different (p=0.06). Hardness values of BSU varied between 0.55 and 1.04 GPa with a mean (± stdev) of 0.77 ±0.13 GPa.
Indentation modulus and hardness were also homogeneous within single BSU but varied with high statistical significance between BSU (p<0.0001). Hardness showed some correlation with indentation modulus (R^2=0.4). Both indentation modulus (R^2=0.41) and hardness (R^2=0.35) showed a correlation with MDMB. However, indentation modulus of distinct BSUs with the same average MDMB showed differences as high as 40%. The LSI explained 40 % of the variation for hardness and 13 % of the variation of indentation modulus.
Longitudinal wave modulus obtained by SAM varied between 26.3 GPa and 52.7 GPa with a mean and standard deviation of 38.3 ±8.3 GPa and showed a correlation with indentation modulus (R^2=0.68) and with MDMB (R^2=0.7). Surprisingly, the local tissue density obtained by scanning acoustic microscopy did not show any relationship with mineral content represented by MDMB (R^2=0.018).
Table 1 shows the correlation coefficients of the mechanical and morphological data of the 86 year old female.

30-year old male:

The characterized BSU/regions of the 30-year old male showed a mineralization ranging from 1.05 to 1.28 g/cm^3 with a mean (±stdev) of 1.17±0.055 g/cm^3. For the LSI a range of 1.34 to 4.97 with an average value (±stdev) of 3.4 ±0.83 was measured.

Indentation modulus of individual BSU ranged from 18.1 to 35.3 GPa with an average (± stdev) of 24.9±4.8 GPa. Osteonal and interstitial bone did not show significant differences (p=0.2). Results for hardness varied between 0.49 and 1.04 GPa with a mean (± stdev) of 0.77±0.1 GPa. The two mechanical parameters, indentation modulus and hardness, showed a correlation of R^2=0.66.

Again BSU was a factor of high statistical significance for both hardness (p=0.0002) and indentation modulus (p<0.0001).

Neither hardness (R^2=0.06) nor indentation modulus (R^2=0.01) showed any correlation with mineral content. LSI was again a poor predictor for hardness (R^2<0.01) and indentation modulus (R^2=0.03).

The stiffness based on the SAM-scans was on average 35.5 ±4.37 GPa. The SAM-modulus showed some correlation with mineral content (R^2=0.54) but not with indentation modulus (R^2=0.01). Again the local tissue density based on the SAM-results did not show any relationship with the mineral content MDMB (R^2=0.05). See Table 1 for overview of the correlation coefficients of both donors.

Table 1: Correlation coefficients between morphological and mechanical parameters for the structures of the 30-year old male */ 86-year old female*. Coefficients above 40% are bold.

R^2 **M30 / *F86***	*E_{ind}*	*hardness*	*MDMB*	*LSI*	*SAM-modulus*	*SAM-ρ*
E_{ind}	1					
hardness	**0.66 / *0.4***	1				
MDMB	0.01 / ***0.41***	0.06 / *0.35*	1			
LSI	0.03 / *0.13*	0.003 **/ *0.4***	0.11 / *0.17*	1		
SAM-modulus	0.01 / ***0.68***	0.05 / *0.32*	**0.54 / *0.7***	0.06 / *0.09*	1	
SAM-ρ	0.18 / *0.14*	0.19 / *0.2*	0.05 / *0.02*	0.01 / *0.16*	0.08 / *0.05*	1

Global correlation for both data sets: F86 & M30:

Figure 5 left shows the indentation modulus for both data sets (donors) separately for osteonal and interstitial bone. Figure 5 right compares the LSI, SAM-modulus and MDMB. Note that the mean MDMB of the 86 year old female is 32 % higher than for the male.

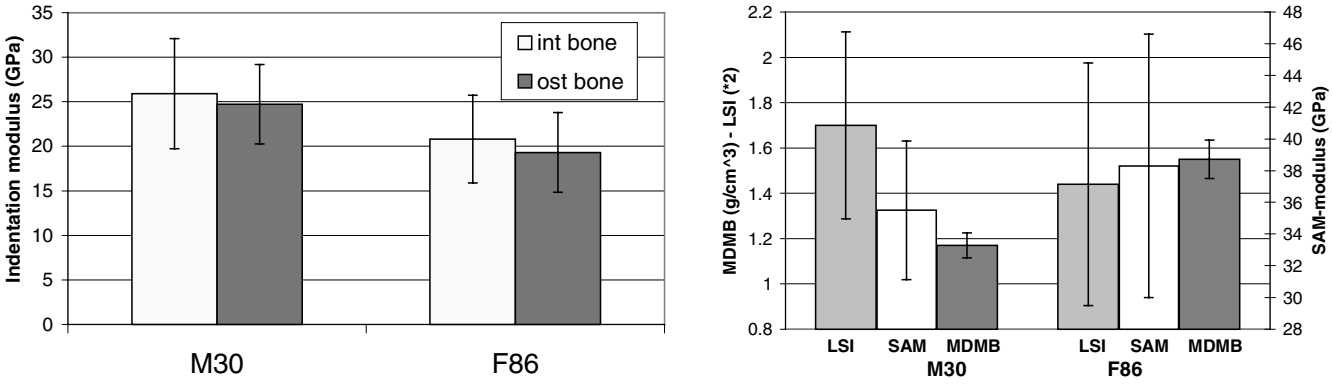

Figure 5 left: Results for indentation modulus for both donors separately for interstitial and osteonal bone. Note that the BSU of the female donor showed a 32% higher mean MDMB. **right:** Longitudinal structure index (LSI), SAM-modulus (SAM) and mineralisation (MDMB) for both donors.

Figure 6 shows the results for indentation modulus versus hardness for both donors. The correlation between these two mechanical parameters R^2=0.66 was higher for the male donor than for the female donor (R^2=0.4). For identical hardness values, the tissue from the older donor showed lower and more heterogeneous indentation moduli.

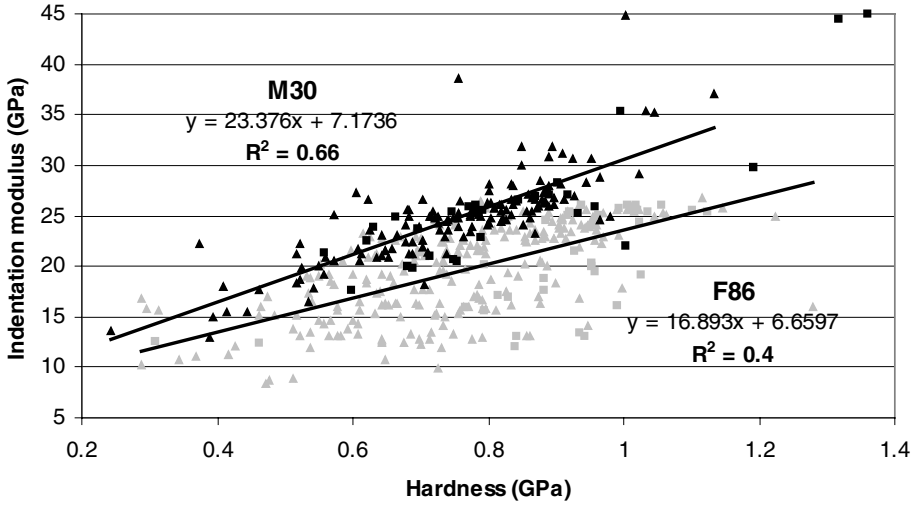

Figure 6: Correlation of two mechanical parameters indentation modulus and hardness. Black data points indicate the male donor (R^2=0.66) while bright data points represent the female (R^2=0.4). Interstitial tissue is represented by squares and osteonal bone by triangles.

Figure 7 (top) shows the SAM-modulus versus the mineral content (MDMB) and longitudinal structure index (LSI) for both donors. The two data sets result in distinct curves, both with an

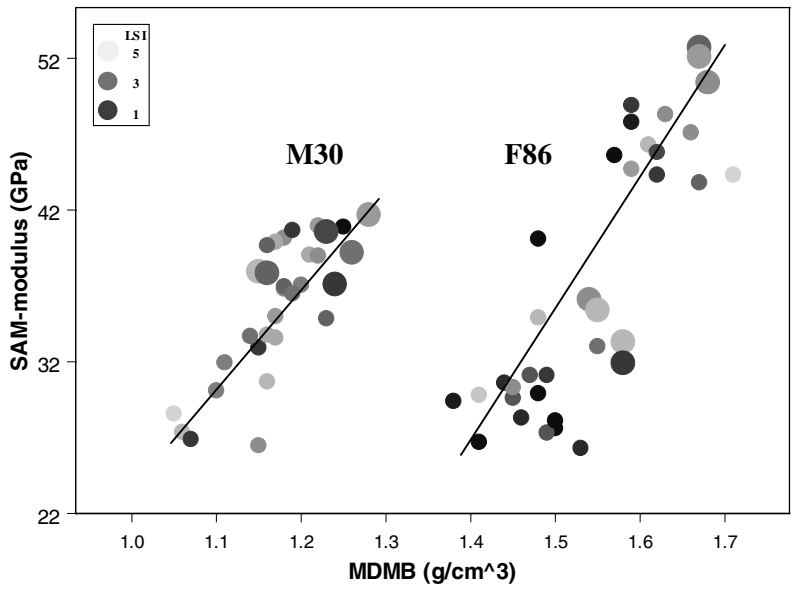

Figure 7 Mechanical parameters as a function of mineral content (MDMB) and longitudinal structure index (LSI). The two donors show distinct trends as a function of mineralisation. Small circles indicate osteons and large circles represent regions of interstitial bone. Increasing brightness of the colour represents increasing LSI.
(top): SAM-modulus as a function of MDMB and LSI.
(bottom): Indentation modulus as a function of MDMB and LSI

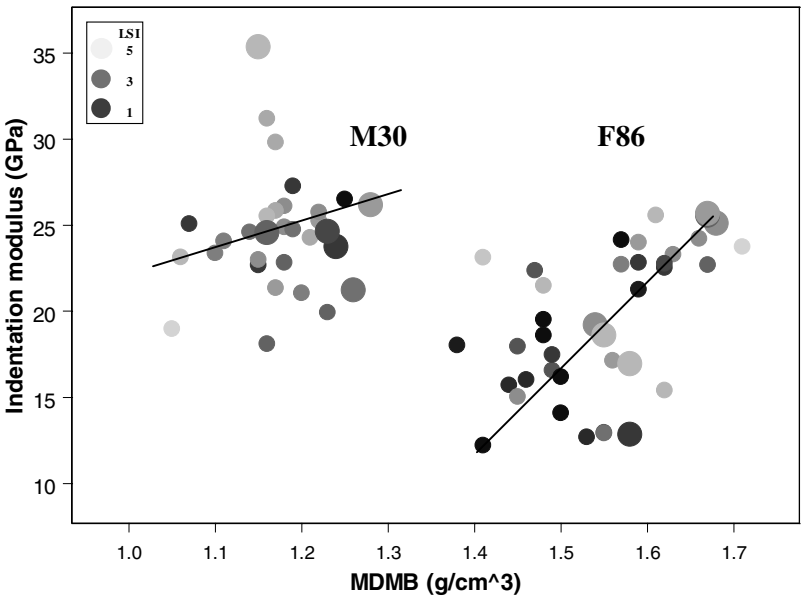

individual dependence on MDMB. Note that despite the lower mineralisation the structures of the male donor showed similar stiffness values obtained by SAM. Pooling the two data sets, the mineral content explained 15% of the global variations of the SAM-stiffness while the LSI explained only 1%.

Figure 7 (bottom) shows the results for indentation modulus as a function of both morphological parameters, MDMB and LSI. A similar pattern of the two data sets was found for hardness. Pooling both data sets, the indentation modulus and hardness showed a low correlation with longitudinal structure index (LSI), R^2=0.15 and R^2=0.13 respectively. With mineralisation, the indentation modulus showed a global correlation of R^2=0.15 (note here R=-0.39 is negative) while for hardness a value of R^2=0.07 was determined.

SAM-modulus of both data sets correlated globally to 15% with indentation modulus. Additionally, the mineral content MDMB showed a poor correspondence with SAM-density as determined by the ratio $\rho=Z/v$. Since the SAM-modulus is calculated by $C=Z^2/\rho$, we propose here a "corrected" acoustic modulus based on the measured SAM-impedance (only the back-reflected signal) and the tissue density calculated with MDMB and equation (1) and (2).

Figure 8 shows the "corrected" SAM-modulus versus indentation modulus. Please note the improvement of the correlation from 15% to 48% between the two mechanical tests. The alternative, to calculate the acoustic modulus with the measured sound speed (only transmitted signal) and the tissue density based on MDMB by $C=\rho v^2$, reduces this correlation to R^2=0.0002 !

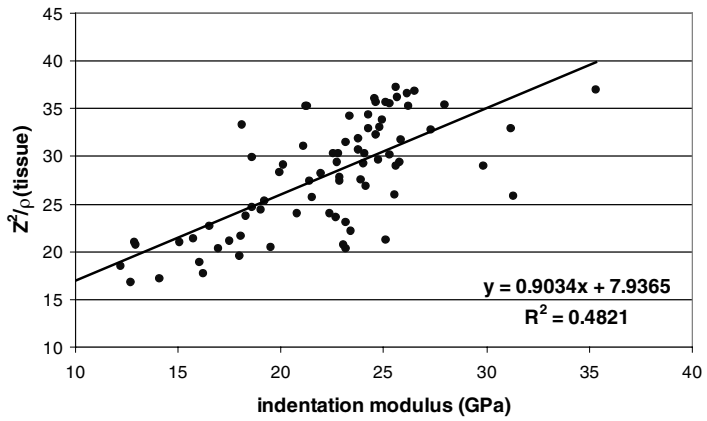

Figure 8 "corrected" SAM-modulus (with impedance Z and tissue density based on MDMB) versus indentation modulus for both data sets. This correction results in an increase in correlation from 15% to 48%.

Discussion

Biomechanical aspects: This study applied four different techniques to a set of 72 BSU and 13 regions of interstitial tissue from the femoral diaphysis of a 86 year old female and a 30 year old male. The BSUs were analysed in terms of morphology by microradiography and PLM and in terms of micromechanical properties by nanoindentation and scanning acoustic microscopy (SAM).

The high significance of BSU for both indentation modulus and hardness confirms that beside

representing the basic structural unit of the bone matrix and the associated remodeling process, the BSU represents also the homogeneous brick element of the bone construct in terms of mechanical properties. This result confirms the two basic ideas of this study a) to apply the four different characterization methods on the identical BSU and b) to consider these structural units for statistical analysis as separate samples.

The microradiography results showed distinct mineralisation levels for the two data sets. According to clinical data of the INSERM institute (Boivin, 2001), the structures of the 86-year old female had high MDMB values while for the 30-year old male the mineral content was normal. The two data sets may therefore represent two extremes not only in terms of lifetime and sex, but also in terms of compositional properties. The comparison of the mechanical properties provided two distinct curves for the two donors. Both nanoindentation and SAM confirmed that, despite the higher mineralisation level, the BSU of the female donor did not show greater mechanical properties than the BSU of the male donor.

Indentation modulus and hardness showed a higher correlation for the tissue of the 30-year old donor than for the older female. We hypothesize that reduced postyield properties like ultimate strength and energy to failure has a greater influence on hardness than indentation modulus. A decreasing correlation of these two mechanical parameters may therefore reflect decreasing tissue quality. This point should be clarified by further studies.

For each individual donor, the SAM-modulus showed a correlation with mineral content (R^2=0.54 for the male and R^2=0.7 for the female). However, pooling the two data sets, MDMB explained only 15% of the variations of SAM-modulus.

Indentation modulus and hardness showed a moderate correlation with MDMB for the structures of the female donor. Surprisingly, no correlation of the nanomechanical parameters with mineralisation was found for the tissue of the 30-year old male. Mean indentation modulus of the young donor was higher in spite of lower mineral content. This resulted in a globally poor negative correlation.

This similarily applies to the proposed quantification of the collagen fiber orientation. For the female donor, LSI correlated to 40% with the hardness results. Pooling both donors, an increasing LSI explained only 13 to 15% of the global increase of hardness and indentation modulus respectively. This finding may be supported by Martin who reported a positive trend between LSI and macroscopic postyield properties (Martin & Ishida, 1989) . However, LSI does not sufficiently enlighten the question why the BSUs of the two donors show distinct trends with mineralisation.

The reported importance of these two morphological factors for the macroscopic level could not be confirmed by our data obtained at the BSU level. A great limitation of this study is evidently the inclusion of only two (quite different) donors. We indeed believe that tests of further donors will result in a positive general trend of the mechanical data with mineralisation. However, this

limited data set allows the statement that further factors probably play an important role. As it can be seen in Figure 7, BSU of identical MDMB and similar LSI of a single donor can show 40% variation of mechanical properties. This variation within a single donor will probably remain unclear if the continuation of this study only accounts for an extension of donors.
These findings suggest that ultrastructural properties, like the quality of the collagen meshwork may play an important role. Zioupos (2001) reported a moderate but significant correlation of the collagen shrinkage temperature with age. This parameter gives an estimate of the mechanical stability of the collagen meshwork that maybe quite different for the 56 year elder female donor. It is also possible that the cross-links between the collagen fibers are of importance for the mechanical properties. However, studies focussing on the influence of these hydroxypyridinium links reported controversial results (Oxlund et al, 1995; Zioupos, 2001).
The spatial arrangement of the hydroxyapatite platelets may be of high importance. Discussing Small-Angle-X-Ray-Scattering (SAXS) data on bovine bone, Sasaki (Sasaki et al, 1991) found that the HAP-platelets show a global orientation along the long axis of the bone. The relative amount of hydroxyapatite crystals with this orientation may somehow vary between different BSUs and lead to different mechanical properties. The mechanical bonds of the mineral to the organic matrix may also influence the mechanical properties of the individual BSU. Targeting a study on the electronic structure of the bone material, Dekhtyar (Dekhtyar et al, 1998) recently recognized the latter point. In this perspective, the matrix of the older tissue may have reduced its capacity to bind the apatite crystals. This effect could be responsible for the fact that the tissue of the female donor did not have greater mechanical properties than the young tissue in spite of the greater mineralisation. The study of Evans, who reported quite different mechanical properties for bone tissue and a bone analogue of identical hydroxyapatite content, support this point. He attributed this discrepancy to the differences how bone tissue and the bone analogue bind the HAP-crystals (Evans et al, 1990).
Saturation often called hypermineralisation may have occurred in the tissue of the female donor. Amprino, who addressed this aspect in his study reported a decrease of microhardness above a certain level of mineralization (Amprino, 1958).
Concluding the biomechanical aspects of this discussion, we may suggest for further study to extend - apart of the number of donors - also the spectrum of techniques to characterize the tissue morphology.

Technical aspects A correction of SAM-modulus was obtained by employing the tissue density based on MDMB. The correction was greater, when the tissue density (based on MDMB) was combined with impedance Z instead of the propagation speed v. This implies the occurrence of artifacts that differently affect the measured reflectivity of the upper surface and the propagating sound signal. It is possible that dispersion of the sound wave leads to an altered propagation

speed, an effect that is not considered by these formulae. Dispersion is a frequency-dependent phenomenon of waves that strongly depends on the absorption properties of the propagation medium and does not reflect elasticity.

In spite of those corrective steps, the correlation between the acoustic measurements and the nanoindentation tests remains a moderate 48%. Hoffler et al (1999) also detected a weak correlation of 34% between the SAM-modulus (applying 150 MHz) and indentation modulus. A main effect is probably due to the different spatial resolution that these two tools provide. The acoustic measurements are based on pulses with 30μm wave length (50 MHz in water) and each data point represents an average that is also strongly influenced by the vascular porosities while nanoindentation at 1μm depth characterizes lamellar packets.

Indentation modulus for the 86-year old female was about a factor two and for the 30-year old male about a factor 1.4 lower than SAM-modulus. Taking into account that the indentations were done on the dried sample and the acoustic measurements under fully wet conditions may even increase these factors by approximately 70% (see chapter 2b). Equations (4) and (7) show that both stiffness values represent a different combination of Young's modulus and Poisson ratio. Setting equation (7) into (4) and assuming a Poisson ratio of $\nu=0.3$ shows that $C=1.23*E_{ind}$ that does not sufficiently explain this difference. To clarify this point the frequency-dependent response of the collagen fibers should be considered. Mechanical tests of rat-tail tendon at a quasi-static strain rate obtained a longitudinal Young's modulus of approximately 1 GPa (Cusack & Miller, 1979). An ultrasonic wave propagation study applying 100 MHz reported a value of 4 GPa for the longitudinal modulus of mouse tail tendon (Cusack & Miller, 1979). This increase of stiffness by a factor four when varying the strain rate by several orders of magnitude may explain the different absolute values obtained by nanoindentation and SAM. It is therefore very likely that the viscoelastic behavior of the collagen fibers plays a major role at the strain rates applied by acoustic measurements.

A further important technical aspect pertains to polarized light microscopy. We suggest a critical use of the longitudinal structure index as parameter to characterize a mean collagen orientation. The absolute angle to which the polarisation plane of the light is rotated should be proportional to the thickness of the sample. Since the intensity varies with $I \propto sin^2(\Theta)$ with the rotation angle Θ, the birefrigence of structures become lower or may even disappear when a certain sample thickness is exceeded. A quantification with LSI can only be appropriate for rotation angles between 0 and $\pi/2$. It could help to take PLM-images of the same region for different sample thicknesses. Optical activity is a frequency-dependent phenomenon, which suggests employing monochromatic instead of white light.

Concluding the technical aspects of this discussion, we suggest extension of the knowledge of the two techniques SAM and PLM. This helps to avoid misleading interpretation of data that are strongly influenced by artifacts.

References

- Ascenzi A (1988) The micromechanics versus the macromechanics of cortical bone - a comprehensive presentation. J Biomech Eng **110**:357-363
- Amprino R (1958) Investigations on some physical properties of bone tissue. Acta Anatom **34**:161-168
- Boivin GY, Chavassieux PM, Santora AC, Yates J, Meunier PJ (2000) Alendronate increases bone strength by increasing the mean degree of mineralization of bone tissue in osteoporotic women. Bone **27/5**:687-694
- Boivin GY (2001) private communication
- Briggs A (1992) Acoustic microscopy, Clarendon Press Oxford
- Carter DR, Hayes WC (1977) The compressive behavior of bone as a two-phase porous material. J Bone Jt Surg **59A**:954-962
- Currey JD (1988) The effect of porosity and mineral content on the Young's modulus of elasticity of compact bone. J Biomech **21/2**:131-139
- Cusack S, Miller A (1979) Determination of the elastic constants of collagen by Brillouin light scattering. J Mol Biol **135**:39-51
- Dekhtyar Y, Katashev A, Mironova N, Noskov V, Pavlenko A (1998) Electron structure of bone affects its mechanical properties. Proceedings ESB 1998
- Eriksen EF, Axelrod DW, Melsen FM (1994) Bone Histomorphometry. 1ed. Raven Press Ltd, New York
- Evans GP, Behiri JC, Currey JD, Bonfield W (1990) Microhardness and Young's modulus in cortical bone exhibiting a wide range of mineral volume fractions, and in a bone analogue. J Mat Sc: Mat Med **1**:38-43
- Gebhardt, 1906 über funktionell wichtige Anordnungsweisen der feineren und gröberen Bauelemente des Wirbeltierknochens. II. Spezieller Teil.: der Bau der Haversschen Lamellensysteme und seine funktionelle Bedeutung. Arch Entw Mech Org **20**:187-322
- Hodgskinson R, Currey JD, Evans GP (1989) Hardness, an indicator of the mechanical competence of cancellous bone. J Orthop Res **7**: 754-758
- Hoffler CE, Zhang N, Kozloff KM, Grimm MJ, Goldstein SA (1999) Comparison of scanning acoustic microscopy and nanoindentation measures of the elastic properties of human bone lamellae. Proceedings ASME 1999
- Martin RB, Ishida J (1989) The relative effects of collagen fiber orientation, porosity, density and mineralization on bone strength. J Biomech **22/5**: 419-426
- Meunier PJ, Boivin G (1997) Bone mineral density reflects bone mass but also the degree of mineralization of bone: therapeutic implications. Bone **21**:373-377, 1997
- Oliver WC, Pharr GM (1992) An improved technique for determining hardness and elastic modulus using load and displacement sensing indentation experiments. Mat Res Soc **7/6**:1564-1583
- Oxlund H, Barckman M, Ortoft G, Andreassen TT (1995) Reduced concentrations of collagen links are associated with reduced strength of bone. Bone **17/4**:365-371
- Sasaki N, Ikawa T, Fukuda A (1991) Orientation of mineral in bovine bone and the anisotropic mechanical properties of plexiform bone. J Biomech **24/1**:57-61
- Weiner S, Traub W (1992) Bone structure:from angstroms to microns. FASEB J **6**:879-885
- Zioupos P (2001) Ageing human bone: factors affecting its biomechanical properties and the role of collagen. J Biomat App **15**:187-229

Chapter 5
How is the indentation modulus of bone tissue related to its macroscopic elastic response? A validation study

Introduction

Nanoindentation, which evolved from the traditional Vicker's hardness test, has been established as a characterization method of mechanical properties of bone tissue down to the lamellar level. Among recent work, differences were reported between donors, anatomical sites, microstructures (Hoffler et al, 2000a & b; Zysset et al, 1999), BSU and bone lamellae (Rho et al, 1999d; Hengsberger et al, 2002).

However, it still remains unclear how the indentation modulus can be converted into the elastic response of the bone tissue on the macroscopic level. The strong motivation behind this issue pertains to the potential to understand mechanical competence of whole bones in the light of its bone structural units resulting from its metabolic activity.

The elastic recovery that is measured when the nanoindenter is unloaded can be attributed to an average response of the tissue extracellular matrix and the canalicular porosity. On the other hand, the mechanical properties on the bone tissue level are influenced by porosities due to lacunae, vascular canals and resorption sites. Carter & Hayes (1977) reported for both cancellous and compact bone that Young's modulus depends on a power law of the porosity. A first naive approach may therefore consider the intrinsic tissue properties weighted by a power law of the intervening porosities in order to achieve the macroscopic response. For human femoral bone, Rho et al (2001) has recently reported a high and significant correlation between the macroscopic bending modulus and a variable including indentation modulus, the relative area covered by osteonal and interstitial bone, and porosity. However, Rho did not provide a way to convert the indentation modulus into an absolute Young's modulus of the macroscopic sample. For this purpose the employed tissue properties must be representative for the entire macroscopic sample. The problem arises that the nanoindentation tests represent local material properties that make a representative characterization of heterogeneous structures difficult. The homogeneous bovine bone with a low presence of secondary osteons represents a good choice for this issue.

A further aspect concerns the characterization of anisotropic bone tissue by nanoindentation and other mechanical tests. The indentation modulus represents some weighted average of the material properties in all directions that raises difficulties for comparisons with other mechanical tests. Fan et al (2001) solved this problem by basing a numerical simulation of the indentation experiment on stiffness values provided by ultrasonic measurements.

The objective of this work was to validate if an identical longitudinal matrix modulus could be derived from a traction test of a microsample when the porosity is considered and indentation tests when the aforementioned anisotropy effects are corrected.

For this purpose traction tests of cylindrical microsamples of 4 mm in length and 300 micrometer in diameter were performed (Section A). The microsamples were further analyzed in terms of porosity by 3D-tomography applying synchrotron radiation (Section B). The results of the traction test and the porosity of the sample were employed to calculate a longitudinal matrix modulus.

The microsamples were then characterized by nanoindentation in a longitudinal and in a transverse plane (Section C). A recently developed numerical algorithm was then employed to calculate a longitudinal matrix modulus based on the nanoindentation data (Section D).

Finally the longitudinal matrix moduli as obtained by the traction experiments and the tomography scans were compared with the longitudinal matrix moduli obtained by nanoindentation and the numerical code.

Materials and Methods

Three cortical bone specimens were dissected from the femoral diaphysis of a cow and dried for 24 hours at 50° Celsius. The samples were milled down to cylindrical shape of 12mm length and 2mm diameter, their long axis being aligned with the longitudinal direction of the diaphysis.

After this preparatory step the specimens were installed on a combined lathe and traction machine (Figure 1). This device allows for both milling down the central part of the cylindrical specimen to a smaller diameter and performing a traction test. Figure 2 represents the resulting microsample where the central part of 4 mm length was milled down to a diameter of approximately 300 micrometer.

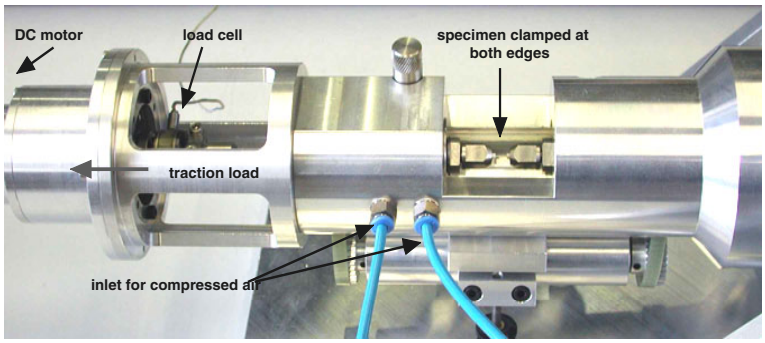

Figure 1 Photo of the combined lathe and traction machine for microsamples. A cylindrical specimen can be milled and tested in traction afterwards without further manipulation. During the traction test, a DC motor drives a moving bar applying a load to one extremity of the sample (moving end). The other extremity of the specimen is fixed (fixed end). The load cell provides the force signal. The resulting strain is determined with help of an optical microscope (see Text). Compressed air reduces internal friction of the machine.

A: Traction test of the microsample

During the traction test a force is applied to an extremity of the specimen while the axial movement of the other extremity is fixed (see Figure 1 and 2 left). A 10 N transducer acquires the force signal while the resulting strain is determined optically. A digital camera is attached to an optical microscope and provides pictures of the spots A and B (see rectangles in Figure 2 left) at 250 micrometer field of view. A commercially available software package (IMAC-Vision) performs image correlation routines that allow determining the absolute displacement of both extremities as a function of the applied force (See Figure 2 right). The difference in slope of these two "displacement versus force"-curves corresponds to the compliance $\frac{\Delta l}{F}$. This is the ratio between the absolute deformation of the bone matrix between the spots A and B and the applied force. Section B demonstrates the calculation of the longitudinal apparent and matrix modulus based on this parameter $\frac{\Delta l}{F}$ and the 3D tomography scans. A tensile test consisted of loading in five steps up to 0.3% strain applying a strain rate of $\dot{\varepsilon} = 10^{-4}/s$ followed by five unloading steps. Between successive steps a holding period of 60 seconds was applied and pictures of the actual position of the spots A and B were done. Each experiment was preceded by ten preconditioning tests up to 0.3% strain in order to reach reproducible deformation. A proper calibration of the traction machine was validated with a polycarbonate sample. Tests with a commercial MTS traction system showed a mean Young's modulus of 2.37 GPa that compared favourably with the 2.31 GPa as obtained by the microtraction machine. Please see the report of J. Enstroem (Enstroem, 2001) for more detailed information.

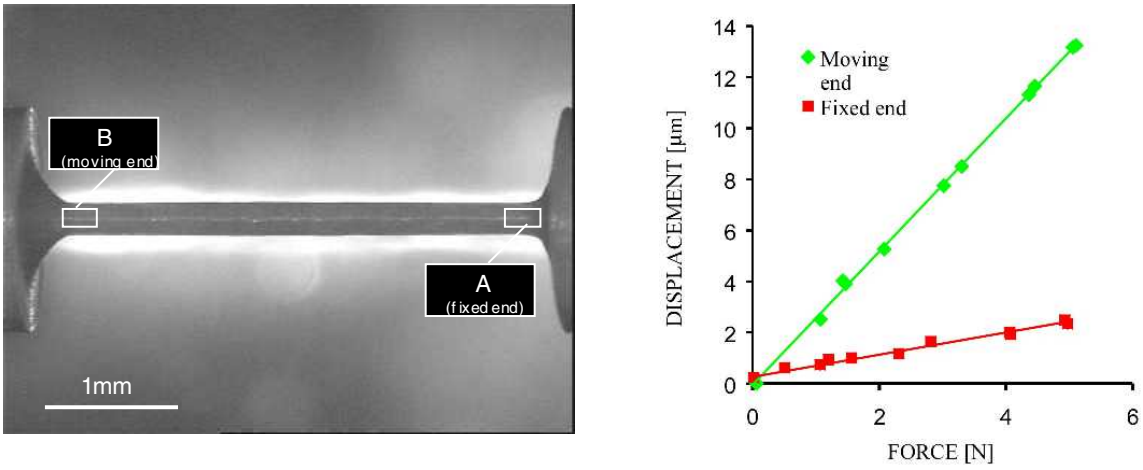

Figure 2 left: Microsample of bovine cortical bone at 5mm field of view. For the determination of the strain, the displacement of the spots A (moving end) and B (fixed end) are observed at 250µm field of view (rectangles). **right:** Displacement versus force curve for both extremities, the moving end where the force is applied and the fixed end. Note the non-negligible displacement of the fixed end. The strain is determined by the difference of the slope of these curves. Note that this allows calculation of the apparent and matrix modulus of the bone matrix volume between these two spots. This avoids the influence of artifacts due to the specimen clamps.

B: μCT-measurements applying synchrotron radiation

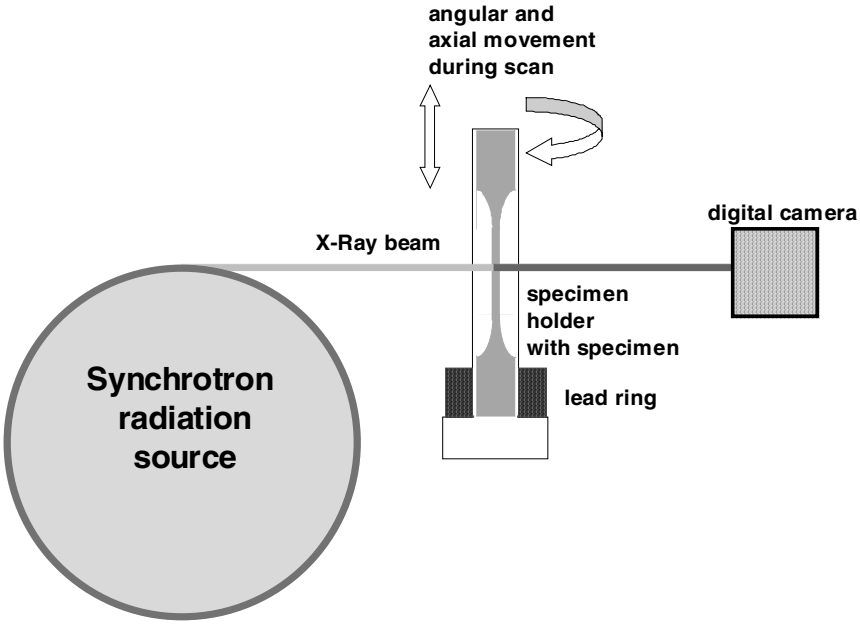

Figure 3: Setup of the 3-dimensional reconstruction experiment. The long axis of the sample is installed perpendicular to the incident X-ray beam. The system manipulator allows for axial and angular movement of the sample while a digital camera acquires 2-dimensional absorption images. A lead ring covers a small volume of the sample that is used for characterization by nanoindentation (the components are not drawn to scale).

The characterization of the vascular and lacunar porosity was performed with 3D synchrotron tomography attached to a beamline of the European Synchrotron Radiation Facility (ESRF/Grenoble).

The bone sample is installed on a stage that allows for angular and axial movement. Hereby the long axis of the cylindrical specimen is perpendicular to the incident photon beam (see Figure 3). The installation includes a FRELON camera providing images with 1024x1024 pixels at 0.95mm field of view. Due to a specimen length of 4mm and the confined field of view of the camera, each specimen was measured in 5 successive scans, whereby each the specimen was shifted axially by 0.95mm. During a scan the specimen is turned around its longitudinal axis for a range

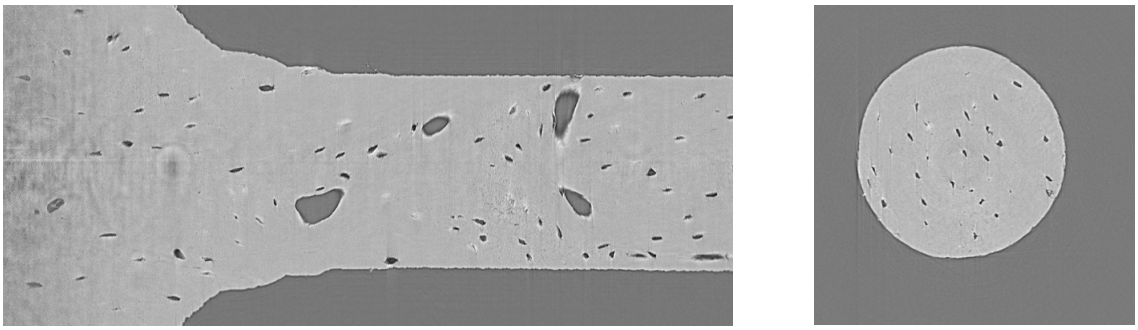

Figure 4 Slices of a 3-dimensional reconstruction of a bovine bone sample: longitudinal cut (left) showing a 650μm x 400μm window where the increasing diameter of the sample close to an extremity can be seen. The right picture shows a transverse cut of 400μm x 400μm size.

of angles between 0° and 180°. At each angular position the digital camera provides a two-dimensional absorption image.

For the three bovine samples a photon energy of 12keV was selected and the samples were turned in steps of 0.2° while the exposure time for each two-dimensional absorption image was set to 2 seconds. The spatial resolution of approximately 0.95 micrometer is determined by the number of voxels and the field of view of the digital camera. A lead ring was set on the sample to protect a small volume close to an extremity of the microsample against radiation (see Figure 3). This part was used for characterization by nanoindentation.

Based on the two-dimensional absorption images, a 3D-reconstruction was calculated. The gray level of the reconstruction is directly proportional to the local X-ray attenuation coefficient $\eta(12keV)$ of each volume element at this photon energy. To quantify the mineral content of the

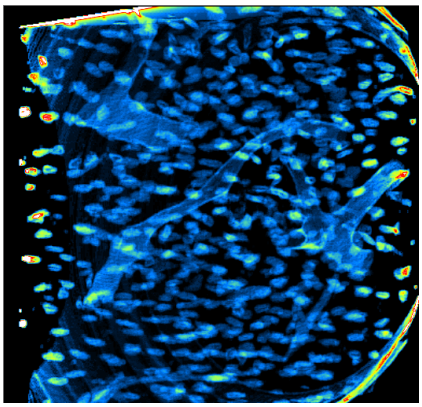

Figure 5: Volume of 400x400x128 μm^3 containing 128 adjacent transverse cuts (see Figure 3 right). The gray levels were segmented and inverted to show the contours of the porosities. The smaller porosities represent lacunae and the larger porosities may be due to resorption sites, Volkmann or Haversian canals.

bone samples, an aluminum sample of known attenuation coefficient $\eta(12keV) = 41.42 \frac{1}{cm}$ was scanned with identical measurement parameters.

Figure 4 represents a longitudinal (left) and transverse (right) cut of a three-dimensional reconstruction. The longitudinal cut includes the sample extremity where the diameter increases. The dark areas within the bone matrix can be attributed to lacunar, vascular and resorption porosities while the canaliculae are beyond the spatial resolution. Figure 5 shows a volume containing 128 adjacent transverse cuts where the gray levels of the bone matrix and the porosity were first segmented and then inverted. Note the presence of lacunae (ellipsoidal shape), vascular canals and resorption sites.

Based on the three-dimensional reconstruction, the apparent Young's modulus of the microsample was determined. For this purpose, a segmentation of the gray levels was performed to distinguish the matrix from the porosities and the background. The following integration over the total length *L* of the sample was done:

$$E_3^{app}(traction) = \frac{F}{\Delta l} \sum_{k=1}^{\frac{L}{ds}} \frac{1}{A_k} ds \tag{1}$$

Here *ds*=0.95µm represents the thickness of each transverse slice and *L/ds* the number of slices. A_k represents the bone cross-section of each slice including the porosities and $\frac{F}{\Delta l}$ is the ratio of the applied force and the relative strain that is supplied by the traction test (see Section A). This parameter is called "apparent modulus" since it only accounts for the outer dimensions of the bone sample.

For the calculation of the matrix modulus the bone sample was divided into N=35 sections containing 128 slices. Based on the assumption that the stiffness varies as a quadratic power law of the volume fraction (Zysset et al, 1994; Rice et al., 1988), each section was weighted with its individual average volume fraction $\rho = 1\text{-}porosity$ raised to the power of two. The contributions of the sections were finally summed up:

$$E_3^{matrix}(traction) = \frac{F}{\Delta l} \sum_{i=0}^{N-1} \frac{1}{\rho_i^2} \sum_{j=1}^{128} \frac{1}{A_k} ds \qquad \text{with } k=i*128+j \tag{2}$$

C: Nanoindentation in transverse and longitudinal directions

After the three-dimensional reconstruction experiments the bovine samples were tested by nanoindentation. The indents were done on transverse and longitudinal cuts of the volume that was protected against radiation by the lead ring during the scan. The resulting slices were polished with successive grades of carbide paper, finished with 0.25µm diamond paste and again dried for 24 hours at 50° Celsius. On each bovine sample 40 indents were done, 20 in the longitudinal and 20 further indents in the transverse direction. The indents were run to 900nm maximum depth that was followed by a 5 seconds holding period. The indentation modulus was derived from the unloading part applying an approximate strain rate of $\dot{\varepsilon} = 0.066 / s$. This parameter represents a combination of the local isotropic Young's modulus and Poisson ratio (Oliver & Pharr, 1992) with

$$E_{ind} = \frac{E^{Young}}{1 - \nu^2} \tag{3}$$

D: Predicted modulus calculated with the Swadener and Pharr model

The experimental indentation modulus represents a weighted average of the elastic properties in all directions. The following procedure was employed to derive a longitudinal matrix modulus from indentations in longitudinal and transverse direction.

A recently developed model (Swadener & Pharr, 2001) was applied that is based on the following equation that holds for an indentation on an anisotropic elastic halfspace by a rigid frictionless cone.

$$E_{ind} = \frac{4\pi}{\int_0^{2\pi} \left\{ a_{3i} B_{ij}^{-1} a_{3j} / \left[\frac{a_1}{a_2} cos^2\gamma + \frac{a_2}{a_1} sin^2\gamma \right]^{1/2} \right\} d\gamma} \tag{4}$$

Here a_{ij} indicate the direction cosines of the angles between the indentation direction and the coordinate system of the elastic stiffness tensor. The components B_{ij} derive from the first Barnett Lothe tensor (Barnett & Lothe, 1976) and depend on the elastic stiffness tensor $\mathbb{C}_{ijkl}$ of the material. The ratio between a_1 and a_2 is determined iteratively and represents the eccentricity of the contact area that is elliptical for anisotropic materials. This ratio depends also on B_{ij} and therefore on the elastic stiffness constants. Equation 4 holds for a conical indenter with an included semi-angle close to α=90°. Based on a finite-element analysis, Hay et al (1999) has shown that errors of 6% occur for a tip with $\alpha \approx 70°$ (close to Berkovich geometry) indenting an isotropic medium with a Poisson ratio of ν=0.25.

This model calculates the indentation modulus from a complete set of mechanical constants. Please note, that in this context the (experimental) indentation modulus is known and the model has to be used to extract a tensorial component. For this purpose, the following transverse isotropic compliance tensor was assumed for the bovine bone specimens (Cowin, 1989).

$$\mathbb{Q} = \frac{1}{\varepsilon_o} \begin{bmatrix} \frac{1}{m_1^2} & -\frac{\nu_o}{m_1^2} & -\frac{\nu_o}{m_1 \cdot m_3} & 0 & 0 & 0 \\ -\frac{\nu_o}{m_1^2} & \frac{1}{m_1^2} & -\frac{\nu_o}{m_1 \cdot m_3} & 0 & 0 & 0 \\ -\frac{\nu_o}{m_1 \cdot m_3} & -\frac{\nu_o}{m_1 \cdot m_3} & \frac{1}{m_3^2} & 0 & 0 & 0 \\ 0 & 0 & 0 & \frac{(1+\nu_o)}{m_1 \cdot m_3} & 0 & 0 \\ 0 & 0 & 0 & 0 & \frac{(1+\nu_o)}{m_1 \cdot m_3} & 0 \\ 0 & 0 & 0 & 0 & 0 & \frac{(1+\nu_o)}{m_1^2} \end{bmatrix} \tag{5}$$

This tensor is reduced to three parameters: bone matrix anisotropy $(m_3/m_1)^2$ and the two intrinsic constants ν_o and ε_o. The eigenvalues m_1 (=m_2) and m_3 of the texture tensor are mathematically bound by $\sum_{i=1}^{3} m_i = 1$ and indicate with $\frac{\varepsilon_3}{\varepsilon_1} = \frac{\varepsilon_3}{\varepsilon_2} = \frac{m_3^2}{m_1^2}$ the anisotropy of the mechanical constants in the principal directions. This tensor was originally derived from an experimental data set of bovine trabecular bone (Zysset, 1994). However, Zysset could show that for volume fractions of ρ=0.9 this tensor gives an excellent approximation for the elastic constants of bovine cortical bone. The numerical model was used to derive the component $1/Q_{33}=\varepsilon_o(m_3)^2$ (the longitudinal matrix modulus) from the indentations. For this purpose, the program code from Swadener and Pharr was performed for several anisotropy ratios $\frac{m_3^2}{m_1^2}$ between *1* and *4* setting ν_o*=0.32* and ε_o*=1*.

The following fit was found between the eigenvalues m_1 and m_3 and the anisotropy ratio of the indentation modulus:

$$\left(\frac{m_3}{m_1}\right)^2 = 0.998 \cdot \left(\frac{E_{ind}(long)}{E_{ind}(trans)}\right)^{1.612} \tag{6}$$

This fit allows calculation of the intrinsic anisotropy of the bone matrix based on the indents in the longitudinal and transverse direction.

A further fit was performed of the absolute longitudinal and transverse indentation moduli (as multiples of the intrinsic constant ε_o) with dependence on the bone matrix anisotropy (see Figure

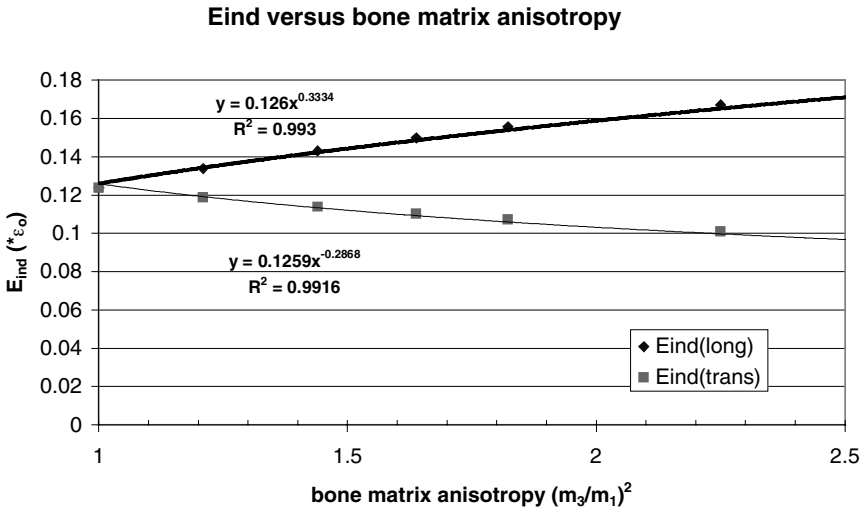

Figure 5: Longitudinal (diamonds) and transverse (squares) indentation modulus as multiples of the intrinsic constant ε_o for different bone matrix anisotropy ratios. The power fits are indicated near the respective curves.

5). Based on this fit, the constant ε_o can be calculated with:

$$\varepsilon_o = 7.94 E_{ind}^{long} \cdot \left(\frac{m_3}{m_1}\right)^{-0.67} = 7.94 E_{ind}^{trans} \cdot \left(\frac{m_3}{m_1}\right)^{0.57} \quad (7)$$

The eigenvalues m_1 and m_3 and the intrinsic constant ε_o can therefore be derived from the ratio and the absolute values of the transverse and longitudinal indentation moduli. A longitudinal matrix modulus can then be derived by

$$E_3^{matrix}(nano) = \varepsilon_o (m_3)^2 \quad (8)$$

Results

A: Traction test

Table 2 (left column) presents the results of the displacement versus force curves of the traction tests. The parameter $\frac{\Delta l}{F}$ is the difference of slopes of the moving and the fixed end and will be used to calculate the apparent and matrix modulus with equation (1) & (2). The error due to the optical determination of the strain was calculated to be 5.9%, while the error of the force transducer was negligible (Enstroem, 2001).

B: Mineral content, outer diameter and porosity derived from μCT-scans

The three bone samples exposed a similar and very homogeneous mineralisation. The ratio of the attenuation coefficient and the density of pure hydroxyapatite $Ca_{10}(PO_4)_6(OH)_2$ for 12keV photon energy is given by $\frac{\eta}{\rho^{HAP}} = 28.2 \frac{g}{cm^2}$ (Nuzzo, 2001). Table 1 shows the measured attenuation coefficients of the bone matrix and the corresponding mineral content for a density of hydroxyapatite of $\rho^{HAP} = 2.8 \frac{g}{cm^3}$ (Nuzzo, 2001). Bovine 7 with 1.41g/cm^3 had the lowest mineralisation while the mineral content was higher in bovine 8 with 1.5g/cm^3 and bovine 10 with 1.48g/cm^3.

	attenuation coefficient η [1/cm]	mineralisation of matrix [g/cm^3]
bovine 7	39.75 ±1.6	1.41 ±0.06
bovine 8	42.4 ±0.8	1.5 ±0.03
bovine 10	41.8 ±0.8	1.48 ±0.03

Table 1: mean attenuation coefficient of the bone matrix and the corresponding mean mineral content of the three bovine samples. Note the low standard deviations indicating a very homogeneous mineralisation.

Figure 6 shows the outer diameter (left) and the porosity (right) along the length of the microsample bovine 10. The porosity is averaged over 128 adjacent slices. Bovine 10 showed a porosity of Φ=3.1±0.95%, bovine 7 Φ=3.4±1.4% and bovine 8 of Φ=3.1±1%. Table 2 summarizes the results of the traction experiments and the 3D tomography scans. The apparent modulus was calculated by integrating the outer dimensions of the sample (see equation 1). The matrix modulus is derived by additionally taking into account a power law of the porosity (see equation 2).

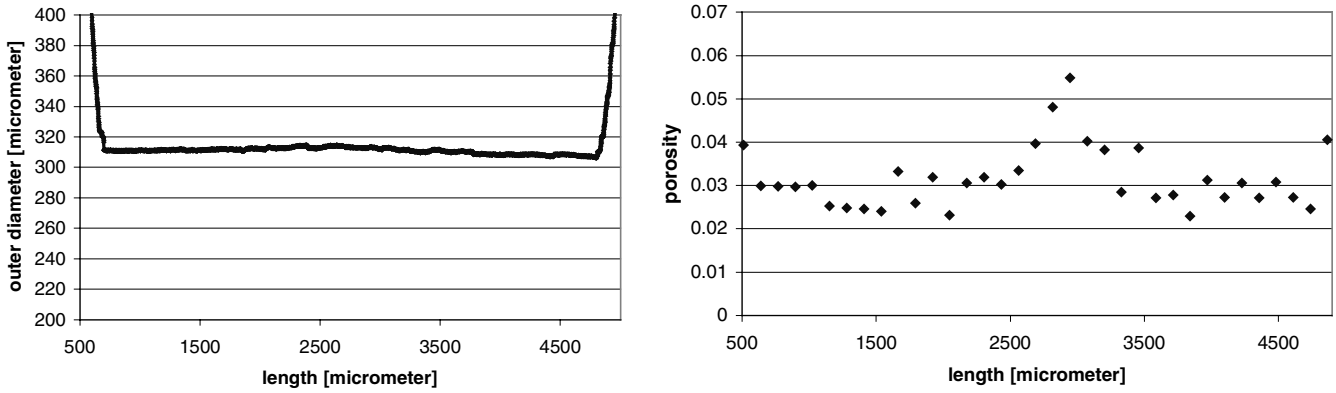

Figure 6: left: outer diameter of the microsample bovine10 as determined by the µCT-scans. **right**: porosity of the microsample bovine10. Each data point represents an average of 128 adjacent slices.

	$\frac{\Delta l}{F}$	$E_3^{app}(traction)$	$E_3^{matrix}(traction)$
bovine 7	*2.82 ±0.17 µm/N*	20.3 ±1.2	22.1 ±1.3
bovine 8	*2.92 ±0.17 µm/N*	27.6 ±1.6	30.0 ±1.8
bovine 10	*1.98 ±0.12 µm/N*	26.0 ±1.5	28.2 ±1.7

Table 2: Summary of the traction test results and the 3D-reconstructions. The parameter $\frac{\Delta l}{F}$ is supplied by the traction experiment. Taking into account the outer diameter of the bone sample, the apparent modulus (middle) was calculated. The matrix modulus (far right) derived by additionally taking into account the porosity of the sample. The error margins of 5.9% were determined by taking into account the error of the optical strain measurement.

C: Nanoindentation results:

Table 3 and Figure 7 show the results of the nanoindentations in transverse and longitudinal direction for the three bovine bone samples.

		E_{ind} *(GPa)*
bovine 7	long	22.1 ±3.6
	trans	18.6 ±1.5
bovine 8	long	27.9 ±3.1
	trans	20.7 ±1.2
bovine 10	long	31.6 ±3.3
	trans	23.7 ±3

Table 3 (top) & Figure 7 (bottom): Nanoindentation results in transverse and longitudinal direction for the three samples. For bovine 10 the longitudinal indentation modulus was $E_{ind}^{long} = 31.6 \pm 3.3\,GPa$, 33% greater than the transverse indentation modulus $E_{ind}^{trans} = 23.7 \pm 3\,GPa$. The sample bovine 7, 22.1 ±3.6 GPa, showed the lowest longitudinal indentation modulus.

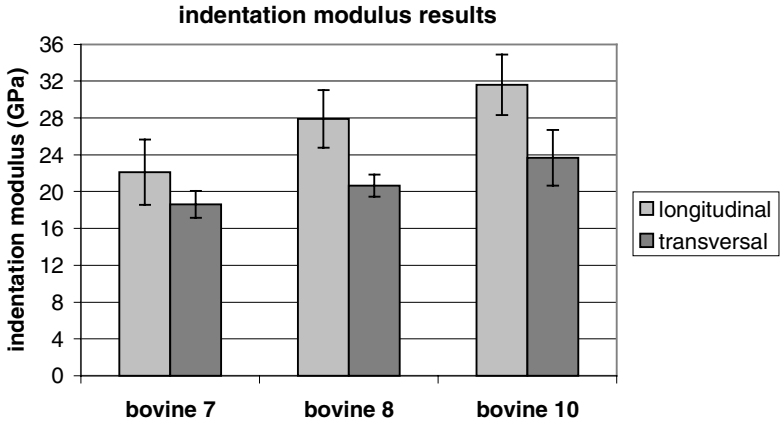

D: Calculated matrix modulus based on nanoindentation

Table 4 represents the bone matrix anisotropy derived from equation (6) based on the ratio of the longitudinal and transverse indentation modulus.

	E_{ind} anisotropy	calculated bone matrix anisotropy $(m_3/m_1)^2$
bovine 7	1.19	1.32
bovine 8	1.35	1.62
bovine 10	1.33	1.58

Table 4: Bone matrix anisotropy (right) for the three bovine samples derived from the indentation modulus anisotropy (left) and equation (6).

With help of equations (7) & (8) the matrix modulus $E_3^{matrix}(nano)$ was calculated. Table 5 and Figure 8 show the matrix modulus derived from the nanoindentation tests in combination with the model of Swadener & Pharr (Section C&D). This is compared with the matrix modulus derived from the traction experiments in combination with the 3D tomography scans (Section A&B). Note that the results for sample bovine 7 and bovine 8 match within the error bars. For bovine 10 the longitudinal matrix modulus derived from the nanoindentation tests was 13% higher than from the traction test.

	$E_3^{matrix}(nano)$	$E_3^{matrix}(traction)$
bovine 7	21.29 ±3.5	22.1 ±1.3
bovine 8	28.53 ±3.2	30.0 ±1.8
bovine 10	32.0 ±3.4	28.2 ±1.7

Table 5 & Figure 8: Comparison of the longitudinal matrix modulus derived from the nanoindentation tests and the model developed by Swadener & Pharr (Section C&D) with the matrix modulus determined from the traction tests and the 3D tomography scans (Section A&B). Note the high correlation for bovine 7 and bovine 8.

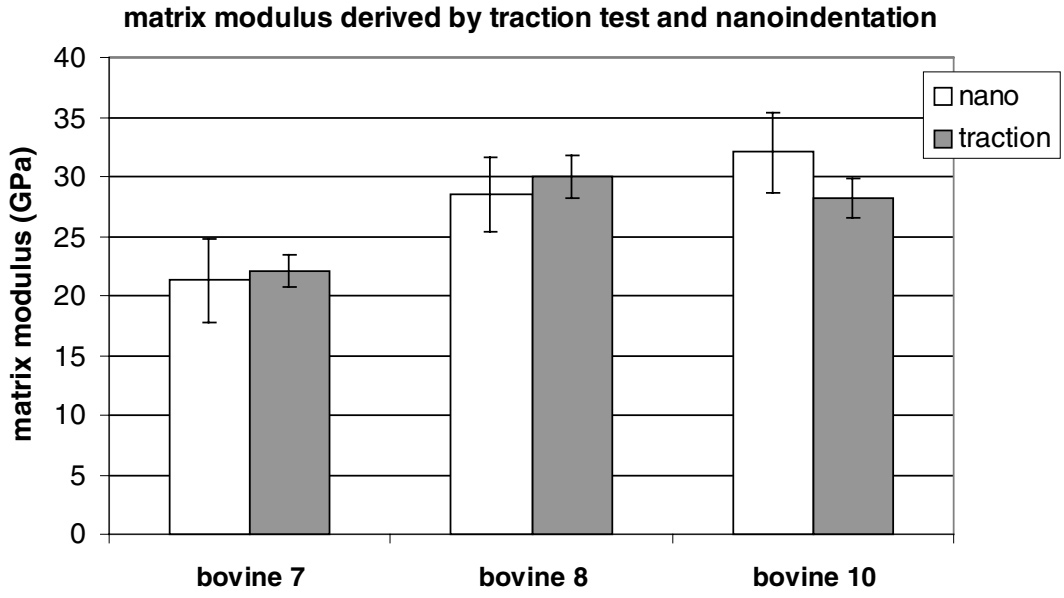

Discussion

For this project we successfully machined a set of three bovine microspecimens and acquired force-displacement curves by utilising a combined lathe and traction machine. The longitudinal matrix modulus was calculated by accounting for the dimensions and porosity of the samples by employing 3D-tomography scans. The calibration of the machine could be validated with a polycarbonate sample. Nanoindentations were done on the bone specimen in transverse and longitudinal direction. The longitudinal matrix modulus was extracted from the indents applying a recently developed program code (Swadener & Pharr, 2001). This method allowed correction of the effect that indentation experiments represent a weighted average of the stiffness constants in all direction. The goal of this study was to compare the matrix moduli derived from these two independent mechanical tests (traction test versus nanoindentation).

For bovine 7 and bovine 8 both matrix moduli match within the error bars. For bovine 10 the matrix modulus derived from the nanoindents is 13 % lower than the corresponding value derived from the traction test. The latter difference may correlate with the fact that the volume for the indentation tests was not identical with the volume characterized by the traction test and the μCT scans. This experimental constraint was due to the 3D-reconstructions that applied radiation doses with destructive effects on the mechanics of the bone matrix. This validation experiment was therefore based on the hypothesis that adjacent volume elements of bovine bone showed negligible differences in terms of mechanical properties. However, it cannot be excluded that the aforementioned variation is due to slight inhomogeneities of the bovine matrix.

In bovine 7 we observed the highest presence of osteonal bone. This sample showed the lowest indentation modulus and the lowest matrix modulus for the traction test that compares with reported results (Martin & Ishida, 1989; Currey, 1959). They reported a weakening of the plexiform structure by Haversian remodeling what they attributed to a lower amount of longitudinal collagen fibers in osteonal bone. The presence of vascular channels probably causes the slightly higher mean porosity of Φ=3.4%. The vascular channels may also explain that the standard deviation of the porosity was by 40% greater than for the two plexiform specimens.

For bovine 7 the lowest degree of mineralisation was measured which compares favorably with the fact that osteons in human bone tissue are on average less mineralised than the surrounding interstitial bone.

The anisotropy ratio of the matrix also varied among the samples being with 32% lowest for bovine 7 and with approximately 60% similar for the two plexiform samples. According to Hasegawa et al (1994), the anisotropy of the bone matrix is mainly determined by its mineral component. The orientation of the apatite crystals could play a key role in the aforementioned anisotropy ratio. For bovine plexiform bone, a preferred mean orientation of the HAP-platelets along the long axis of the bone was reported (Sasaki et al, 1991). It is possible that for secondary

osteons the mean orientation of the mineral crystals is different and/or less pronounced with respect to the fast growing plexiform structure.

An important point pertains to the applied strain histories for the two mechanical tests. The applied holding period of 60 seconds between successive steps for the traction experiment contrasts with the 5 seconds holding time that preceded the unloading of the indenter. Additionally, the traction tests of the microspecimens were run at a strain rate that was by a factor 600 lower than the applied strain rate for the indentation tests. To clarify this point, we applied a torsion test of a dried bovine bone specimen that was dissected from the same femur. In the low frequency range the shear modulus increased by 4.3% when the frequency was increased by factor 1000 (Schaller, 2001). This test provided evidence that the strain rate dependent effects for the elastic response of dried tissue are in the low frequency range of minor importance.

In conclusion this study demonstrated that the identical longitudinal matrix modulus could be derived from a traction experiment in combination with porosity and from nanoindentation tests in combination with a numerical code. The critical reader may argue that this does not represent a straightforward procedure to convert the nanoindentation modulus into the macroscopic elastic response.

However, based on this excellent correspondence, the following straightforward procedure can be proposed. The ratio $(m_3/m_1)^2$ and the factor ε_o can be determined by nanoindentation and the equations (6) and (7) assuming a transverse isotropic stiffness tensor. This allows for a direct calculation of the matrix modulus with $E_3^{matrix} = \varepsilon_o (m_3)^2$. The apparent modulus for tensile tests can then be determined by additionally employing the outer dimensions and the porosity of the macroscopic sample. For this purpose, some modifications of the equations in section B have to be made.

This study could validate this procedure for homogeneous structures like bovine bone and may represent a first step for a conversion of the indentation modulus into the mechanical response on the organ level. However, further work is required to complete this task.

References

- Barnett DM, Lothe J (1975) Line force loadings on anisotropic half-spaces and wedges. Physica Norvegica **8/1**:13-22
- Carter DR, Hayes WC (1977) The compressive behavior of bone as a two-phase porous material. J Bone Jt Surg **59A**:954-962
- Cowin SC (1989) Bone Mechanics. CRC Press, Inc. Boca Raton, Florida
- Currey JD (1959) Differences in the tensile strength of bone of different histological types. J. Anat. **98**:87-95
- Enstroem J (2001) Micromechanics of compact bone. Diploma thesis DGM/EPFL-Lausanne
- Fan Z, Swadener J, Rho JY, Roy M, Pharr G (2001) Anisotropy nanoindentation properties

of human cortical bone. Proceedings, Orth Res Soc 2001, San Francisco

- Hasegawa K, Turner CH, Burr DB (1994) Contribution of collagen and mineral to the elastic anisotropy of bone. Calcif Tissue Int **55**:381-386
- Hay JC, Bolshakov A, Pharr GM (1999) J Mater Res **14**:2296
- Hengsberger S, Kulik A, Zysset PK (2002) Nanoindentation discriminates the elastic properties of individual human bone lamellae under dry and physiological conditions. Bone: in press
- Hoffler CE, Moore KE, Kozloff K, Zysset PK, Brown MB, Goldstein SA (2000a) Heterogneity of bone lamellar-level elastic moduli. Bone **26/6**:603-609
- Hoffler CE, Moore KE, Kozloff K, Zysset PK, Goldstein SA (2000b) Age, gender, and bone lamellae elastic moduli. J Orth Res: Official Publication of the Orthopaedic Research Society, **18/3**:432-437
- Martin RB, Ishida J (1989) The relative effects of collagen fiber orientation, porosity, density and mineralization on bone strength. J Biomech **22/5**: 419-426
- Nuzzo (2001) ESRF/Grenoble. private communication
- Oliver WC, Pharr GM (1992) An improved technique for determining hardness and elastic modulus using load and displacement sensing indentation experiments. Mat Res Soc **7/6**:1564-1583
- Rho JY, Zioupos P, Currey JD, Pharr GM (1999d) Variations in the individual thick lamellar properties within osteons by nanoindentation. Bone **25/3**:295-300
- Rho JY, Zioupos P, Currey JD, Pharr GM (2001) Microstructural elasticity and regional heterogeneity in human femoral bone of various ages examined by nanoindentation. J Biomech: in press
- Rice JC, Cowin SC, Bowman JA (1988) On the dependence of elasticity and strength of cancellous bone on apparent density. J Biomech **21**:155-168
- Sasaki N, Ikawa T, Fukuda A (1991) Orientation of mineral in bovine bone and the anisotropic mechanical properties of plexiform bone. J Biomech **24/1**:57-61
- Schaller (2001) EPFL/Lausanne. private communication
- Swadener JG, Pharr GM (2001) Indentation of elastically anisotropic half-spaces by cones and parabolae of revolution. Phil Mag A, **81/2**:447-466
- Zysset (1994) A constitutive law for trabecular bone. Ph.D. thesis. EPFL-Lausanne
- Zysset PK, Guo XE, Hoffler CE, Moore KE, Goldstein SA (1999) Elastic modulus and hardness of cortical and trabecular bone lamellae measured by nanoindentation in the human femur. J Biomech **32**:1005-1012

Chapter 6
The influence of ovariectomy, low protein diet and treatment with essential amino acids on the tissue properties of rat vertebrae: a preclinical study

Introduction

Nanoindentation has proven to be a powerful tool to determine the mechanical properties of bone tissue. The characterization of the tissue quality provides a probe to investigate the influence of medical agents on the bone remodeling process at the level of the bone cells. For this purpose, vertebral bodies of rats that experienced bone loss due to estrogen deficiency and low protein intake followed by a treatment with essential amino acids were measured by nanoindentation. In this context the nanomechanical tests represent an additional characterization tool for an already completed preclinical study that includes histomorphometry and macroscopic mechanical tests. The prospect of this study was to determine if estrogen deficiency and low protein intake affect the mechanical properties of bone tissue in the rat. In the following, a summary of the material and methods as well as experiments and results of the preclinical study will be described. Our contribution with the nanoindentation tests will then be presented and combined with the macroscopic mechanical and histomorphometrical properties.

Materials and methods

For a more detailed description see Amman et al. (2002).

Animals and treatment

Nine 26-weeks old female Sprague-Dawley rats were included in this study. The rats were divided into three groups. The first group contained three sham operated rats that received during the following 26 weeks a 15% casein diet.

The six other rats were ovariectomized and fed with an isocaloric 2.5% casein diet resulting in loss of bone mass. After 10 weeks of adaptation three of these six rats received an addition of 5% essential aminoacids (EAA) for further 16 weeks. See Table 1 for an overview of the different treatments.

group \ week	**26**	**26-36**	**36-52**
SHAM	sham operated	15% casein	15% casein
OVX	ovariectomized	2.5% casein	2.5% casein
EAA	ovariectomized	2.5% casein	2.5% casein + 5% essential aminoacids

Table 1: Treatment of the three groups before the macroscopical mechanical tests and the nanoindentations were performed. Each group contains three rats. Note that the "OVX" and "EAA" group were both ovariectomized and fed with low protein diet.

Mineralisation

Bone mineral density (BMD) of the lumbar spine was characterized by Dual X-ray Absorptiometry (DXA) using a Hologic QDR-1000 densitometer that was adapted to small animals.

Histomorphometry

Volume fraction and trabecular architecture of the vertebrae were characterized using a high-resolution micro-CT system. Based on the micro-CT images, the thickness of the cortical shell and the stereological parameters of trabecular bone volume fraction (BV/TV) were determined on the L4 vertebral body.

Macroscopic mechanical tests

The 52-week old rats were sacrificed and the L4 vertebral bodies were dissected at the level of the intervertebral disks. Ultimate strength (US), stiffness (Stiffness) and energy to failure (Energy) were determined by an uniaxial traction experiment applying an electromechanical system (Instron 1114, Instron Corp., High Wycombe, UK) applying a displacement rate of 2 mm/min.

Nanoindentation

The L5 vertebral body of each rat was also dissected at the level of the intervertebral disks. The bone specimens were kept frozen until preparation for the mechanical tests by nanoindentation. Each vertebra was cut transversally in the middle of the approximately 8mm high body. The samples were embedded in PMMA and the face of the transverse cut was polished finishing with a 0.25µm diamond solution. After these preparation steps, the specimen were dried for 24 hours at 50° Celsius.

The mechanical tests included 9 indents on the cortical shell of each vertebral body, 3 indents at the posterior, three at the lateral and three further on the anterior site.

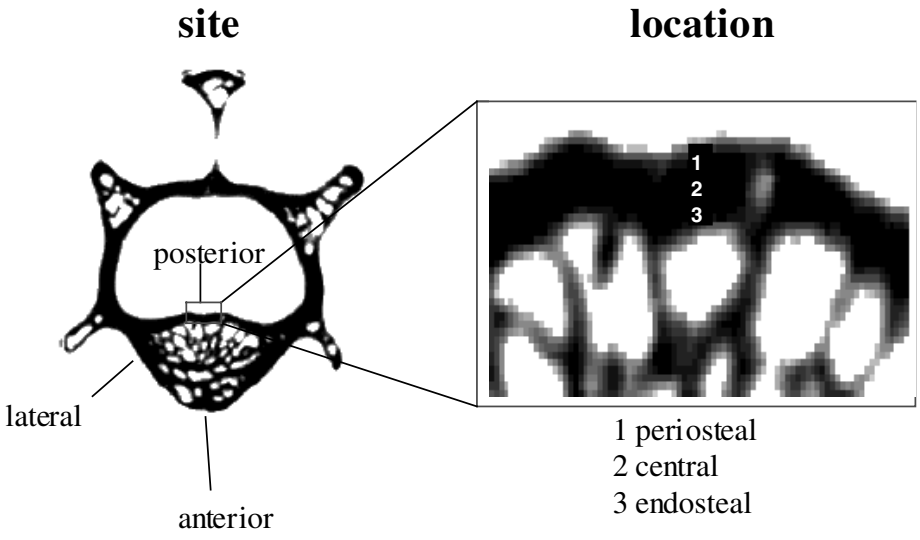

Figure 1: Schematical representation of the indent areas. On transversal slices three sites of the vertebral body were chosen: anterior, posterior and lateral site (see left figure). On each site three locations were defined as structure of interest: the periosteal, the central and the endosteal location (see right figure).

On each site, three indents were done on the periosteal, the central and the endosteal location of the bone matrix. See Figure 1 to have an overview of the chosen areas of the nanomechanical tests. The indents were run to 900nm maximum depth applying an approximate strain rate of $\dot{\varepsilon} = 0.066\frac{1}{\mathrm{s}}$. At the point of initial unloading hardness was evaluated after 5 seconds holding period. The indentation modulus was derived from the unloading part (Oliver & Pharr, 1992) for which an identical strain rate was employed. The thermal equilibrium conditions resulted in a drift of less than 0.1nm/s.

Statistical analysis

For statistical analysis, multiple-way-ANOVAs were run that were based on a parametric mixed model. The factors "treatment" (SHAM, OVX or EAA), "site" (anterior, lateral, posterior) and

"location" (periosteal, central and endosteal) were set to fixed effects while "sample" (3 samples per group) was treated as a random factor.
MANOVAs for the relative hardness values were based on "treatment", "site" and "location" as fixed effects. A significance level of p=0.05 was chosen.

Results

Mineralisation

The sham-operated group with 15% protein intake, BMD=0.142 ±0.011g/cm^2, showed greatest bone mineral density (BMD) among the three groups. Bone mineral density, 0.085 ±0.012g/cm^2, was lowest for the ovariectomized group receiving low protein intake (OVX). The ovariectomized group with low protein intake and 16 weeks treatment with essential aminoacids (EAA) showed a mineralisation of 0.119 ±0.01g/cm^2 (see Table 2).

Histomorphometry

Cortical thickness was greatest in the SHAM group, 198 ±35 μm. In the OVX group a thinning of the compact bone shell down to 134 ±26 μm was observed. For the group treated with essential aminoacids (EAA) a complete recovery of the cortical shell to 198 ±5 μm was seen (see Table 2). The trabecular volume fraction (BV/TV) was greatest in the SHAM group by 25%. In the OVX group this parameter was decreased due to an increased resorption activity. This resulted in a change of the trabecular number, connectivity and structure (rods instead of plates). The EAA-treated group showed BV/TV=15%, an uncompleted recovery of trabecular volume fraction.

Macroscopic mechanical tests

For ultimate strength and energy to failure the OVX group showed lowest values, while for the stiffness results OVX was not significantly different from EAA (p=0.66). See Table 2 for an overview of the histomorphological and mechanical data and the global significance level of the treatment group for each parameter.

Table 2: Results of the histomorphometric and macroscopical mechanical tests of the 52-week old rats. From left to right: Bone mineral density (BMD), cortical thickness (cort thick), trabecular volume fraction (BV/TV), ultimate strength (US), energy to failure (Energy) and Stiffness (Stiffness). The bottom line shows the global significance level of the treatment group for each parameter.

	BMD (g/cm^2)	cort thick (μm)	BV/TV	*US (N)*	*Energy (Nmm)*	*Stiffness (N/mm)*
SHAM	0.142 ±0.011	198 ±35	0.25 ±0.06	*155 ±12.4*	*27.1 ±9.2*	*489 ±99.7*
OVX	0.085 ±0.012	134 ±26	0.08 ±0.04	*72.6 ±11*	*10.2 ±3.9*	*322 ±7.4*
EAA	0.119 ±0.010	198 ±5	0.15 ±0.025	*148.8 ±14*	*38.6 ±5.7*	*312 ±36*
p-level	0.002	0.03	0.008	*0.0003*	*0.015*	*0.02*

Indentation modulus

The indentation modulus was 19.7 ±3.9 GPa (mean ±stdeva) for SHAM, 17.8 ±5.3 GPa for OVX and 17.6 ±6.2 GPa for EAA and were not significantly different (p=0.77). The ratio of the standard deviation and the mean value was for the OVX (30%) and EAA (35%) group greater than for the SHAM group (20 %). Figure 2 left presents the boxplots of the indentation modulus results.

The indentation moduli in the anterior regions were 15.4 ±5.4 GPa significantly lower (p<0.0001) than for the lateral, 20.3 ±5.3 GPa, and the posterior sites, 19.4 ±3.6 GPa.

According to 4-way-ANOVA the sample (p<0.0001) and the site (p<0.0001) were highly significant factors while location (p=0.066) and treatment (p=0.77) were not globally significant.

By pooling treatment, 2-way ANOVAs were performed for each location. The anatomical site was significant (p=0.011) for the indents made at the periosteal locations but not significant (p=0.26) for endosteal indents.

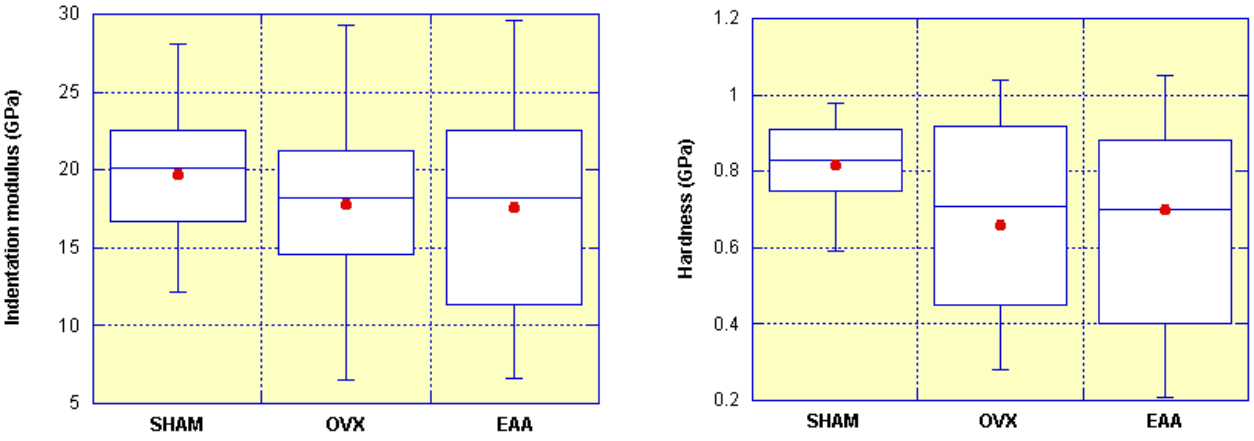

Figure 2 Boxplots for indentation modulus (**left**) and hardness (**right**). The whiskers indicate minimum and maximum of the value range, the boxes show the upper and lower quartiles. The line within the boxes indicates the median and the point the average value.

Hardness

The hardness values were 0.82 ±0.13 GPa for SHAM, 0.66 ±0.25 GPa for OVX and 0.7 ±0.24 GPa for EAA and were not significantly different among the three groups (p=0.41 with 4-way-ANOVA). The ratio between standard deviation and mean value was therefore 15% for SHAM and was increased up to 38% for OVX and 34% for EAA. See Figure 2 right for the boxplots of the hardness results.

According to 4-way-ANOVA, the sample ($p<0.0001$) and site ($p<0.0001$) were again of global significance while the location ($p=0.1$) and the treatment ($p=0.41$) did not reach global significance.

3-way-ANOVAs with sample, site and location as factors were run separately for each treatment group. Within the SHAM group, the samples were not significant ($p=0.32$), in the OVX-group a moderate ($p=0.02$) and in the EAA-group a high significance ($p=0.0002$) of the sample was seen (see Figure 3a).

Pooling the three treatment groups, 2-way-ANOVAs were performed separately for each indentation location. As for indentation modulus, the periosteal hardness values were significantly different among the sites ($p=0.0013$) while for the endosteal indents this factor had no statistical influence ($p=0.51$).

Despite the low global significance of the treatment, some trends can be observed. Figures 3b shows the hardness values for the anterior site. This graphic represents the results separately for the treatment groups and for the location of the indent. Among the three anatomical sites, the anterior region showed 0.7 ±0.14 GPa for SHAM, 0.42 ±0.18 GPa for OVX and 0.61 ±0.24 GPa for EAA, the greatest variations with treatment. The group treated with essential aminoacids showed for the anterior site an increase of the endosteal hardness values that reached the level of the SHAM rats. For the periosteal indents on the anterior site the effect of treatment with essential aminoacids seemed to be lower. 3-way-ANOVA (with sample, location and treatment as factors) did not show significance of the treatment for the anterior hardness ($p=0.2$). However, pooling the three samples (or excluding the factor "sample") within each group, treatment achieved significance ($p=0.02$).

Figure 4 represents the relative hardness values whereby each indent was normalized with respect to its adjacent central indent. This representation is based on the interest to detect relative variation of tissue properties. This normalization may also help to account for the individual variation among the rats. A 3-way-ANOVA of the relative hardness values was performed with site, location and treatment as factors. The interaction term site*location was globally significant ($p=0.015$). Figure 4 shows that the effect of the treatment with essential aminoacids on the endosteal surface was different among the three sites. 2-way-ANOVA of the endosteal indents showed a moderate significance of the interaction site*treatment ($p=0.05$), that shows a site-dependent effect of the treatment. 2-way-ANOVA of the periosteal indents did not show significant interaction of site*treatment ($p=0.83$), indicating that for these indents the effect of the treatment was not site-dependent.

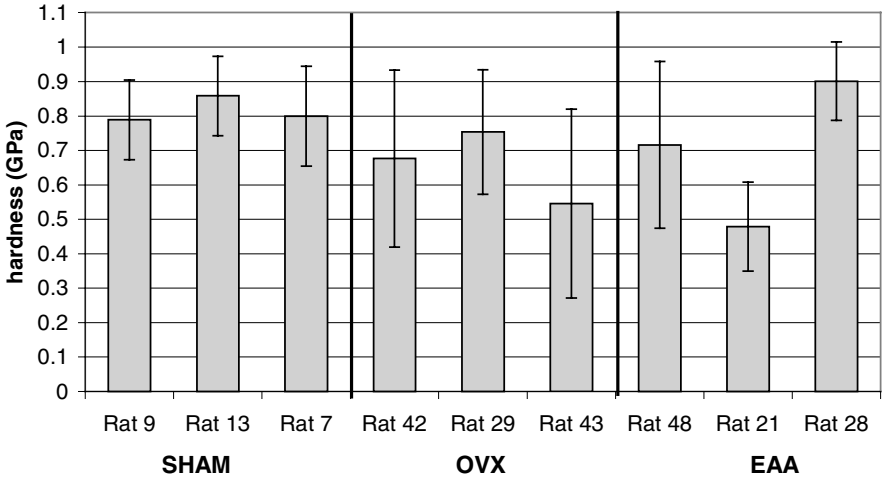

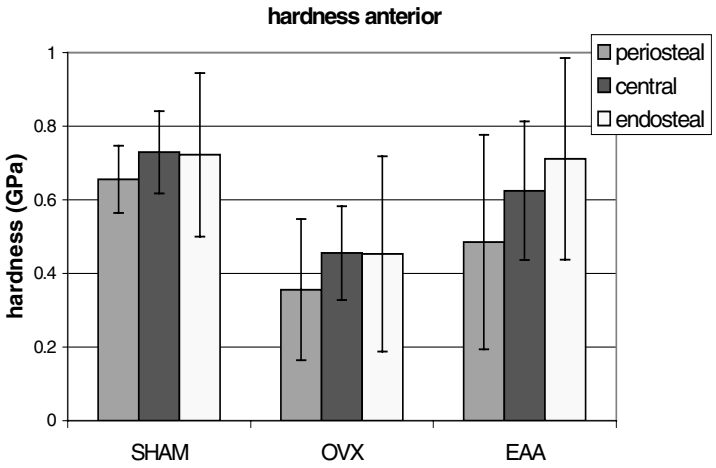

Figure 3a (top) Mean hardness values for the nine individuals The three SHAM-samples were not significantly different, while within the OVX and EAA-group the samples were significant.
Figure 3b (left): Hardness values for the anterior site of the three treatment groups separately for the periosteal, the central and endosteal location.
Each column represents mean ± stdeva and contains 9 (top) or 3 (left) indents.

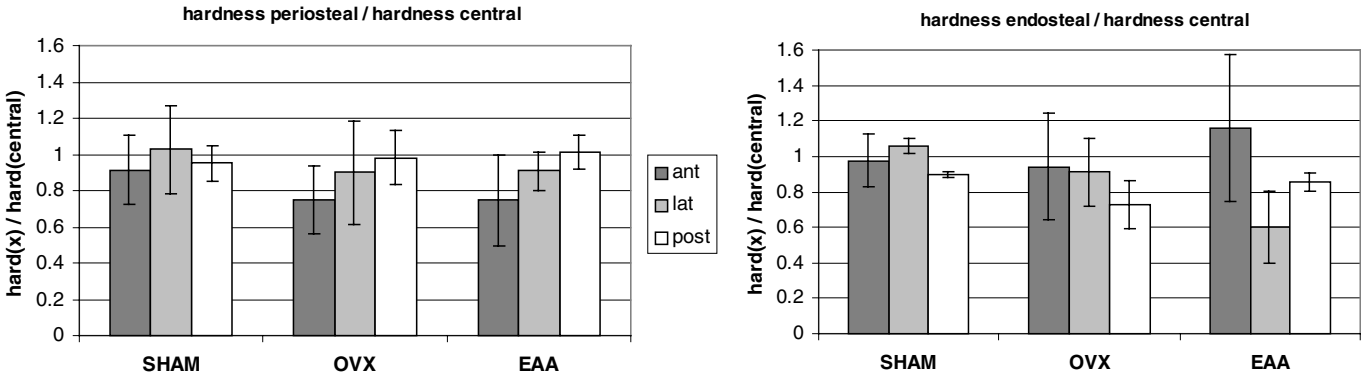

Figure 4: Relative hardness, where each indent was normalized by the value of the adjacent "central" indent. This representation accounts for the individual variation of the rats within each group. The results are shown separately for the three anatomical sites: anterior (ant), lateral (lat), posterior (post). **on the left** the relative hardness values for the periosteal location and **on the right** the relative hardness values for the endosteal location . The interaction of treatment*site reached significance (p=0.05) for the endosteal indents but not for the periosteal indents (p=0.83).

Macroscopic mechanical competence versus histomorphometry and tissue properties

Table 3 represents the regression results of the macroscopic mechanical properties. For each rat the mean values of hardness and indentation modulus were employed. BMD explained 81% of variation of ultimate strength, while the correlation between stiffness and BMD was moderate (R^2=0.22). Energy to failure showed a correlation with both, BMD (R^2=0.7) and hardness (R^2=0.75).

	regression	**R^2**
Ultimate strength	US= 2641*BMD$^{1.42}$	0.81
	US= 145*hardness$^{0.6}$	0.1
Stiffness	Stiffness= 1011*BMD$^{0.47}$	0.22
	Stiffness= $(E_{ind})^{0.21}$	0.03
Energy to Failure	Energy= 2310*BMD$^{2.2}$	0.7
	Energy= 59.3*hardness$^{3.76}$	0.75

Table 3: Regression of the macroscopic mechanical parameters as functions of BMD or the nanomechanical properties. For Ultimate strength, BMD showed a higher correlation than hardness. Both BMD and indentation modulus (E_{ind}) showed a low correlation with stiffness. For Energy to failure, BMD and hardness explained 70 and 75% of the variation, respectively.

Discussion

This study determined the micromechanical properties of L5 vertebral bodies from nine rats. Six animals were ovariectomized and fed with a low protein diet, three of them additionally received essential aminoacids.

The high statistical significance of the factor "sample" shows the difficulties involved in the determination of the influence of the treatment. For the control (SHAM) rats the "sample" was not a significant factor. Within the OVX group the samples were moderate statistical significance and high within the EAA group. This implies an individual response of the rat tissue to ovariectomy and low protein diet, particularly with addition of essential aminoacids. It should be noted that the high standard deviation of hardness and indentation modulus in the EAA-group is also due to significant differences between the animals. This study could not show a global significance of the treatment on the intrinsic tissue properties. Since the high variability of the "sample" has decreased the significance level of the factor "treatment" (this was demonstrated for the anterior hardness results), further studies with a greater number of animals are crucial. However, this study could demonstrate some trends of the nanomechanical parameters that are probably results of the treatments.

Ovariectomy and low protein intake lead to an extension of the hardness and the indentation modulus range particularly towards lower values. Obviously the greater resorption activity is also accompanied by a certain formation activity. Areas of lower mechanical properties probably

indicate the presence of new-modelled units with low mineral content and poor collagen organisation. According to Oxlund et al (1995), a lower degree of hydroxypyridinium cross-links in ovariectomized rats may also play a role for the decreased mechanical properties.

The histomorphometric analysis of the L4 vertebral bodies of the same animals determined a thinning of the cortical wall as a result of ovariectomy and low protein intake. An almost complete recovery of the cortical wall was observed due to the treatment with essential aminoacids. Hereby the apposition of new tissue seems to take preferentially place on the endosteal surface of the bone while the outer dimensions of the vertebral body remained almost constant.

This histomorphometric observation may be discussed in the light of the relative hardness values (that were normalized with respect to the corresponding central indent). For the anterior and posterior site a relative increase of endosteal hardness and for the lateral site a relative decrease of endosteal hardness was observed for the EAA group. Statistically this site-dependent effect of treatment on the endosteal part reached significance.

This variable response of the three sites may be due to a locally varying time delay and/or amplitude of the remodeling stimulation. An immediately high cellular activity at the anterior endosteal surface due to EAA-treatment could explain a greater maturity and mineralisation of these structures. Further studies incorporating tetracycline labels and an analysis of the degree of cross-linking could be helpful at this point. Heterogeneity of the remodeling activity could be correlated with an inhomogeneous mechanical stimulation. Effects like a variation of the muscular competence change the mechanical stresses imposed on the vertebral body. The comprehensive preclinical study also included the analysis of the muscle weight of the lower limbs. The mean muscle weight was by 20% lower for OVX with respect to SHAM group and was after EAA treatment even by 6% higher than for the control rats. The muscle weight change of the lower limbs may reflect variations of the weight and the associated mechanical competence of the back muscles. This could result in inhomogeneous variations of compressive forces in the lumbar spine that differently stimulates the remodeling activity among the sites. Checking these additional information a moderate positive correlation was found anterior hardness being a power function of muscle weight (R^2=0.47).

A set of regressions was presented fitting the macroscopic mechanical properties as functions of BMD or nanoindentation parameters. Surprisingly, the energy to failure showed a high correlation with both hardness (R^2=0.75) and BMD (R^2=0.7). This finding may be of potential clinical interest since a set of nine local nanomechanical tests in combination with BMD allow predicting 81% of a macroscopic parameter. It may be interesting to check the validity of this relationship for the human vertebra.

However, at least 19% variation of the macroscopic mechanical competence cannot be explained by these regressions. The EAA group showed a complete recovery of ultimate strength and

energy to failure, while the BMD value remained by approximately 16% below the level of the control group. Based on the hypothesis that mineral content is homogeneously distributed in the matrix, the relative influence of volume changes of trabecular and cortical bone on BMD can be estimated. For a cylindrical body of 8mm length and 4mm outer diameter a change of cortical thickness from 200μm to 135μm results in a 6% decrease of BMD. A change of trabecular volume fraction from 25% to 8% leads to a BMD decrease of more than 15%. It is therefore probable that the recovery of cortical thickness for the EAA-rats explains that the relative increase of the macroscopic mechanical competence is greater than is reflected by the BMD.

Concluding the discussion, an important point should be addressed. Is the rat vertebral body a good biomechanical model for the human vertebrae? Based on numerical work, Homminga et al (2000) reported that for intact rat vertebrae the trabecular structure contributes only to 11.3% to the macroscopic mechanical response. For ovariectomized rats the spongy bone was with 3.3% even less involved in the macroscopic competence. Obviously this does not reflect the conditions of human vertebrae where the trabecular bone structure plays the major role for the mechanical integrity of healthy and osteoporotic tissue. This point does not speak against the inclusion of mechanical tests like nanoindentation to characterise the intrinsic tissue properties. Medical agents could show equivalent stimulation of the cellular activity for human and rat bone although the effects on the macroscopic mechanical properties are quite different.

References

- Ammann P, Laib A, Bonjour JP, Meyer JM, Rüegsegger P, Rizzoli R (2002) Dietary essential aminoacid supplements increase bone strength by influencing bone mass and microarchitecture in osteoporotic adult rats. JBMR in press
- Homminga J, Weinans H, Ederveen AGH, Kloosterboer HJ, Schlatmann R, Oosterbroek M, Huiskes R (2000) The rat vertebra is not a good model for testing the mechanical quality of cancellous bone. Proceedings ESB 2000, Dublin
- Oliver WC, Pharr GM (1992) An improved technique for determining hardness and elastic modulus using load and displacement sensing indentation experiments. Mat Res Soc **7/6**:1564-1583
- Oxlund H, Barckman M, Ortoft G, Andreassen TT (1995) Reduced concentrations of collagen links are associated with reduced strength of bone. Bone **17/4**:365-371

Conclusions and outlook

Nanoindentation was the central technique of this thesis that focussed on the structure-function relationship of bone. Mechanical and morphological properties were discussed on the tissue, BSU and the lamellar level of human, bovine and rat bone. In conclusion, a synthesis of all the information provided by these studies may be done. This outline presents the results following the decreasing hierarchical organisation of bone. Technical limitations as well as suggestions for further studies will also be provided.

Nanoindentation was applied in the frame of a preclinical study targeted for the treatment of osteoporosis. Indentation tests were done on rat vertebrae that experienced bone loss by low protein intake and ovariectomy followed by a treatment with essential aminoacids. Whole bone and tissue properties were compared with changes in bone mineral density, histomorphometry and muscle weight. The latter point suggested a discussion of tissue properties in the light of the entire muskuloskeletal system that represents the highest functional level for biomechanics. The detected variation of mechanical properties on the tissue level was weak with respect to the whole bone level. The extended range of hardness and indentation modulus towards lower values suggests apart of the increased resorption a certain formation activity for bone of ovariectomized rats with low protein intake. Here nanoindentation provided a probe to detect areas of bone formation. Further studies may include tetracycline labelling to enable a more thorough identification of newly remodeled structures. The tissue properties of the rats showed an individual response to the treatments. An inappropriate proportion between the number of samples and the biological variability might have suppressed statistical significance of some factors. In spite of the low statistical contrast, some trends of the anterior hardness values were identified that call for tests of additional animals. It is possible that the performed treatments remain globally insignificant for the tissue properties. If this applies, the macroscopic mechanical properties depend mainly on geometrical and histomorphological changes.

Hardness explained 75% of the variation of the energy to fracture. This again raises the need for tests of further individuals, since this suggests a great potential to determine macroscopic competence with indents on small volumes. In the light of preclinical studies, indentation experiments could serve as a complementary tool to detect intrinsic tissue changes. The fact that small volumes (<mm^3) are sufficient for nanoindentation tests may be of great advantage for this purpose.

The latter point raises the need to extend the knowledge of the relationships between the mechanical integrity on the organ level and the level characterized by nanoindentation. In an effort to satisfy this task for the micromechanical versus nanomechanical level, a validation study was targeted. Traction tests were done with microspecimen of bovine bone that contained several

BSUs. Longitudinal tissue modulus was calculated from indentation modulus and compared with the value derived from a traction experiment taking into account a power law of the porosity. The excellent correspondence of these values supported the hypothesis that the main factors, that distinguish nanomechanical and micromechanical tests, are porosity and anisotropy. Numerical calculations were employed in this context to extract the stiffness constant in the direction of the indentation. The presented curve fits that were based on a model for bovine bone may be extended to human bone in future work. If the effect of bone anisotropy on the measured indentation modulus is known for any microstructure, the absolute tissue properties can be determined in their physiological loading direction.

Another problem of nanoindentation that is still not fully understood regards the influence of damage on the measured elastic indentation modulus. However, the comparison with an elastic traction experiment raises confidence in the absolute value of indentation modulus. The ratio between the volume analysed by an indentation test and by microtraction was approximately $1{:}10^6$. Further studies should focus on microspecimen of greater size and on the more heterogeneous human bone. It is possible that for higher variability of mineralisation this parameter should also be taken into account. The traction test of the three bovine samples showed that differences as high as 35% in elastic modulus could occur between microsamples dissected from the same femoral diaphysis.

Individual properties of the plexiform and osteonal microstructures and/or individual properties of the BSUs may play a role.

The former point was addressed by a comparison of trabecular, osteonal, interstitial and bovine plexiform microstructures. The elastic properties of the bovine plexiform structure were not significantly different from human interstitial bone at this depth. Human interstitial tissue was significantly stiffer than osteonal tissue, and the osteonal microstructures were significantly stiffer than trabecular BSUs. The latter confirmed observations at the human femoral neck (Zysset et al, 1999; Hoffler et al, 2000a).

The second point, the variability of the individual BSU for identical microstructures was tested for human interstitial and osteonal bone. It could be shown with clear significance that the BSU represents the basic unit of the bone construct with individual mechanical properties. The individual mechanical properties of each BSU are probably a result of individual morphological properties. The structure-function relationships were therefore studied on the BSU-level. Hereby, two morphological parameters were chosen for which an influence on the macroscopic mechanical competence was reported.

Surprisingly, the subset of the hypermineralised structures of the 86-year old female (and not of the 30-year old male) confirmed some moderate correlations that were reported for the macroscopic level. The 30-year old male showed similar hardness values and higher indentation moduli than the female donor in spite of lower mineral content. Indentation modulus showed a

poor general correlation with both, mineralisation (determined by MDMB) and the orientation of the collagen fiber (determined by LSI). A poor correlation with the latter parameter was also attributed to possible limitations of the applied PLM technique.

An interesting finding may be that the correlation between hardness and indentation modulus was more heterogeneous for the older female donor. We hypothesised that hardness correlates with macroscopic postyield properties like ultimate strength and energy to failure. This hypothesis is supported for the latter parameter by the findings of the rat study. Hardness may therefore better reflect changes in tissue quality than indentation modulus. We suggest to clarify whether a deterioration of tissue quality leads to a decreasing correlation between these nanomechanical properties.

The weakness of this work is due to the low number of donors. Instead of investigating many BSUs of a few donors, few BSUs of many donors should be studied in future work. However, it could be proven that the dependence of nanomechanical on morphological properties is more complex and can hardly be explained by our proposed quantitative measures. Apart of the extension to further donors, other parameters like the orientation of the HAP-crystals, the quality and degree of cross-linking of the type-I-collagen should also be considered. Experimental difficulties may arise from the fact that these parameters have to be determined for individual BSUs.

The moderate correlation of indentation tests with ultrasound measurements implied that artefacts may occur that are still badly understood. The influence of vascular porosity and dispersion effects on the propagation of the sound wave was suggested. The correlation was improved by using an independent measure of local density. It seems that a combination of impedance measurement (back-reflected wave) and microradiography represents an appropriate alternative to quantify a SAM-modulus. Further studies may apply SAM in a higher frequency range (>400 MHz, for which absorption is too high for a simultaneous detection of the transmitted wave) in combination with MDMB. This alternative also provides an improved spatial resolution to distinguish single BSUs (Katz & Meunier, 1993; Briggs, 1992).

Properties of BSUs were determined with indents at 1μm depth that represent an average of a few lamellae. The bone lamellation theories suggest that the collagen fiber orientation and/or mineral content may vary between adjacent thick and thin lamellae.

The proposed bone lamellation models motivated tests within single bone lamellae, where the aforementioned factors were assumed to be more homogeneous. For this purpose, we introduced a recently developed device that allows topography scans and indentation experiments applying the same tip. The great precision to position the indenter tip was used to extract the properties of single lamellae. Differences were seen between thin and thick lamellae in terms of indentation modulus, depth dependency of indentation modulus and relative increase of stiffness after drying. Approximately 90 years after Gebhardt has published the first bone lamellation model (Gebhardt,

1906), the mechanical tests have reached the submicron level. The discussion of the mechanical lamellar properties did not allow a choice of an appropriate bone lamellation theory. However, the detected depth-dependency of indentation modulus suggests that even within single lamellae the morphological properties may not be homogeneous. Collagen fiber orientation and/or mineral content may even vary within single lamellae. We prefer at this point an organisation of the collagen matrix that was proposed by Giraud-Guille (1998). Based on TEM-measurements (Figure 1, middle), Giraud-Guille explained the lamellar appearance by successive orientation changes between adjacent collagen fibrils (see Figure 1, left). Collagen fibrils in the centre of adjacent lamellae therefore show the greatest orientation difference. This model, that allows a comparison with the cholesteric growth of liquid crystals, may explain the smooth depth-trends the thick lamellae have shown. In an effort to characterise the collagen fiber orientation we scanned some trabecular bone lamellae employing scanning electron microscopy (SEM). A comparison of our SEM-scan (Figure 1, right) with the TEM-scan by Giraud-Guille does not speak against the cholesteric model. Next steps should therefore combine morphological (TEM, AFM and/or SEM) and mechanical analysis (nanoindentation) on identical lamellae. It is also possible that the detected differences between adjacent bone lamellae vary with the orientation in which this cholesteric structure is tested. The generality of our results has to be moderated by the fact that lamellae of one single (hypermineralised) donor were tested. It can't be excluded that the high mineral content has influenced the detected trends.

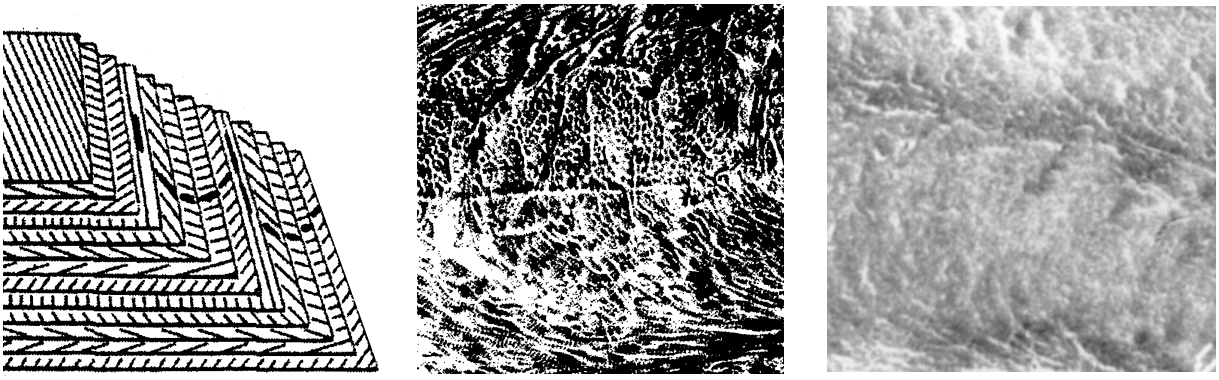

Figure 1 left: Cholesteric organisation proposed by Giraud-Guille where successive orientation changes of collagen fibrils are responsible for the lamellar structure.
middle: TEM-scan on which the cholesteric model is based (scan size 10 μm x 10 μm).
right: SEM of demineralised trabecular bone (scan size approximately 8 μm x 8 μm) performed in our lab. The SEM-scan seems to support a cholesteric organisation.

Future studies should also investigate the intrinsic anisotropy of single lamellae. For this purpose, the identical lamella should be measured twice, in a transverse and longitudinal plane. Bovine osteonal bone is probably a good choice for this issue. The intrinsic longitudinal and transverse

lamellar modulus can be extracted employing the theoretical basis that we presented and validated for bovine bone. This test may give better insight into the bone lamellation theory. An anisotropic indentation modulus may exclude the model of randomly oriented collagen fibers where only the density alternates between adjacent lamellae (Marotti, 1993).

The intrinsic lamellar anisotropy could in a further step be determined under fully wet conditions and again after drying. This experimentally challenging task could clarify the shrinkage behaviour of the collagen fiber when the water content is removed. Evidently this test has to be combined with some morphological analysis of the collagen fiber orientation.

The extracellular matrix, the composite within single lamellae is the next level in the bone hierarchy. Here we reach the current technical limitations of nanoindentation, which provides an average response of the complex hydroxyapatite (HAP) and collagen framework. As it was suggested in this thesis, the mechanical links between collagen and HAP-crystals and/or the collagen cross-links could play an important role. Fundamental research in biomechanics has therefore a strong interest for a further development and application of nanomechanical devices.

As it was mentioned in the introduction, current treatment of osteoporosis mainly includes agents that inhibit bone resorptive processes. However, little is known if the mechanical properties of the remaining tissue change with time. It is possible that effects like damage accumulation occur in this purely remodeled tissue. Further it is unclear if these antiresorptive agents also affect the quality of the newly formed tissue. The potential of nanoindentation is to analyze the unresorbed and/or newly remodeled structures, those components that still contribute to the macroscopic mechanical competence. Future work may establish possible relationships between the nanomechanical parameters (like hardness and/or the hysteresis included by the indentation curve) and damage accumulation.

A possible alternative treatment may replace a general inhibition of bone resorption by a stimulation of targeted remodeling. According to Burr (2000), 30% of the overall remodeling activity is targeted. It becomes widely accepted that the osteocyte-canalicular network plays a major role for these site-dependent processes. Further work may investigate if this proportion of targeted remodeling can be increased and if the cellular activity can be directed to remodel mainly those structures with deteriorated mechanical properties and preserve intact bone areas. In this context, the nanoindentation tests can be employed to identify the areas where tissue formation is necessary and to characterize the quality of the new-formed structures. Further strategies to treat osteoporotic bone may evolve from an effort to improve the latter parameter.

As a first step, in vitro studies may be done employing a combined perfusion/loading chamber (Mertens et al, 1998). This mechanical testing device allows uniaxial loading of macroscopic bone specimens combined with a long-term culture of their bone cells (viability for more than 60 days). Bone areas subjected to remodeling could be analyzed in terms of nanomechanical

properties. This experiment could give better insight into the complex mechanism of how bone turnover is linked to the nanoscopic and macrosopic bone mechanical properties.

References

- Briggs A (1992) Acoustic microscopy, Clarendon Press Oxford
- Burr DB (2000) Damage detection and behavior in bone. Proceedings ESB, Dublin
- Gebhardt W (1906) über funktionell wichtige Anordnungsweisen der feineren und gröberen Bauelemente des Wirbeltierknochens. II. Spezieller Teil.: der Bau der Haversschen Lamellensysteme und seine funktionelle Bedeutung. Arch Entw Mech Org **20**:187-322
- Giraud-Guille MM (1998) Plywood structures in nature. Curr Op Solid State & Mat Sc **3**:221-227
- Hoffler CE, Moore KE, Kozloff K, Zysset PK, Brown MB, Goldstein SA (2000a) Heterogneity of bone lamellar-level elastic moduli. Bone **26/6**:603-609
- Katz JL, Meunier A (1993) Scanning acoustic microscope studies of the elastic properties of osteons and osteon lamellae. J Biomech Eng (Transactions of the ASME) **115**:543-548
- Marotti G (1993) A new theory of bone lamellation. Calcif Tissue Int **53**(Suppl I):47-56
- Mertens F, Bröckmann E, Kratz M, Smith E, Jones D (1998) A novel combined perfusion/loading chamber for bone biomaterials studies. Poster presentation, Davos Conference "Cells & Materials"
- Zysset PK, Guo XE, Hoffler CE, Moore KE, Goldstein SA (1999) Elastic modulus and hardness of cortical and trabecular bone lamellae measured by nanoindentation in the human femur. J Biomech **32**:1005-1012

Acknowledgements

First of all, I would like to thank my supervisor Professor Philippe Zysset who followed this thesis during more than three and a half years. His continuous availability, enthusiasm and interest in this work constituted a great basis for a fruitful friendly collaboration. I owe to him many constructive propositions for this thesis and an introduction in the world of scientific writing. I remember many conversations where I could profit from his extended comprehension of the fascinating world of biomechanics.

I further wish to express my thanks to Dr Andrej Kulik (IGA – DP – EPFL) for his respective contributions to this work. It was a particular concern for me to stay with one foot within the interesting world of physics. I liked to profit from his experimental experience as well as from his fascinating ability to know a person for any problem.

My deepest thanks to Professor Alain Curnier for many fruitful discussions and advises. I enjoyed to work as an assistant for his lectures during three terms.

I would like to thank Professor John Botsis to welcome me to his lab. The amazing environment of his lab was a great basis for productive work. I therefore express my thanks to Liliana Rincon & Eric Charriere for the friendly collaboration within the biomechanics (nano)group. I further wish to thank Johanna Enström et Marc Jeanneret for their respective contributions to this thesis.

My thesis work in the LMAF was additionally enriched by many friendly colleagues and friends. Here I would like to thank Michel Studer, Christian Talon, Federico Bosia, Colin Sanctuary, Jörn Justiz, Francois Erdemli, Kara Peters, Philippe Bonhôte, Jaroslaw Pietrzyk, Laurent Humbert and Professor Bargmann.

I wish to express my thanks to Professor J. Currey, Professor R. Rizzoli, Professor J.-J. Meister and Professor J. Giovanola to have accepted a contribution to the jury of this thesis.

In the frame of many collaborations with AO-ASIF/Davos, INSERM/Lyon, the university of Geneva and the ESRF/Grenoble, I had the pleasure to get many acquaintances. I particularly owe many thanks to Professor B. Rahn, Laurent Feuz & Christoph Sprecher (both from Davos), Dr G. Boivin (Lyon), Dr P. Ammann (Geneva), Dr F. Peyrin and Stefania Nuzzo (both from Grenoble).

I further would like to thank Christian Azcoitia and Dr A. Karimi for their respective support for a large part of the nanoindentation measurements.

I owe many thanks to Michael Bonfert, Dirk Thomas, Tillmann Seidel and Holger Schwenk who enjoyed me with their generous proofs of deep friendship in spite of this great distance.

Last but not least I particularly express my deepest thanks to my parents. This thesis is dedicated to my father and particularly to my mother who left us recently but stay with us in memory. I would like to thank my brother Matthias Hengsberger, his wife Cynthia Hengsberger (Beuret) and their son Lucas Jan Alexandre Hengsberger who have enriched our family with very much joy.

Curriculum vitae

Born in July 21st in 1971 (Saarbrücken/Germany)
Nationality: German
Marital status: Single

Current professional address:
LMAF DGM EPFL
CH-1015 Ecublens
Tel. +41 (0) 21 693 3871
e-mail: stefan.hengsberger@epfl.ch

- **July 1977-June 1990** Primary & high school in Homburg/Saar

- **July 1990- July 1991** ABC-Soldier in Zweibrücken/Pfalz

- **Oct.1991-Sept. 1997** Student in Physics at University of Saarbrücken
  March 1993 Intermediary exam in Mathematics & Physics
  April 1995-Sept. 1997 Diploma student. Diploma thesis in solid state physics:
  "*Photoelectron spectroscopy on $NbSe_2$*"

- **Oct. 1997-May 1998** Research assistant at Fraunhofer Institute for Biomedical Techniques Miami/Florida

- **July 1998-Feb. 2002** PhD-student at EPFL/Lausanne

Publications

[1] S. Hengsberger, A. Kulik, Ph. Zysset (2001) A combined atomic force microscopy and nanoindentation technique to investigate the elastic properties of bone structural units. Cells & Materials **1**:12-16

[2] S. Hengsberger, A. Kulik, Ph. Zysset (2002) Nanoindentation discriminates the elastic properties of individual human bone lamellae under dry and physiological conditions. Bone: **30/1**:178-184

Contributions to international conferences (abstract & talk)

[1] S. Hengsberger, A. Kulik, Ph. Zysset (1999) A combined AFM and nanoindentation technqiue to investigate the elastic properties of bone lamellae. Cells & Materials Conference, Davos 1999

[2] S. Hengsberger, A. Kulik, Ph. Zysset (2000) A combined AFM and nanoindentation technique to measure the elastic properties of single bone lamellae under physiological conditions. ESB 2000, Dublin

[3] S. Hengsberger, G. Boivin, Ph. Zysset (2001) Mineral content is a poor predictor of mechanical properties in single bone structural units of human cortical bone. ISB 2001, Zürich